ALGEBRAIC MODELS IN PHYSIOLOGY & UNDERGRADUATE RESEARCH

A Dissertation

by

THOMAS WILLIAM STILES

Submitted to the Office of Graduate and Professional Studies of
Texas A&M University
in partial fulfillment of the requirements for the degree of

DOCTOR OF PHILOSOPHY

Chair of Committee,	Christopher Quick
Committee Members,	Ranjeet Dongaonkar
	Randolph Stewart
	Burgrahan Yalvac
Head of Department,	Larry Suva

December 2018

Major Subject: Biomedical Sciences

ABSTRACT

Algebraic models are developed to provide qualitative insights and novel tools for experimentalists and clinicians to investigate processes involved in heart failure and renal fluid balance. The models employed graphical analysis to conceptualize how equilibrium behaviors in complex systems emerge from the interactions between mechanical processes. In contrast to numerical modeling methods, the models yielded explicit and general algebraic formulas for clinically relevant variables. Algebraic formulas were obtained by (1) characterizing the functional behavior of the most salient elements of the system, (2) constraining the scope of the model by assuming all global and local feedback acts through the physical properties of the system, and (3) assuming the relationships that characterize the functional elements of the system are linear. Because these models were developed through joint team research with undergraduate research scholars, a third study was conducted to identify the vocational identities and team attributes that predict undergraduate career goal change. Findings regarding the interactions between participant traits and team attributes inform the design of undergraduate research programs that seek to amplify and diversify the nation's workforce of knowledge-producers.

CONTRIBUTORS AND FUNDING SOURCES

The works contained herein were done in collaboration with research faculty and undergraduate research scholars at Texas A&M University. This work was supported by a dissertation committee consisting of Professor Christopher Quick (Chair), Professors Ranjeet Dongaonkar and Randolph Stewart of the Department of Veterinary Physiology and Pharmacology, and Professor Burgrahan Yalvac of the Department of Teaching, Learning and Culture. Contributing authors for the heart failure model (Chapter II) included Professors Christopher Quick of the Department of Veterinary Physiology and Pharmacology as well as research scholars Alejandra Morfin, Hyunjin Lee, Wesley Fuertes, Thad Adams, and Fazal Dalal of the Michael E. DeBakey Institute. Contributing authors for the renal fluid balance model (Chapter III) included Professors Christopher Quick, Ranjeet Dongaonkar, Randolph Stewart, and John Stallone of the Department of Veterinary Physiology and Pharmacology as well as undergraduate research scholars Gabrielle M. Lessen, Madison C. Johnson, Ryan S. Kvinta, and Scott J. Mash of the Michael E. DeBakey Institute. Contributing authors for the undergraduate research vocational goal change model (Chapter IV) included Professors Christopher Quick of the Department of Veterinary Physiology and Pharmacology and Professor Burgrahan Yalvac of the Department of Teaching, Learning and Culture.

Graduate study was supported by assistance from Department of Veterinary Physiology and Pharmacology as well as funding for the Aggie Research Scholars Program provided by Texas A&M University's Tier-One Program.

TABLE OF CONTENTS

Page

LIST OF FIGURES

Page

Page

LIST OF TABLES

Page

CHAPTER I

INTRODUCTION

Mathematical models in physiology aim to characterize how the global behaviors emerge from the interactions among the parts of a complex living system. There are many different types of models in physiology, and each exhibit particular ontological, epistemological, and axiological commitments as to what constitutes a good prediction. Numerical methods are particularly dominant in the field of physiology due to the computational power afforded by modern machine processors. With so much computing power at their fingertips, physiologists have been able to employ large sets of equations and parameters to accurately predict the observed behaviors of physiological systems (208). Multi-scale, nonlinear models incorporating feedback are the most common types of models being published today (128, 194, 282, 294). The algebraic modeling methods of classical physiologists, like Otto Frank, Ernest H. Starling, and Author C. Guyton, have thus lost much of their sway in physiology communities. However, in our laboratory at the Michael E. DeBakey Institute for Comparative Cardiovascular Science and Biomedical Devices led by Professor Christopher M. Quick, undergraduate and graduate research scholars have sought to develop predictive models that offer insights into how complex physiological systems work. Elevating concerns for understanding system mechanics, we have labored to construct models from parsimonious sets of first-order relationships to discover which occult interactions are the most influential in determining system behavior. To this end, we have adopted methods that classical physiologists employed to approximate functional relationships and graphically explore how parts interact. We have also devised novel analytical strategies to construct conceptual frameworks that can inform the work of experimentalists and clinicians.

Managing system complexity by mathematically characterizing the functional behavior of the most salient elements of the system. Physiological systems are amazingly complex, involving physical, chemical, and electrical interactions within and between anatomical structures. Distributed models regard the spatial arrangements of anatomical structures as important parameters influencing system behaviors. Network models regard the order of interactions to be important. Another modeling approach is to disregard anatomical details of similar structures in order to mathematically characterize their overall behavior as a distinct functional element. Referred to as “lumping”, this entails grouping similar structures into compartments that each have singularly distinct set of properties and relationships (223). In the renal fluid balance model (Chapter III), convoluted proximal tubules in the kidney and the capillary network surrounding them were lumped into two separate rigid compartments each characterized by osmotic and oncotic pressures. The heterogeneous interstitial space between them through which fluid must pass during reabsorption was also lumped into an intervening third compartment. The complex membrane structures of the tubule and capillaries were also lumped together in effort to focus the model on their overall fluid filtration function. In the closed-loop circulatory model, microvascular beds, large vessels, and ventricles were characterized as resistive Beds, compliant chambers, and elastic pumps. Each element is described by a mathematical relationship and arranged with the other elements to provide a minimal, yet sufficient functional representation of the circulatory system.

By characterizing the most salient functional parts, modelers are able to manage system complexity to ensure algebraic methods can be applied. Models that attempt to characterize the behavior of an entire organ or system from every known part will amass a large number of starting equations. Kidney models have been developed for the entire length of the nephron and the effects of millions of nephrons have been added up to predict whole organ function (208). Circulatory

models will also include detailed arrangements of blood storage and resistance to more accurately model behavior (128, 282). Large sets of starting equations, however, often require numerical methods to solve. And though algebraic solutions can sometimes be obtained from a large set of equations, the length and over-complexity of the solutions prevents modelers from being able to understand their meaning. Since the goal of algebraic modeling is to understand how complex systems work, we have striven to craft parsimonious sets of starting equations. Both the renal and circulatory model has five starting equations; and each model has less than twenty parameters. In our laboratory, we have found this to be sufficient level of complexity that enables solving the system algebraically and yields expressions that can be understood by students and researchers.

Constraining the scope of the model by assuming all global and local feedback acts through the physical properties of the system. To ensure model components are necessary and sufficient, the scope of the model must be carefully constrained. Computational modelers often build models that span several levels of function. This often entails concerns about how to model system feedback. Arterial and cardiopulmonary baroreflex as well as renal fluid reabsorption all function to maintain blood volume levels to optimize cardiac filling pressures and output (94). These feedback mechanisms are interdependent and often unbalanced in abnormal physiological states such as heart failure (99). However, with respect to blood volume, the effects of these regulatory mechanisms on equilibrium behaviors can all be evaluated with alterations in the total stressed volume. The same is true for the local and global signaling regulating cortical fluid balance. Control of efferent arteriolar resistance alters capillary hydrostatic and protein osmotic pressures (158). Active solute transport alters tubule hydrostatic and osmotic pressures. The simple idea that regulation acts through physical properties provides justification for constraining what is required for the study of steady-state behaviors.

Because regulation can function to maintain homeostasis, another way to limit the scope of a model is to regard the target parameter as a constant. The best example of this is systemic arterial pressure. Mechanosensors in the carotid and aortic arteries detect pressure changes and provide feedback to systemic arteries, the heart, and the splanchnic vasculature to adjust the physical properties of the cardiovascular system, resistance and blood storage compliance, in a coordinated effort to maintain a steady perfusion pressure to the visceral organs. Numerical models have estimated the sensitivities that physical properties have to controlled systemic arterial pressure changes. Most conventional cardiovascular models regard systemic arterial pressure as a variable to predict while treating systemic resistances as constant parameters (128, 195). However, consider that when blood volume is increased in humans, systemic arterial pressure remains relatively constant whereas total systemic resistance changes by several factors (74). Systemic arterial pressure does change some, as all parameters in the circulatory system do when perturbed. However, it does not change much, especially when compared to total systemic resistance that is being dramatically altered by the baroreflex in order to keep systemic arterial pressure close to constant as possible. In contrast to conventional modeling approaches that treat resistances as constant parameters, the heart failure model assumed resistance is variably controlled by baroreflex mechanisms to maintain perfect arterial pressure homeostasis. That is, systemic arterial pressure was treated as a constant. The model was thus able to constrain its scope to the physical cardiovascular properties without having to incorporate additional equations to characterize how parameters may be more or less sensitive to autonomic control.

Predicting global behaviors algebraically by assuming the relationships that characterize the functional elements of the system are linear. Algebraic models in physiology aim to discover how the global behaviors of a system emerge from the interactions among the parameters of

different functional parts (127, 273). Because the focus is on understanding how the system works, there is less concern for predictive accuracy and greater attention given to being able to identify and understand the most influential interactions. Given this purpose, a good algebraic model may exhibit 30% predictive error and still yield general and valid insights about the mechanics of the system. In the renal fluid balance model, the explicit algebraic solutions reveal how reabsorption across the tubule membrane depends on an overall effective filtration coefficient comprised of both tubule and capillary filtration coefficients. In the heart failure model, the explicit algebraic solutions reveal how the effective circulatory volume, which is commonly assumed to be the total stressed volume, is actually the total venous stressed volume augmented by the pumping actions of the left and right ventricle. In both cases, algebraic methods produced explicit expressions for global behaviors that revealed the most important interactions of the system that were not apparent when examining the numerical output of equivalent, more accurate numerical models.

To obtain general algebraic solutions, the starting equations of the model must be a set of linear relationships. Physiological relationships, however, are rarely linear. Many of the pressure-flow and volume-pressure relationships between physical variables, however, are close to being linear under specified conditions (250, 258, 287). For the high flow conditions across the tubule and capillary barriers of the renal cortex, the flow of fluid may be assumed to be linear with compartmental pressures (76, 136, 292). For the volume-pressure relationships of compliant blood-storage chambers of the cardiovascular system, a constant compliance may be assumed as blood volume changes over a normal physiological range of pressures (258, 287). In contrast, the end-diastolic pressure-volume relationship (EDPVR) of the left and right ventricle is highly nonlinear with a slope that steepens as ventricular filling pressures increase (47). Considered to have the most impact on the behavior of the cardiovascular system, many heart failure models

retain this nonlinearity and solve the model numerically (275). To obtain algebraic solutions, others have assumed EDPVR of each ventricle to be linear (127). Following this approach, the heart failure model used the linear EDPVR relationship for the right and left ventricles. This approximation proved to be suitable for modest perturbations in parameter values. In the present work, an important facet of algebraic modeling involves testing the conditions or cases in which linear assumptions remain valid.

Conceptualizing system equilibrium as a balance point. Though numerical modeling dominates in the field of physiology today, the algebraic and graphical methods that Guyton developed over a half-century ago still provide a powerful means for conceptualizing and predicting how equilibrium behaviors emerge from the interactions within a complex system (23, 181). Under conditions of mass conservation, Guyton showed how equilibrium cardiac output and filling pressure could be predicted as a balance point that emerges from the pressure-flow relationships of the cardiopulmonary and systemic parts of a closed-loop system (120, 122). An algebraic expression for the blood returned by the systemic vasculature was derived. Specifically, the slope depended on interactions between resistances and compliances, while the intercept was shown to be a circulatory filling pressure (Figure 1.1A). The derivation of algebraic slopes and resistances provided researchers and students an intuitive method for manipulating parameter values and predicting changes in the balance point based on those parameter changes affected the slopes and intercepts of the two intersecting blood flow relationships. While graphical analysis was hailed as a ‘monumental’ methodological achievement by Guyton’s contemporaries and the venous return model is still depicted in physiological textbooks as a way of conceptualizing the regulation of cardiac output (129, 181), critics have identified several difficulties with Guyton’s applications.

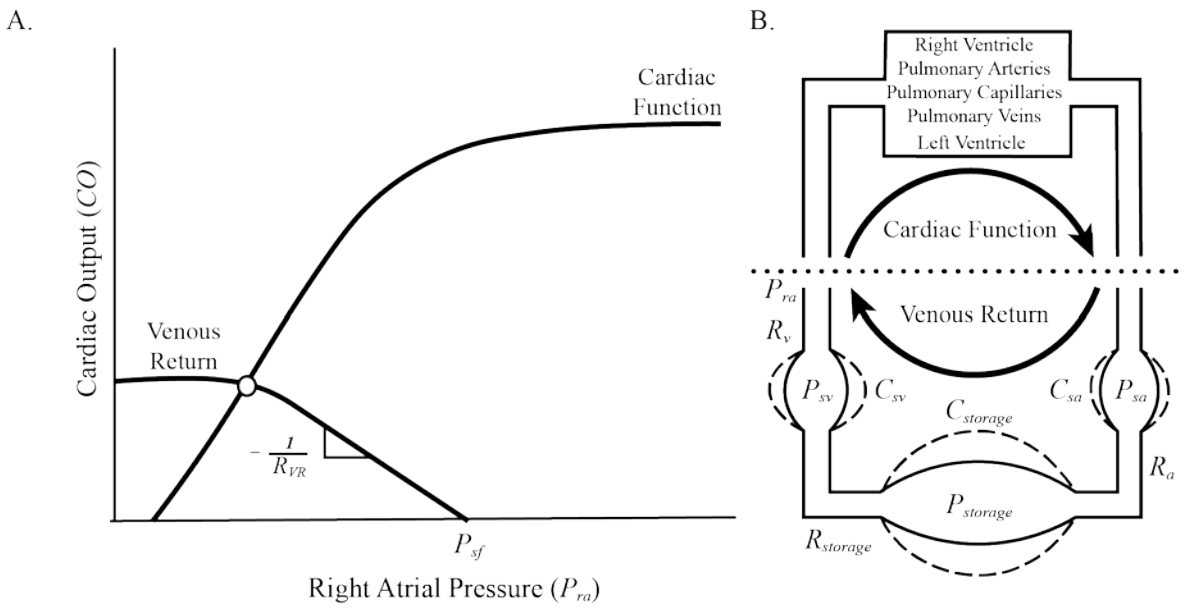

Figure 1.1 Guyton's experimental, closed-loop venous return model. A: Graphical representation of system equilibrium. B: How Guyton experimentally partitioned the cardiovascular system and parameterized the functional elements of the systemic vasculature.

One issue complicating Guyton's model was shifting blood volume between the chosen compartments. Guyton partitioned his model of the cardiovascular system based on the experimental apparatus he set up to measure the flow of blood from the systemic vasculature and the pressure within the right atrium of the heart (Figure 1.1B). In his 1973 book *Cardiac Output and Its Regulation, 2nd*, Guyton labored over how to deal with the shifting blood volume in an intact circulatory system (279). Guyton of course appreciated the value of characterizing the slopes and intercepts algebraically. However, to get the model to predict observed values of pressure and flow, Guyton resorted to an iterative numerical method. The problem Guyton faced highlights a principle of graphical analysis, which is that a complex system must be partitioned in a way to establish independent, yet interactive processes. Each process should be conceptualized as a subset of elements functioning together to affect equilibrium behavior. In the heart failure model, the

stressed volumes of the four chamber are partitioned into an independent compartment. Arterial and cardiopulmonary baroreflex therefore act on the stressed volumes contained within a single compartment. From the mathematical relationships characterizing this compartment a flow equation for cardiovascular return was derived. Likewise, a flow equation was developed for left ventricular function. Plotting these two flows together revealed how system equilibrium emerged from the interaction of cardiovascular return and left ventricular function.

Graphical analysis is a way of conceptualizing how equilibrium emerges from interacting processes. Each process is characterized by an algebraic relationship, e.g., fluid or blood flow, which can be plotted together. Slopes and intercepts for each relationship can be derived for each of these linear relationships. Altering a parameter value will shift an intercept or change a slope of one of the relationships; and this in turn will alter where the linear relationships intersect. This intersection is the point at which all variables exist in steady-state and is called the balance point. If the full set of equations are solved for system variables, the solutions for these variables can be rather complex and will often lack physiological meaning. Using simple algebraic rearrangements or substitutions, we can begin to organize terms in a way that can be interpreted. In graphical analysis, the slopes and intercepts are smaller expressions characterizing more complex processes and their groupings are often straight forward. These grouping often have physiological meaning, and can be used to organize the more complex full equilibrium solutions. In both the renal fluid balance model and the heart failure model, this technique was instrumental in understanding the interactions determining equilibrium flows and pressures. Not just a means to visually predict equilibrium changes, graphical analysis is a tool for organizing the parameters of a complex solutions into formulas with physiologically meaningful terms.

CHAPTER II

HEART FAILURE MODEL

Management of acute decompensation heart failure (ADHF) has focused extensively on understanding how patients tolerate high filling pressures or low cardiac output. Forrester et al. (100, 101) identified these variables as key dimensions for classifying pump performance as well as the particular disorders underlying symptoms requiring hospitalization. Critically elevated filling pressure causes volume overload of the left ventricle and has been associated with pulmonary edema (84, 263). Critically diminished cardiac output results in peripheral hypoperfusion. Clinical profiles based on these variables have been used to predict outcomes for heart failure patients (216). The post-discharge outcomes of patients at-risk for subsequent decompensation are assumed to depend on individuals' capacity to tolerate subsequent hemodynamic perturbations (283). Studies have revealed that discharged patients having heart failure with reduced ejection fraction (HFrEF) contend with various levels of hypervolemia and elevated filling pressures (8, 204). However, the majority of patients who develop critical symptoms do not experience increases in total blood volume prior to hospitalization (58). This has raised questions about how heart failure patients tolerate changes in the stressed portion of blood volume (87, 94). Yet, despite consensus on the importance of monitoring volume status (308), little is known about the stressed volume interacts with physical properties to determine the range of asymptomatic filling pressure and cardiac output that heart failure patients can tolerate.

Although his classic venous return model has limitations, Guyton's algebraic methods still provide a powerful means for predicting how equilibrium behaviors emerge from blood volume interactions with vascular and ventricular properties. Guyton showed how equilibrium cardiac

output and filling pressure could be predicted as a balance point that emerges from the pressure-flow relationships of the cardiopulmonary and systemic parts of a closed-loop system (98). An algebraic expression for the blood returned by the systemic vasculature was derived (122). Specifically, the slope depended on interactions between resistances and compliances, while the intercept was a circulatory filling pressure determined by the system's stressed blood volume and total vascular compliance (120). While this provided researchers and students an intuitive method for predicting changes in equilibrium behavior when blood volume is altered (181), limitations arise from the way Guyton's model partitioned the cardiovascular system to suit experimental conditions. On the cardiopulmonary side, Guyton relied on data to plot a pressure-flow curve and thus never defined cardiac performance in terms of ventricular mechanical properties (252). The empirical cardiac performance curve, moreover, depended on the function of both ventricles and was therefore not useful for predicting the effects of isolated ventricular dysfunction on equilibrium behaviors. On the systemic side, resistance to blood flow was implicitly assumed to be constant rather than variably controlled by the baroreflex response to maintain systemic arterial pressure homeostasis (23, 193). Another difficulty, especially for in vivo applications, was the confounding effect of shifting blood volume between the two partitions (279). Finally, Guyton's model partitioned the cardiovascular system to predict cardiac output and right ventricular filling pressure. To understand how cardiovascular properties determine equilibrium cardiac output and left ventricular filling pressure, researchers have sought to overcome these limitations through mathematical modeling (279).

Unlike Guyton's empirical cardiac output and venous return model, more recent minimal closed-loop models have been used to predict hemodynamic variables by lumping cardiovascular structures into phenomenologically distinct functional elements. Ventricles, large vessels, and

microvascular beds, for instance, have been mathematically characterized as elastic pumps, compliant chambers, and resistive Beds (69, 223, 275). Other complexities, e.g., baroreflex regulation of systemic pressures, are sometimes included to investigate multi-level processes (236, 282). Nonlinear behaviors, e.g., ventricular end-diastolic pressure-volume relationships, also increase model complexity to the extent that numerical methods become necessary to solve model equations (218). Insights about interactions among properties are typically limited to univariate sensitivity analysis and graphing the effects of one or perhaps two parameters (48, 128, 195). How equilibrium emerges from different combinations of parameter interactions is therefore difficult to explain (232, 238). In a closed-loop model of left ventricular dysfunction, Magder, et al. (195) further demonstrated how inferences drawn from numerical solutions are contingent upon the specific parameter values assumed. While accurate if parameter values are well known, numerical methods are limited for purposes of gaining generalized insights about complex parameter interactions in closed-loop models.

Where numerical methods have fallen short, algebraic methods have provided generalized insights that have been useful in the clinical study of left ventricular heart failure. Extending algebraic methods to a minimal closed-loop model, Sunagawa et al. (265) obtained algebraic formulas for cardiac output and arterial pressures by linearizing the end-diastolic pressure-volume relationship of both ventricles. The resulting formulas were expressed in terms of heart rate, ventricular elastances, vascular resistances and compliances, and total blood volume. While this addressed the issue of shifting blood volume between compartments, systemic arterial pressure was regarded as a variable. However, to identify the ventricular-cardiovascular interactions that determine acute decompensation, i.e., critically low cardiac output or critically high ventricular filling pressure, an algebraic model must assume an intact baroreflex response

that variably controls vascular resistance to maintain a constant systemic arterial pressure. Therefore, the purpose of the present work is to derive general algebraic formulas for equilibrium cardiac output and ventricular filling pressure for a minimal closed loop model with arterial pressure regulation.

METHODS

Three model elements. To construct a minimal closed-loop model, microvascular beds, large vessels, and ventricles were characterized as resistive Beds, compliant chambers, and elastic pumps (Fig. 2.1). These mathematical characterizations followed a standard modeling approach used for reducing the anatomical complexity of the cardiovascular system to its most salient functional elements (72). Firstly, the small vessels of a microvascular network through which blood flows between large arterial and venous vessels were lumped into an overall pathway called a resistive Bed. Assuming inertial effects on blood flow to be negligible, the cardiac output (CO) of a Bed was assumed to be a linear function of the arterial-venous pressure difference ($P_a - P_v$) and dependent on a total vascular resistance (R). Secondly, large vessels were assumed to have negligible resistance to blood flow and were instead characterized by their blood storage capacity. Networks of large vessels were thus lumped into singular compliant chambers whose blood volume changed linearly with pressure (251). The blood volume within each chamber (V) was therefore assumed to be a function of transmural pressure (P) and dependent on the vascular compliance (C) and the unstressed volume (V_o), the chamber volume at zero pressure. Finally, each ventricle was characterized as an elastic pump whose cardiac output depends upon the heart rate (HR) and the stroke volume. The stroke volume is the difference between the end-systolic and end-diastolic volumes ($V_{es} - V_{ed}$) and is governed by two

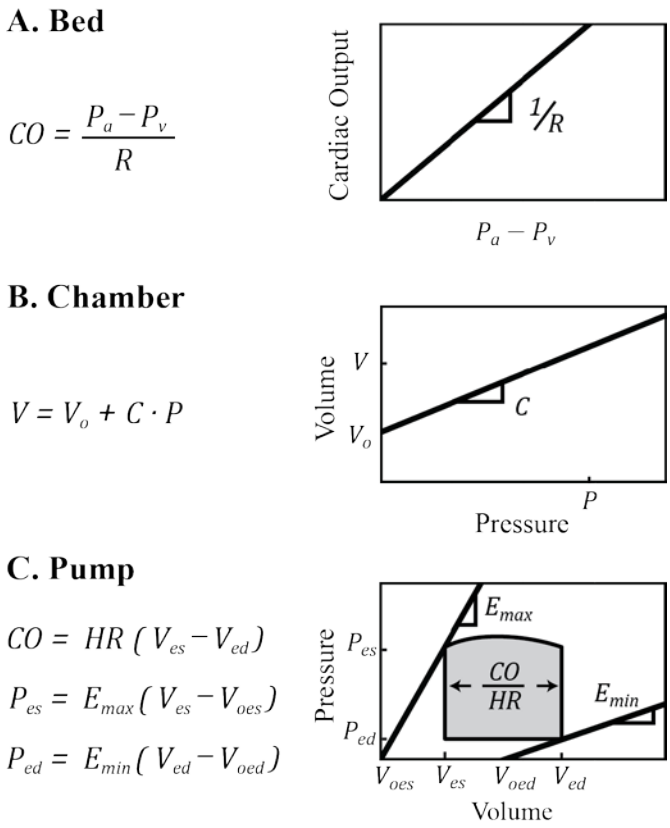

Figure 2.1 Functional elements of the minimal closed-loop model represented mathematically and graphically. A: Resistive conduits represent cardiac output (*CO*) from microvascular beds in terms of arterial-venous pressure difference ($P_a - P_v$) and vascular resistance (*R*). B: Compliant chambers represent the blood storage of large vessels in terms of pressure (*P*), vascular compliance (*C*) and unstressed blood volume (V_o). C: Elastic pumps represent cardiac output (*CO*) in terms of heart rate (*HR*) and stroke volume ($V_{es} - V_{ed}$). End-systolic pressure (P_{es}) is expressed in terms of end-systolic volume (V_{es}), maximum elastance (E_{max}) and end-systolic unstressed volume (V_{oes}). End-diastolic pressure (P_{ed}) is expressed in terms of end-diastolic volume (V_{ed}), minimal elastance (E_{min}) and end-diastolic unstressed volume (V_{oed}).

pressure-volume relationships. The end-systolic pressure-volume relationship (ESPVR) is linear over an extended range of end-systolic pressures (11, 46, 249). End-systolic pressure (P_{es}) was therefore assumed to be a function of end-systolic volume (V_{es}) and dependent on the maximum elastance (E_{max}) and end-systolic unstressed volume (V_{oes}). In contrast, the end-diastolic pressure-volume relationship (EDPVR) is nonlinear over the physiological range end-diastolic pressures. The EDPVR, however, is commonly approximated by linearizing the pressure-volume relationship over a range of end-diastolic pressures. With this consideration, the end-diastolic pressure (P_{ed}) was assumed to be a linear function of end-diastolic volume (V_{ed}) and dependent on the minimal elastance (E_{min}) and end-diastolic unstressed volume (V_{oed}).

Arrangement of functional elements within the minimal closed-loop model. Standard minimum closed-loop models use the three functional elements previously described to characterize blood flow through the cardiovascular system (48, 139, 260). An arrangement of these functional elements is illustrated in Figure 2.2. Generally, there are two resistive Beds that characterize the function of microvascular beds. There are four compliant chambers that characterize the function of large vessel networks, and there are two elastic pumps that characterize the right and left ventricles of the heart. Including an equation representing conservation of mass, there are thirteen fundamental equations and thirty-seven parameters needed to construct a minimal model. Equations for each particular element are listed below with combinations of subscripts to denote the location of their properties in either the pulmonary or systemic circulation (*p* or *s*), a venous or arterial chamber (*v* or *a*), or the right or left ventricle (*rv* or *lv*).

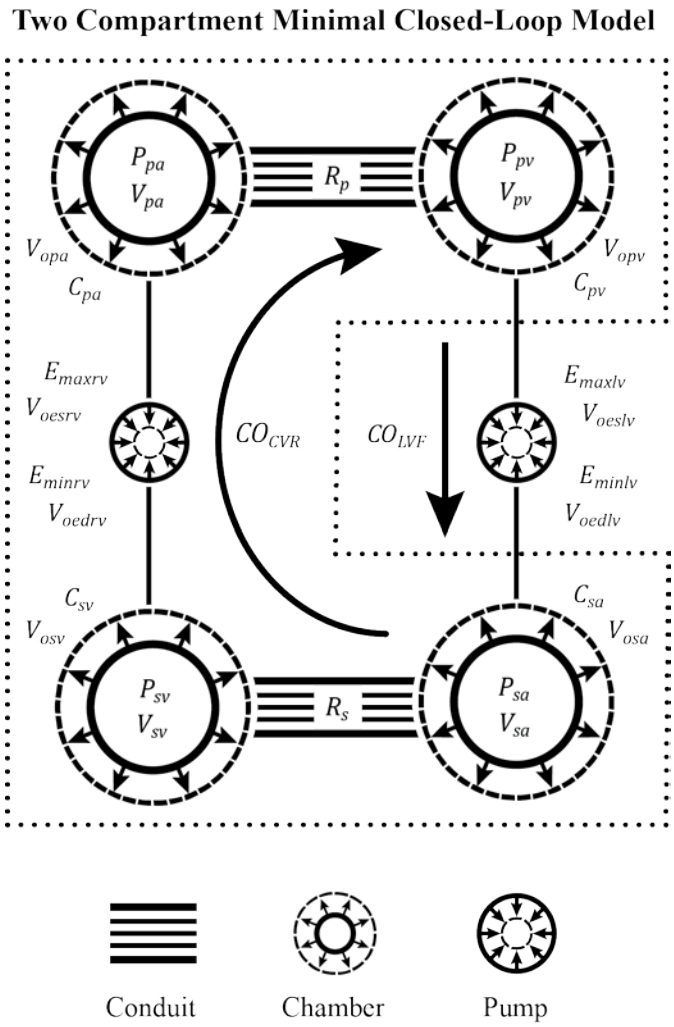

$$CO = (P_{sa} - P_{sv})/R_s \quad (A1)$$

$$CO = (P_{pa} - P_{pv})/R_p \quad (A2)$$

$$P_{eslv} = E_{maxlv}\,(V_{eslv} - V_{oeslv}) \quad (A3)$$

$$P_{edlv} = E_{minlv}\,(V_{edlv} - V_{oedlv}) \quad (A4)$$

$$CO = HR\,(V_{eslv} - V_{edlv}) \quad (A5)$$

$$P_{esrv} = E_{maxrv}(V_{oesrv} - V_{oesrv}) \quad (A6)$$

$$P_{edrv} = E_{minrv}(V_{edrv} - V_{oedrv}) \quad (A7)$$

$$CO = HR\,(V_{esrv} - V_{edrv}) \quad (A8)$$

$$V_{sa} = V_{osa} + C_{sa}P_{sa} \quad (A9)$$

$$V_{pa} = V_{opa} + C_{pa}P_{pa} \quad (A10)$$

$$V_{sv} = V_{osv} + C_{sv}P_{sv} \quad (A11)$$

$$V_{pv} = V_{opv} + C_{pv}P_{pv} \quad (A12)$$

$$V_b = V_{sa} + V_{pa} + V_{sv} + V_{pv} \quad (A13)$$

$$V_{otot} = V_{osa} + V_{opa} + V_{osv} + V_{opv} \quad (A14)$$

Figure 2.2 The arrangement of three functional elements in a two-compartment minimal closed-loop model. Conduits, chambers, and pump are each characterized by mathematical equations (Fig. 2.1). Subscripts denote the location in either the pulmonary or systemic circulation (*p* or *s*), venous or arterial chambers (*v* or *a*), or right or left ventricle (*rv* or *lv*). The dotted line indicates how system was partitioned into two compartments. Large arrows indicate cardiac output owed to left ventricular function (LVF) and cardiovascular return (CVR). *Eqs. A1-14* characterize the relationships between properties.

Parsimonious set of model equations. A parsimonious set of equations characterizing the entire system (*Eqs. 1-5)* was derived from *Eqs. A1-A14* and additional simplifying assumptions. Cardiac output (*CO*) through pulmonary and systemic microvasculature beds are governed by,

$$CO = \frac{P_{sa} - P_{sv}}{R_s}, \quad (1)$$

$$CO = \frac{P_{pa} - P_{pv}}{R_p}, \quad (2)$$

where P_{sa} is the systemic arterial pressure, P_{sv} is the systemic venous pressure, P_{pa} is the pulmonary arterial pressure, P_{pv} is the pulmonary venous pressure, R_s is total systemic resistance, and R_p is total pulmonary resistance. Blood storage of entire system was reduced to a single equation for stressed volume (V_s) by combining *Eqs. A9 –A12.* Given ventricular volumes are relatively small, the sums of the four chamber volumes and unstressed volumes were redefined as the total blood volume (V_b, *Eq. A13*) and total unstressed volume (V_{otot}, *Eq. A14*), respectively. Total stressed volume (V_s), the difference between total blood volume and the total unstressed volume ($V_b - V_{otot}$), was expressed as for the parsimonious set as,

$$V_s = V_B - V_{otot} = C_{sa}\, P_{sa} + C_{sv}\, P_{sv} + C_{pa}\, P_{pa} + C_{pv}\, P_{pv}, \quad (3)$$

where C_{sa}, C_{sv}, C_{pa}, and C_{pv} are compliances of the system arterial, systemic venous, pulmonary arterial, and pulmonary venous chambers, respectively. Ventricular function of the system was reduced to two equations. The ESPVR, EDPVR, and *CO* relations for the right ventricle (*Eqs. A3-A5*) and the left ventricle (*Eqs. A6-A8*) were each solved for *CO*. Following Sunagawa et al. (266), ventricular end-systolic pressures were then approximated as arterial chamber pressures ($P_{eslv} \approx P_{sa}$; $P_{esrv} \approx P_{pa}$), and ventricular end-diastolic pressures were approximated as venous chamber

pressures ($P_{edlv} \approx P_{sv}$; $P_{edrv} \approx P_{pv}$). The differences between V_{oed} and V_{oes} in each ventricle were redefined as the theoretical unstressed stroke volumes ΔV_{orv} and ΔV_{olv}. Equations for the cardiac output (*CO*) from the right and left ventricles were then rewritten for the parsimonious set as,

$$CO = \left(\frac{P_{sv}}{E_{minrv}} - \frac{P_{pa}}{E_{maxrv}} + \Delta V_{orv}\right) HR, \tag{4}$$

$$CO = \left(\frac{P_{pv}}{E_{minlv}} - \frac{P_{sa}}{E_{maxlv}} + \Delta V_{olv}\right) HR, \tag{5}$$

where *HR* is heart rate, E_{maxrv} and E_{maxlv} are the maximum elastances of the right and left ventricles, and E_{minrv} and E_{minlv} are the minimum elastances of the right and left ventricles. The simplifying assumptions specified above allowed the model to be reduced to a parsimonious set of five equations with a total of nineteen properties. From the parsimonious set, analytical solutions for system equilibrium were derived.

Algebraic and graphical analysis of system equilibrium. To characterize steady-state behaviors for a minimal closed-loop model with intact systemic arterial pressure regulation, graphical and algebraic analysis was performed by partitioning the functional elements of the system into left ventricular function (LVF) and cardiovascular return (CVR) compartments (Fig. 2.2). Equations for blood flow were then derived for each of the compartments. Blood flow resulting from isolated left ventricular function (CO_{LVF}) is characterized by mechanical properties of the left ventricle. CO_{LVF} therefore corresponds to the cardiac output derived previously as *Eq. 5*. Using *Eq. 5*, CO_{LVF} was plotted as a function of P_{pv}. The P_{pv} intercept at zero flow and the instantaneous slope of *CO* with respect to P_{pv} were also derived from *Eq. 5*. An equation for the blood flow resulting from the functions of two resistive Beds, the four compliant chambers, and the right ventricular pump (CO_{CVR}) was obtained by simultaneously solving *Eqs. 1-4* for the

variables CO, P_{sv}, R_s, and R_p. This solution assumes systemic resistance (R_s) is a controlled variable that regulates systemic arterial pressure (P_{sa}) and pulmonary resistance (R_p) is a controlled variable that regulates pulmonary arterial pressure (P_{pa}). CO_{CVR} was then plotted as a function of P_{pv}. The P_{pv} intercept at zero flow and the instantaneous slope of CO with respect to P_{pv} were also derived from the resulting CO_{CVR} solution. To depict how slopes and intercepts interact to determine the point at which the system is at equilibrium, the two linear flow equations (CO_{LVF} and CO_{CVR}) were plotted simultaneously as a function of P_{pv}. General equilibrium solutions (denoted by asterisks) were derived by simultaneously solving *Eqs. 1-5.* for CO^*, $P_{pv}{}^*$, $P_{sv}{}^*$, $R_p{}^*$, and $R_s{}^*$.

Graphical representation of system equlibrium with changes in left ventricular function. To illustrate how equilibrium shifts with changes to left ventricular function, the pressure-volume loop and balance point graphs were plotted with decreased E_{maxlv}, decreased E_{minlv} and decreased ΔV_{olv}. Alterations in pressure-volume loop properties as well as changes in the equilibrium cardiac output (CO^*) and equilibrium pulmonary venous pressure ($P_{pv}{}^*$) were graphically indicated.

Sensitivities of equilibrium cardiac output and pulmonary venous pressure to changes in stressed volume. Using general algebraic solution, the sensitivity of cardiac output to stressed volume (α) was derived as the derivative of CO^* with respect to V_s. The sensitivity of equilibrium pulmonary venous pressure to stressed volume (β) was derived as the derivative of $P_{pv}{}^*$ with respect to V_s. General algebraic solutions for CO^* and $P_{pv}{}^*$ were then respectively rewritten in terms of α and β. The solutions for CO^* and $P_{pv}{}^*$ were each plotted as a function of V_s with sensitivities α and β indicated.

Errors of linear approximation quantified by comparing results of algebraic solutions to results of a more complex numerical model. The algebraic formulas derived from *Eqs. 1-5* should be interpreted as approximations that assume the end-diastolic pressure of each ventricle is linear

with respect to end-diastolic volume. In contrast, the more complex numerical model incorporated an exponential end-diastolic pressure-volume relationship for each ventricle for each ventricle. The difference between the predictions of the algebraic formulas and the numerical model is the error of approximation. Using the normal parameter values, absolute errors were calculated and plotted for a wide range of stressed volume values.

Model sensitivity analysis. To evaluate the sensitivity of equilibrium cardiac output and pulmonary venous pressure of the algebraic formulas to changes in normal baseline parameters (Table 2.1), a non-dimensional sensitivity index (*SI*) for was calculated for each parameter,

$$SI = \frac{\Delta Var}{Var_0} \Big/ \frac{\Delta Par}{Par_0}, \tag{6}$$

where *SI* represents the change in the variable (ΔVar) normalized by its baseline value (Var_0) for a given change in the parameter (ΔPar) normalized by its baseline value (Par_0). Values of *SI* were estimated by changing the value of each parameter by 10%. Normal *SI* values were compared to *SI* values estimated from a heart failure parameter set (Table 2.1) as well as from a numerical model incorporating nonlinear a EDPVR for each ventricle.

Homeostatic range of stressed volume. To characterize the homeostatic range of stressed volume, two points were defined for the critical symptoms that result from acute decompensated heart failure. Using *Eq. 13*, CO^* was redefined as CO_{cold} to characterize the point at which cardiac output becomes so low that peripheral hypoperfusion develops. The equation was then rearranged to express the stressed volume at which hypoperfusion occurs ($V_{s\ cold}$) as a function of CO_{cold}. Using *Eq. 14*, P_{pv}^* was redefined as $P_{pv\ wet}$ to characterize the point at which pulmonary venous pressure becomes so high that pulmonary edema develops. The equation was then rearranged to express the stressed volume at which pulmonary edema occurs ($V_{s\ we}$) as a function of $P_{pv\ wet}$. The

difference between $V_{s\ wet}$ and $V_{s\ cold}$ was then calculated. The resulting algebraic expression identifies the interactions determining the range of asymptomatic V_s fluctuation (ΔV_s).

Predicting the homeostatic range of stressed volume for normal patients and patients having heart failure with reduced ejection fraction (HFrEF). To evaluate its robustness, the algebraic solution for the homeostatic range of stressed volume (ΔV_s) was evaluated using the measured parameter values from clinical studies of normal and HFrEF patients (Table 2.1). The error of approximation was calculated as the difference between the predicted results of the algebraic formulas and the more complete numerical model incorporating nonlinear end-diastolic pressure-volume relationships for the left and right ventricles. Equilibrium cardiac output, pulmonary venous pressure, systemic venous pressure, total pulmonary resistance, and total systemic resistance were also predicted using previously derived algebraic solutions and the parameters values for the normal and HFrEF cases. To further ensure model validity, the results were compared to reported clinical values.

Numerical minimal closed-loop model. For comparison purposes, a numerical minimal closed-loop model was constructed to simulate the effects of the highly nonlinear end-diastolic pressure volume relationship (EDPVR) of the left and right ventricles. Equation *B1* is the standard exponential relationship characterized the EDPVR of an elastic pump (48, 195),

$$P_{ed} = A\ (exp^{\,B\,V_{ed}} - 1)\ , \tag{B1}$$

where end-diastolic pressure (P_{ed}) is expressed terms of a scaling coefficient (A), chamber stiffness (B), and end-diastolic volume (V_{ed}). Assuming $P_{edlv} \cong P_{pv}$ and $P_{edrv} \cong P_{sv}$ (265), the nonlinear EDPVR relationships of the left and right ventricle were rewritten as,

$$P_{pv} = A_{lv}\ (exp^{\,B_{lv}\ V_{edlv}} - 1)\ , \tag{B2}$$

$$P_{sa} = A_{rv}\ (exp^{\,B_{rv}\ V_{edrv}} - 1)\ . \tag{B3}$$

The numerical model was constructed from *Eqs. A1-14* with *Eqs. B2* and *B2* replacing *Eqs. A4* and *A7* respectively. This equation set was solved numerically for the variables CO, P_{pv}, P_{sv}, R_p, R_s, V_{edlv}, V_{edrv}, V_{eslv}, and V_{esrv} using Newton's method and the parameters specified in Table 2.1.

Baseline Parameter Values. Table 2.1 summarizes the parameter values assumed from clinical studies of normal patients (128, 160, 255, 309) and those having heart failure with reduced ejection fraction (91, 182, 309). Stressed volume (V_s) was estimated as the product of the circulatory filling pressure and the sum total of all chamber compliances ($V_s = P_{cf} \cdot C_{tot}$). P_{cf} was assumed to be 7.0 mmHg for the normal case (244). For the case of heart failure with reduced ejection fraction (EF < 40%), stressed volume was assumed to be 50% higher than normal to reflect an increase in effective circulatory volume present in advanced heart failure. This elevated stressed volume may be due to increased total blood volume and/or decreased total unstressed volume. Minimal elastance values for the left and right ventricles (E_{minlv} and E_{minrv}) were each calculated as the derivative of the exponential EDPVR used in the numerical model (*Eqs. B2* and *B3*). Scaling factors and exponents of the nonlinear EDPVR are not well-known and are often estimated numerically to fit other chosen parameter values (195). Using parameters in Table 2.1 and the numerical model, left and right ventricle scaling factors (A_{lv} and A_{rv}) were estimated to be 0.35 and 4.4 mmHg respectively. Left and right ventricle exponents (B_{lv} and B_{rv}) were estimated to be 0.027 and 0.009 ml^{-1} respectively. Baseline end-diastolic pressures and volumes were obtained from numerical model. At normal baseline, P_{pv} and P_{sv} values were estimated to be 5.6 and 4.2 mmHg respectively; and V_{edlv} and V_{edrv} values were estimated to be 99 and 91 ml respectively. E_{minlv} and E_{minrv} were estimated to be 0.14 and 0.09 $mmHg \cdot ml^{-1}$ at normal baseline, which is consistent with previous studies (35, 128). The theoretical unstressed stroke volumes of the heart (ΔV_{olv} and ΔV_{orv}) were calculated as the difference between end-systolic and end-diastolic

Table 2.1 Baseline parameter value sets for heart failure model.

Parameter	Normal	HFrEF
Stressed Volume		
V_s, ml	800†	1200†
Compliances		
C_{sa}, ml·mmHg^{-1}	1.6 (128)	1.6 (128)
C_{sv}, ml·mmHg^{-1}	100 (128)	100 (128)
C_{pa}, ml·mmHg^{-1}	4.3 (128)	4.3 (128)
C_{pv}, ml·mmHg^{-1}	8.4 (128)	8.4 (128)
Pressures		
P_{sa}, mmHg	88	92 (309)
P_{pa}, mmHg	14 (160)	28 (182)
Heart Rate		
HR, beats·min^{-1}	70 (255)	80 (91)
Maximal Elastances		
E_{maxlv}, mmHg·ml^{-1}	3.7 (309)	1.3 (309)
E_{maxrv}, mmHg·ml^{-1}	0.84 (128)	0.84 (128)
Minimal Elastances†		
E_{minlv}, mmHg·ml^{-1}	0.14†	0.77†
E_{minrv}, mmHg·ml^{-1}	0.09†	0.13†
Unstressed Volumes†		
ΔV_{olv}, ml	64†	97†
ΔV_{orv}, ml	29†	33†

p or *s*, pulmonary or systemic circulation; *v* or *a*, venous or arterial chambers; *rv* or *lv*, right or left ventricle. Sources are in parenthesis. †Calculated values are detailed in Methods.

unstressed volumes. End-systolic unstressed volumes (V_{oeslv} and V_{oesrv}) for each ventricle were assumed to be zero. End-diastolic unstressed volumes (V_{oedlv} and V_{oedrv}) were calculated using *Eqs*. *A4* and *A7*. Following Burkhoff and Tyberg (48), left and right ventricle EDPVR exponents (B_{lv} and B_{rv}) were respectively increased to 0.033 and 0.11 ml^{-1} to reflect ventricular stiffening for the case of HFrEF. Minimal elastances and unstressed volumes for that case were then calculated as previously described.

RESULTS

Algebraic and graphical analysis of system equilibrium. In a two-compartment minimal closed-loop model that assumes systemic resistance (R_s) is variably controlled to regulate systemic arterial pressure (P_{sa}), the cardiac output resulting from left ventricular function (CO_{LVF}) or cardiovascular return (CO_{CVR}) is a function of pulmonary venous pressure (P_{pv}). As illustrated in Figure 2.3A, CO_{LVF} increases linearly with increasing P_{pv}. In *Eq. 7*, the slope of the left ventricular function relationship is shown to be the ratio of heart rate (*HR*) to minimal elastance of the left ventricle (E_{minlv}),

$$slope_{LVF} = \frac{HR}{E_{minlv}}. \tag{7}$$

In *Eq. 8*, the intercept is expressed in terms of systemic arterial pressure (P_{sa}) and mechanical properties of the left ventricle (unstressed stroke volume, ΔV_{olv}; maximum elastance, E_{maxlv}; minimum elastance, E_{minlv}),

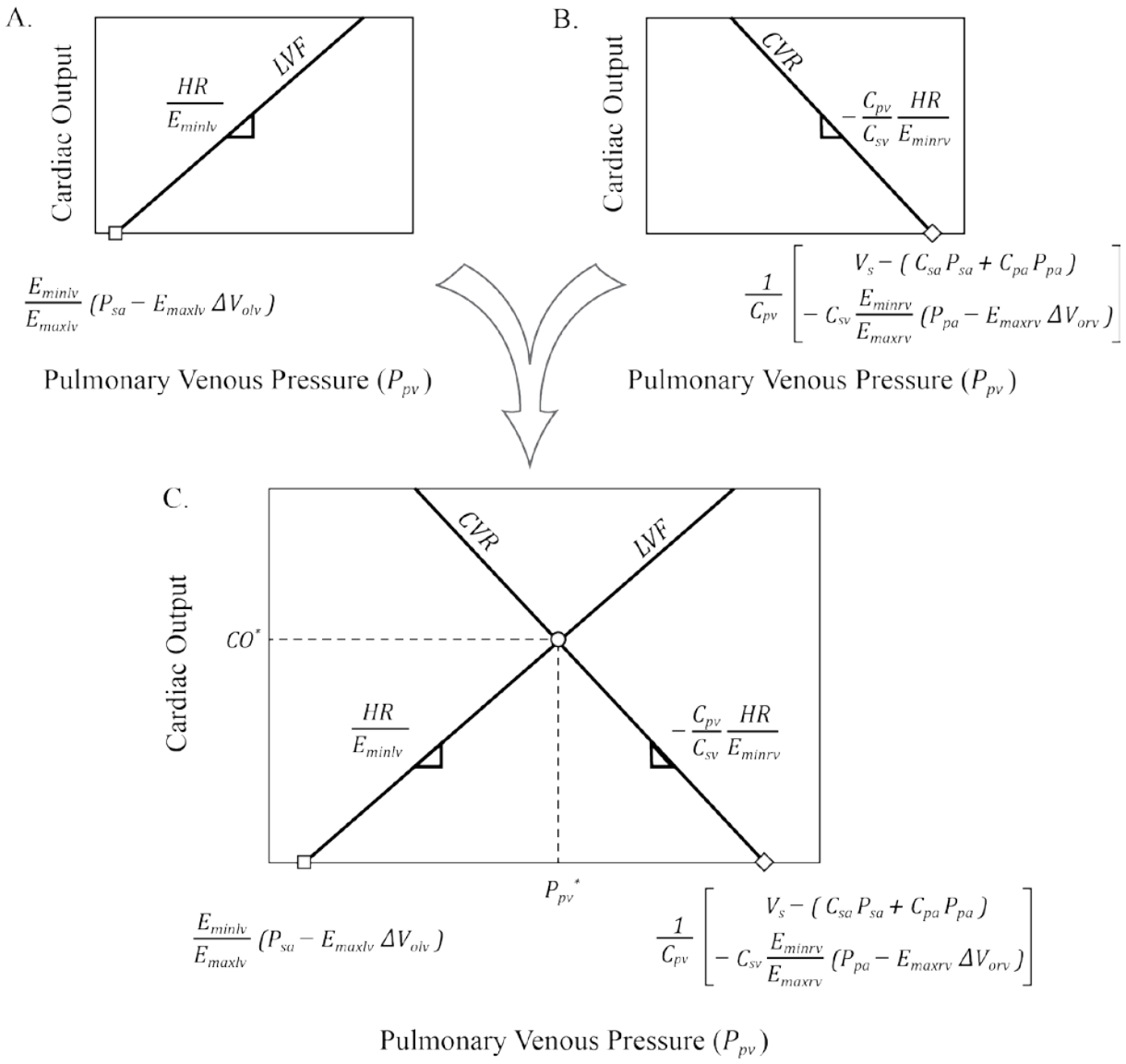

Figure 2.3 Graphical representation of the interaction of left ventricular function (LVF) and cardiovascular return (CVR). A: According to *Eq. 5*, as pulmonary venous pressure (P_{pv}) increases, the cardiac output (CO) resulting from LVF increases linearly. The slope is determined by heart rate (HR) and left ventricle minimal elastance. The intercept (open square) is determined by systemic arterial pressure (P_{sa}) and left ventricle properties (unstressed stroke volume, ΔV_{olv}; maximum elastance, E_{maxlv}; minimum elastance, E_{minlv}). B: According to *Eqs. 1-4*, as P_{pv} increases, the CO resulting from CVR decreases linearly. The slope is determined by heart rate, RV minimal elastance (E_{minrv}), and venous compliances (C_{sv} and C_{pv}). The intercept (open diamond) is determined by total stressed volume (V_s), compliances, arterial pressures, and right ventricle properties (unstressed stroke volume, ΔV_{orv}; maximum elastance, E_{maxrv}; minimum elastance, E_{minrv}). C: The left ventricle function and cardiovascular return relationships (solid lines) intersect at the balance point (open circle) where $CO_{LVF} = CO_{CVR}$. The resulting equilibrium cardiac output (CO^*) and pulmonary venous pressure (P_{pv}^*) are characterized by *Eqs. 13* and *14*.

$$intercept_{LVF} = \frac{E_{minlv}}{E_{maxlv}} \left(P_{sa} - E_{maxlv}\, \Delta V_{olv}\right). \quad (8)$$

As illustrated in Figure 2.3B, CO_{CVR} decreases linearly with increasing P_{pv}. The for the slope and intercept expressions of this relationship assume P_{pa} is relatively constant with respect to a changing total pulmonary resistance (R_p). In *Eq. 9*, the slope of the cardiovascular return relationship is shown to depend on heart rate (*HR*), minimal elastance of the right ventricle (E_{minrv}), and venous compliances (C_{sv} and C_{pv}).

$$slope_{CVR} = -\frac{HR}{E_{minrv}} \frac{C_{pv}}{C_{sv}}. \quad (9)$$

The slope of cardiovascular return is affected by properties of the systemic and pulmonary vasculature as well as the right ventricle. In *Eq. 10*, the intercept is expressed in terms of the sum of the total stressed volume (V_s), arterial stressed volumes ($C_{sa}\, P_{sa}$ and $C_{pa}\, P_{pa}$), and interactions of right ventricle properties (E_{maxrv}, E_{minrv}, ΔV_{orv}) with proximal vascular properties (C_{sv} and P_{pa}),

$$intercept_{CVR} = \frac{1}{C_{pv}} \left[\begin{array}{c} V_s - (C_{sa} P_{sa} + C_{pa}\, P_{pa}) \\ - C_{sv} \frac{E_{minrv}}{E_{maxrv}} (P_{pa} - E_{maxrv}\, \Delta V_{orv}) \end{array} \right]. \quad (10)$$

As indicated, the effects of V_s and other volume terms are modulated by pulmonary venous compliance (C_{pv}). Note also that the total stressed volume minus the sum of the arterial stressed volumes pressures equals sum of the venous stressed volumes (*Eq. 3*). The effective volume resulting from right ventricle interactions depends on the pressure difference between the afterload P_{pa} and a pressure limit determined by $E_{maxlv}\, \Delta V_{orv}$. If the afterload becomes elevated (e.g., heart failure) and approaches the value of the pressure limit ($P_{pa} \approx E_{maxrv}\, \Delta V_{orv}$), then term approaches

zero, and intercept for CVR (*Eq. 10*) simplifies to the total stressed volume minus the sum of the arterial stressed volumes, i.e. the total venous stressed volume. As illustrated in Figure 2.3C, system equilibrium emerges from the interactions between left ventricular function (CO_{LVF}) and cardiovascular return (CO_{CVR}). The equilibrium balance point is represented by the intersection of the two lines, where $CO_{LVF} = CO_{CVR}$ (open circle). At equilibrium, the cardiac output is denoted as CO^* and the pulmonary venous pressure is P_{pv}^*. The full algebraic solutions for CO^* and P_{pv}^* are presented as *Eqs. 13* and *14*. Changes in CO^* and P_{pv}^* may be predicted by evaluating how altered parameter values effect the slopes and intercepts of the CO_{LVF} and CO_{CVR} lines to shift the balance point.

Graphical representation of system equlibrium changes with altered left ventricular function. Figure 2.4 illustrates three alterations in left ventricular properties that increase equilibrium pulmonary venous pressure (P_{pv}^*) and decrease cardiac output (CO^*) from baseline. In Figure 2.4B, an increase in E_{minlv} resulting from a steepening of the end-diastolic pressure-volume relationship (EDPVR) causes the ventricular filling pressure to increase and the end-diastolic volume and stroke volume to decrease. This causes the slope of the CO_{LVF} curve to decrease and its pressure intercept to decrease. In Figure 2.4C, a decrease in unstressed stroke volume (ΔV_{olv}) results in a leftward shift of the EDPVR. This causes ventricular pressure to increase and the end-diastolic volume and stroke volume to decrease. The pressure intercept of the CO_{LVF} curve increases. In Figure 2.4D, a decrease in E_{maxlv} results in a less steep ESPVR causing increased ventricular pressure by increasing end-diastolic volume and decreasing the stroke volume. Decreasing E_{maxlv} thus causes the pressure intercept the CO_{LVF} curve to increase.

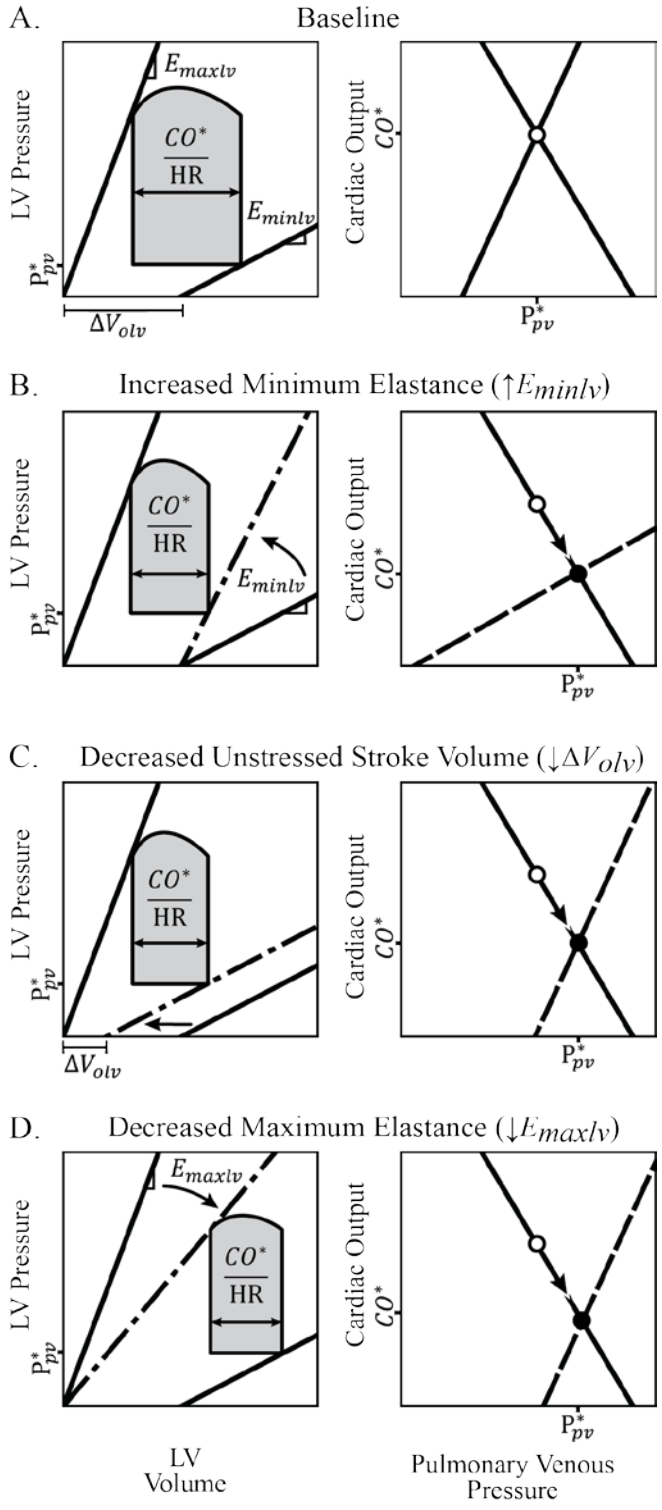

Figure 2.4 Alterations in the left ventricular properties that increase equilibrium pulmonary venous pressure (P_{pv}^*) and decrease cardiac output (CO^*) from baseline. A: Baseline balance. B: Increased left ventricular minimum elastance (E_{minlv}). C: Decreased unstressed stroke volume of left ventricle (ΔV_{olv}). D: Decreased left ventricular maximum elastance (E_{maxlv}). In all three cases, a right downward shift in the balance point (arrow from open to closed circle) indicates increased P_{pv}^* and decreased CO^*.

Sensitivities of equilibrium cardiac output and pulmonary venous pressure to changes in stressed volume. Expressions for the sensitivities of equilibrium cardiac output and pulmonary venous pressure to changes in stressed volume (α and β respectively) are

$$\alpha = \frac{\Delta CO}{\Delta V_s} = \frac{HR}{C_{pv}\, E_{minlv} + C_{sv}\, E_{minrv}}\,, \tag{11}$$

$$\beta = \frac{\Delta P_{pv}}{\Delta V_s} = \frac{E_{minlv}}{C_{pv}\, E_{minlv} + C_{sv}\, E_{minrv}}\,. \tag{12}$$

Sensitivities α and β have a common denominator dependent on coupled minimal ventricular elastance and venous compliance terms. The sensitivity α has heart rate units while sensitivity β has elastance units. As illustrated in Figure 2.5A, a change in CO^* resulting from altered V_s is predicted by the CO^* sensitivity to V_s times the amount that V_s is perturbed, i.e., $\Delta CO^* = \alpha\, \Delta V_s$. Figure 2.5B illustrates how $P_{pv}{}^*$ is predicted by the $P_{pv}{}^*$ sensitivity to V_s times the amount that V_s is perturbed, i.e., $\Delta P_{pv}{}^* = \beta\, \Delta V_s$. Further, the correlation of CO^* to $P_{pv}{}^*$ with alterations in total stressed volume is given by the ratio of their sensitivities, i.e., $\alpha/\beta = HR/\, E_{minlv}$. This correlation is also derived from the left ventricular function equation (*Eq. 5*) as the derivative of CO^* with respect to $P_{pv}{}^*$. This suggests $\Delta CO/\, \Delta P_{pv}$ that in a minimal close-loop model is governed by left ventricular function. In *Eq. 13,* cardiac output at equilibrium (CO^*) is expressed in terms of α, which has heart rate units, and several volume terms,

$$CO^* = \alpha \begin{bmatrix} V_s - (C_{sa} P_{sa} + C_{pa}\, P_{pa}) \\ - C_{pv} \frac{E_{minlv}}{E_{maxlv}} (P_{sa} - E_{maxlv}\, \Delta V_{olv}) \\ - C_{sv} \frac{E_{minrv}}{E_{maxrv}} (P_{pa} - E_{maxrv}\, \Delta V_{orv}) \end{bmatrix}. \tag{13}$$

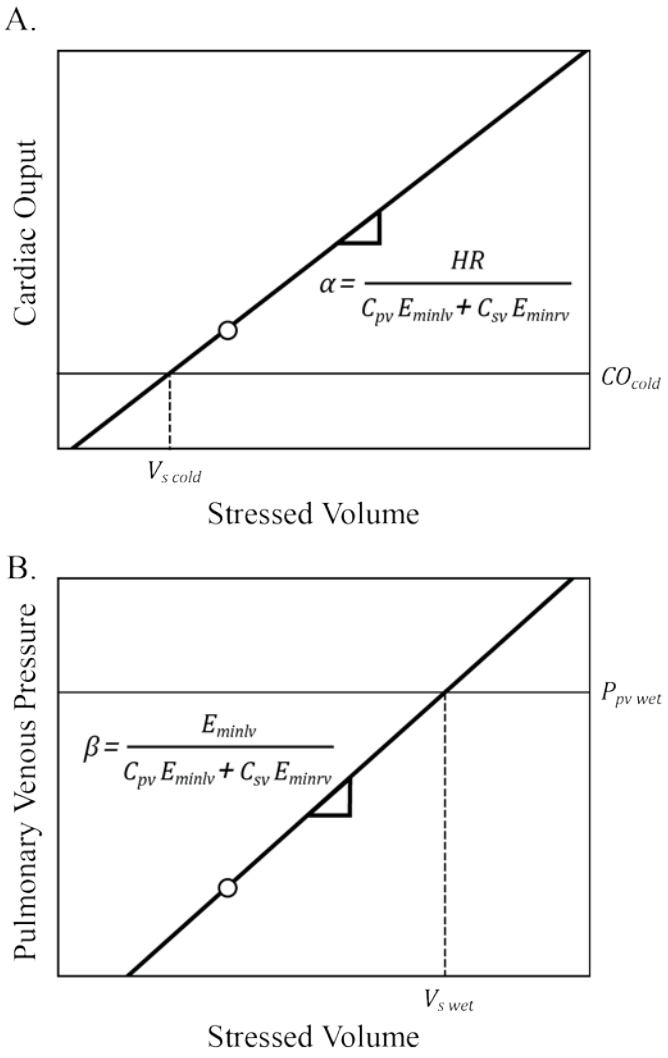

Figure 2.5 Predicting equilibrium cardiac output (CO^*) and pulmonary venous pressure (P_{pv}^*) with altered stressed volume (V_s). Algebraic solutions for (*Eqs. 13* and *14*) are plotted as function of stressed volume (solid lines). A: The change in CO^* from baseline (circle) is approximated by multiplying the amount that stressed volume is perturbed by the sensitivity α. Peripheral hypoperfusion develops when cardiac output is decreased to a critically low level by reducing stressed volume ($V_{s\,cold}$). B: The change in P_{pv}^* from baseline (circle) is approximated by multiplying the amount that stressed volume is perturbed by the sensitivity β. Pulmonary edema develops when P_{pv}^* is increased to a critically high level by increasing stressed volume ($V_{s\,wet}$).

Quantitatively, the dominant term is the total stressed volume (V_s). Vs, however, is modulated by the smaller sum of the arterial stressed volumes and two effective volumes resulting from left and right ventricle interactions with proximal vascular properties. These terms are similar to the intercept expressions for LFV and CVR (Fig. 2.3). Given $E_{maxlv}\,\Delta V_{olv} \gg P_{sa}$ and $E_{maxrv}\,\Delta V_{orv} > P_{pa}$ in normal physiology, ventricular-vascular interactions positively contribute to the overall volume determining cardiac output. In *Eq. 14,* pulmonary venous pressure at equilibrium (P_{pv}^{*}) is expressed in terms of β, which has elastance units, and several volume terms,

$$P_{pv}{}^{*} = \beta \begin{bmatrix} V_s - (C_{sa}P_{sa} + C_{pa}\,P_{pa}) \\ -\,C_{pv}\,\frac{E_{minlv}}{E_{maxlv}}\,(P_{sa} - E_{maxlv}\,\Delta V_{olv})\left(-\frac{C_{sv}\,E_{minrv}}{C_{pv}\,E_{minlv}}\right) \\ -\,C_{sv}\,\frac{E_{minrv}}{E_{maxrv}}\,(P_{pa} - E_{maxrv}\,\Delta V_{orv}) \end{bmatrix}. \qquad (14)$$

Although the expression could be simplified further, this form reveals that all the same volume terms which effect CO^{*} also effect $P_{pv}{}^{*}$. There is, however, an additional term modulating left ventricle interactions. This term is the ratio of the LVR and CVR slopes (*Eqs. 7* and *9*) and depends on venous compliances and minimal elastances. Heart rate (*HR*) cancels out of the ratio and does not affect $P_{pv}{}^{*}$. The ratio is negative and thus modulates left ventricular interactions to reduce the overall volume influencing $P_{pv}{}^{*}$.

Errors of approximation quantified by comparing results of algebraic solutions to results of a more complete numerical model. Figure 2.6 illustrates the error in the equilibrium cardiac output (CO^{*}) and equilibrium pulmonary venous pressure ($P_{pv}{}^{*}$) predicted by the algebraic formulas (*Eqs. 13* and *14*) as stressed volume (V_s) is changed. The error is zero at the origin, i.e., 0 ml stressed volume, because the algebraic formulas are equivalent to the results of the more complex numerical model that incorporates an exponential end-diastolic pressure-volume

relationship for each of the ventricles. When V_s is reduced by 300 ml from baseline, the algebraic model overestimates CO^* by less than 8 ml·s^{-1}. This is within the range of measurement errors observed in thermodilution studies (215). When V_s is increased by 300 ml, the algebraic model underestimates P_{pv}^* by less than 1 mmHg. Modest V_s perturbations (less than 38% change from baseline) therefore yield small errors in CO^* and P_{pv}^*.

Model sensitivity analysis. Figure 2.7 presents the normal baseline sensitivity indices (*SI*) for equilibrium cardiac output (CO^*) and pulmonary venous pressure (P_{pv}^*) of the minimal closed-loop model. The solid bars indicate the sensitivity indices estimated for a modest 10% increase in each parameter's value. The sensitivity indices have the same sign and similar magnitude as the sensitivity indices estimated for the more complete numerical model that incorporated a nonlinear EDPVR for each ventricle. The small differences in magnitudes exhibited by the numerical model sensitivities (which were not apparent on log scale, and therefore not shown) suggest that linearizing the EDPVR of both ventricles has little effect on predicting changes in CO^* and P_{pv}^* for modest parameter perturbations. The sensitivity indices indicate that CO^* and P_{pv}^* are positively correlated when parameters determining cardiovascular return (CVR) are changed. These include total stressed volume, compliances, pulmonary arterial pressure, as well as the elastances and unstressed stroke volume of the right ventricle. Figure 2.7 thus illustrates how elevated stressed volume (V_s) increases both CO^* and P_{pv}^*. Reducing V_s would have converse effects. Indices further indicate CO^* is more sensitive than P_{pv}^* to V_s changes and that both are less sensitive to V_s than other parameters. Together, this suggests that in normal physiology V_s fluctuates across a relatively large range to effect CO^* with more modest effects on P_{pv}^*. In contrast

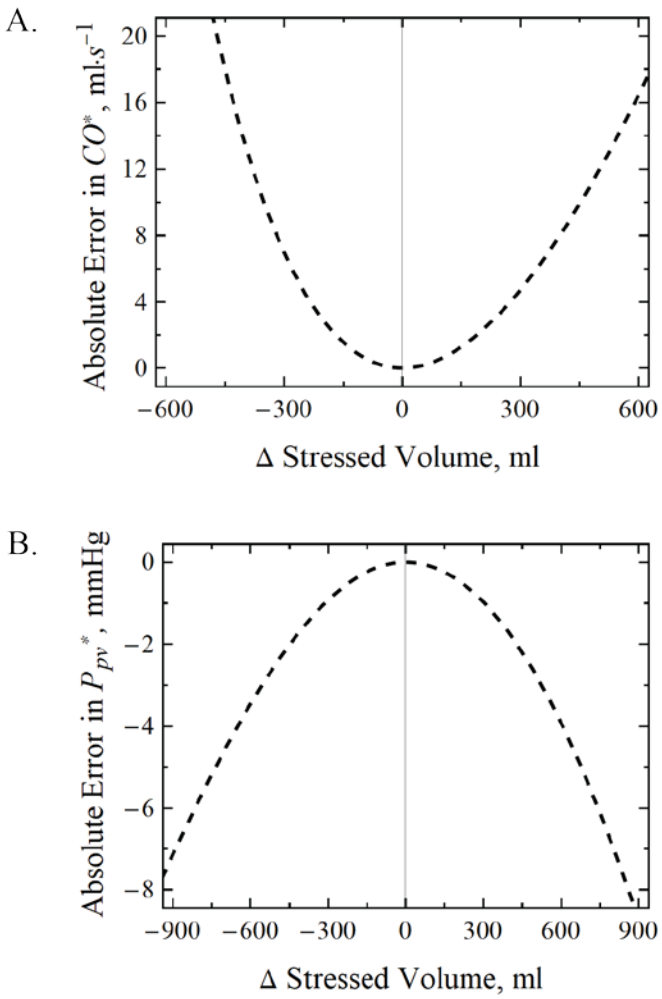

Figure 2.6 Approximation error when predicting equilibrium cardiac output (CO^*) and pulmonary venous pressure ($P_{pv}{}^*$) with small changes in stressed volume (V_s). Using normal baseline parameter values (Table 2.1), absolute error in CO^* and $P_{pv}{}^*$ was calculated as the difference between algebraic and numerical model predictions. A: Reducing stressed volume by 300 ml in the algebraic model overestimates CO^* by less than 8 ml·s^{-1}. B: Increasing stressed volume by 300 ml in the algebraic model underestimates by less than 1 mmHg.

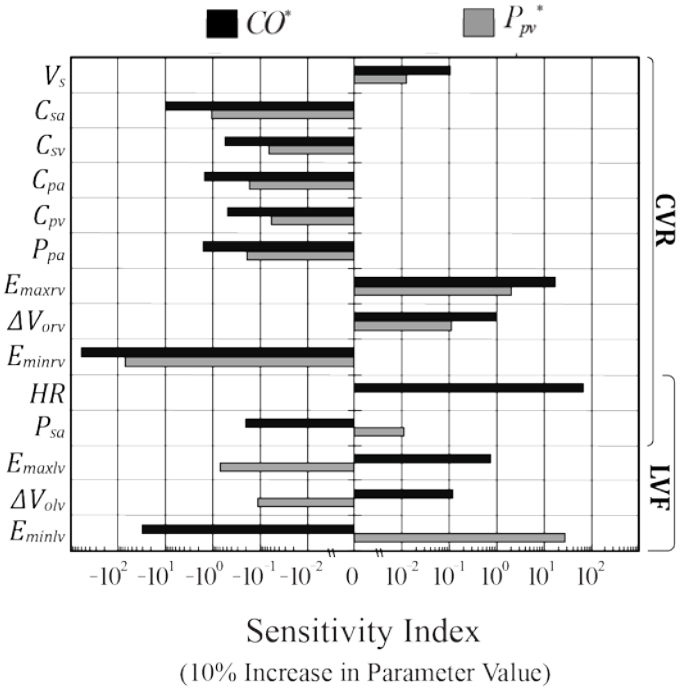

Figure 2.7 Baseline sensitivity indices (*SI*) of equilibrium cardiac output (CO^*) and pulmonary venous pressure (P_{pv}^*). Bars indicate both signs and magnitudes of CO^* and P_{pv}^* sensitivities for the algebraic formulas (*Eqs. 13* and *14*) when the normal baseline value of a property is increased by 10%. For $|SI| > 1$, the fractional change in the variable is greater than the fractional change in the parameter (*Eq. 6*). Vascular properties include stressed volume (V_s), systemic and pulmonary arterial pressures (P_{sa} and P_{pa}), arterial compliances (C_{sa} and C_{pa}), venous compliances (C_{sv} and C_{pv}). Left and right ventricular properties include maximal elastances (E_{maxlv} and E_{maxrv}), minimal elastances (E_{minlv} and E_{minrv}), and unstressed stroke volumes (ΔV_{olv} and ΔV_{orv}). CO^* and P_{pv}^* are negatively correlated when properties determining left ventricular function (LVF) are changed. CO^* and P_{pv}^* are positively correlated when properties determing cardiovascular return (CVR) are changed.

to CVR parameters, sensitivity indices indicate CO^* and $P_{pv}{}^*$ are negatively correlated when any of the parameters determining left ventricular function (LVF) are changed. CO^* increases and $P_{pv}{}^*$ decreases when the maximum elastance or unstressed stroke volume of the left ventricle is elevated. CO^* and $P_{pv}{}^*$ are particularly sensitive to changes in the minimum elastance of the left ventricle (E_{minlv}). Given a $|SI| > 10$, a slight elevation in E_{minlv} decreases CO^* and increases $P_{pv}{}^*$ dramatically. A slight reduction would have converse effects. Heart rate and systemic arterial pressures are the two parameters that effect both CVR and LVF. Their sensitivity indices, however, indicate that they effect CO^* to a greater extent than $P_{pv}{}^*$. Taken together, this suggests that parameters determining left ventricular function may be altered to sustain cardiac output when stressed volume is lowered. The magnitude differences between the sensitivity indices of normal and heart failure cases were minor for all parameter except for maximal elastances. In the case of heart failure with reduced ejection fraction, the *SI* of CO^* and $P_{pv}{}^*$ for a change in E_{maxlv} increased by a factor of 100. The *SI* of $P_{pv}{}^*$ to E_{maxrv} is increases by a factor of 10. In the case of heart failure, increasing right ventricular contractility would thus exacerbate already high pulmonary venous pressure.

Homeostatic range of stressed volume. Acute decompensated heart failure resulting from left ventricular dysfunction occurs when stressed volume exceeds or falls below levels at which critical symptoms develop. Specifically, when cardiac output becomes critically low (CO_{cold}), peripheral hypoperfusion develops. When pulmonary venous pressure becomes critically high ($P_{pv\,wet}$), pulmonary edema develops. Expressed algebraically in *Eq. 15*, the difference in the unstressed volumes between these two critical points identifies the interactions of hemodynamic factors determining the homeostatic range of asymptomatic V_s fluctuation (ΔV_s).

$$\Delta V_s = \left(\frac{1}{\beta}\right) P_{pv\,wet} - \left(\frac{1}{\alpha}\right) CO_{cold} - \left(\frac{1}{\beta}\right)\left(\frac{E_{minlv}}{E_{maxlv}}\right) P_{sa} + \left(\frac{E_{minlv}}{\beta}\right) \Delta V_{olv} \quad (15)$$

This algebraic formula is general and valid for cases that have a relatively modest range of asymptomatic stressed volume fluctuation, e.g., heart failure. As indicated by the expression, the homeostatic range of unstressed volume is determined in part by the pressure and flow at which critical symptoms develop. A decrease in systemic arterial pressure (P_{sa}) will increase ΔV_s. Increasing the unstressed stroke volume of left ventricle (ΔV_{olv}) also increases ΔV_s (Fig. 2.8C). Increasing the maximal elastance of the left ventricle (E_{maxlv}) increases ΔV_s in a limited manner (Fig. 2.8A). Increasing the minimal elastance of the left ventricle (E_{minlv}) decreases ΔV_s (Fig. 2.8B). *Predicting the homeostatic range of stressed volume (ΔV_s) for normal patients and patients having heart failure with reduced ejection fraction (HFrEF).* Table 2.2 reports the predicted equilibrium values for the variables of the algebraic closed-loop model. Predicted values for cardiac output (CO^*), pulmonary venous pressure (P_{pv}^*), systemic venous pressure (P_{sv}^*), total pulmonary resistance (R_p^*), and total systemic resistance (R_s^*) were all consistent with the range of mean values measured and reported in clinical studies of normal and HFrEF patients. This suggests algebraic solutions derived from *Eqs. 1-5* are valid for predicting baseline behaviors. Using *Eq. 15*, ΔV_s for the normal baseline was predicted to be 1855 ml. When compared to the more complete numerical model that incorporated nonlinear end-diastolic pressure-volume relationships (EDPVR), the algebraic solution overestimated ΔV_s by 682 ml (58% error). For the heart failure case, ΔV_s baseline was predicted to be 467 ml. When compared to the numerical model, the algebraic solution for ΔV_s overestimated by 69 ml (17% error). This suggests that the algebraic solution for ΔV_s, which assumes the EDPVR of each ventricle may be approximated with a single

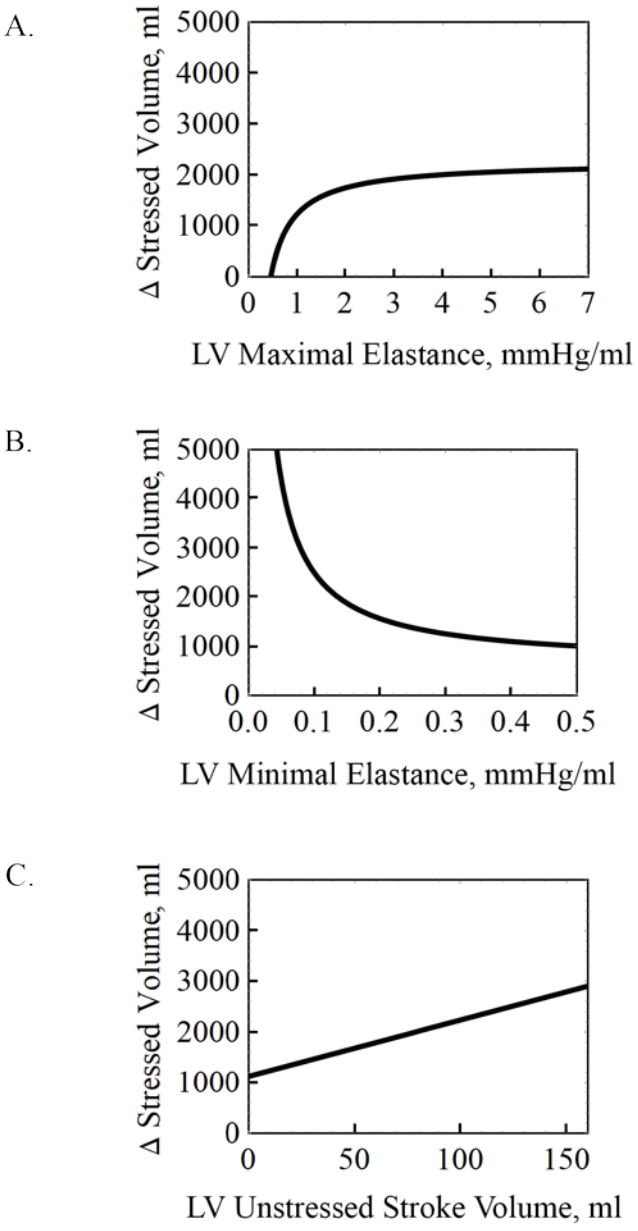

Figure 2.8 Effects of changing left ventricular (LV) properties on the homeostatic range of unstressed volume (ΔV_s). A: Increasing the maximal elastance of the left ventricle (E_{maxlv}) increases ΔV_s in a limited manner. B: Increasing the minimal elastance of the left ventricle (E_{minlv}) will decrease ΔV_s. C: Increasing the unstressed stroke volume of left ventricle (ΔV_{olv}) also increases ΔV_s.

Table 2.2 Predicted variables from parameters reported for normal patients and patients having heart failure with reduced ejection fraction (HFrEF).

	Normal		HFrEF Ejection Fraction < 40%	
Variable	Prediction	Reported	Prediction	Reported
CO^* (ml·s^{-1})	87	60 – 89	75	57 – 80
$P_{pv}{}^*$ (mmHg)	4.7	4.0 – 12	23	19 – 26
$P_{sv}{}^*$ (mmHg)	5.6	0.0 – 8.0	7.4	6.0 – 15
$R_p{}^*$ (mmHg·s·ml^{-1})	0.11	0.11 – 0.19	0.068	0.048 – 0.083
$R_s{}^*$ (mmHg·s·ml^{-1})	0.95	0.68 – 1.1	1.1	0.31 – 1.2
ΔV_s (ml)	1855		467	

Equilibrium cardiac output (CO^*), pulmonary venous pressure ($P_{pv}{}^*$), systemic venous pressure ($P_{sv}{}^*$), total pulmonary resistance ($R_p{}^*$), and total systemic resistance ($R_s{}^*$) were predicted by evaluating from the algebraic solutions derived from *Eqs.1-5* with the parameter values summarized in Table 2.1. Predictions were consistent with the reported ranges of variable values for normal patients (128) and patients having HFrEF (91, 182, 205, 255, 309). Compared to normal, the homeostatic range of stressed volume (ΔV_s) is dramatically lower for the case of HFrEF.

linear equation, is suitable for cases having a relatively modest range of asymptomatic stressed volume fluctuation.

DISCUSSION

The present work is the first to develop and validate algebraic formulas that predict equilibrium cardiac output and pulmonary venous pressure in a minimal closed-loop model with arterial pressure regulation. The present work demonstrates how algebraic methods are used in lieu of numerical approaches for obtaining explicit formulas that reveal how steady-state behaviors emerge from the interaction of left ventricular function and cardiovascular return. Limitations encountered in previous models were resolved by (1) isolating left ventricular function, (2) linearizing end-diastolic pressure-volume relationships, and (3) assuming arterial pressures to be regulated. The formulas reveal that cardiac output and pulmonary venous pressure can be estimated with minimal error over modest ranges of stressed volume change. The resulting algebraic formulas revealed two novel insights when examining effects of total stressed volume and left ventricular dysfunction. First, cardiac output and pulmonary venous pressure are governed by effective volume terms that are not apparent when using numerical approaches (*Eqs. 13* and *14*). Second, the range of asymptomatic stressed volume fluctuation is limited by the properties of the failing left ventricle. In addition to these novel findings, the discussion below details the strategies and assumptions used in developing a basic linear minimal closed-loop model, which cardiovascular researchers can readily extend or modify when investigating particular processes and adaptations resulting from isolated ventricular dysfunction.

To obtain general algebraic formulas that approximate system behaviors, linear relationships were assumed for the Beds, chambers, and pumps of the closed-loop model. With

few exceptions (183, 190), minimal closed-loop models have assumed linear relationships to characterize the cardiovascular system in terms of a relatively small number of parameters (Fig. 2.1). In contrast to numerical models that employ nonlinear relationships having additional, often poorly characterized parameters (66, 175), minimal closed-loop models use linear equations over specified ranges of volumes or pressures (65). Flow-pressure relationships, for instance, have been shown to be fairly linear over a wide range of pulmonary and systemic arterial pressures (250, 258, 287). Similarly, the volume-pressure relationship of the systemic venous chamber has been shown to be relatively linear as pressures rise (258, 287). With respect to pump function, the end-systolic pressure-volume relationship (ESPVR) in normal patients and those with heart failure has been reported to be relatively linear over wide range of end-systolic pressures (11, 46). Linearization of end-systolic volume-pressure relationship has been experimentally validated (264) and has yielded close approximations of numerical simulations (59). In contrast, the end-diastolic pressure-volume relationship (EDPVR) is highly nonlinear with a slope that increases over the normal range of ventricular filling pressures (47). Considered to have the most impact on system behavior, some heart failure models have retained this nonlinearity (275). However, to obtain algebraic solutions, others have assumed EDPVR to be linear (127, 265). For instance, by characterizing EDPVR with a slope (E_{min}) and volume intercept (V_o), Sunagawa, et al. (265) derived a general algebraic formula for cardiac output. The formula revealed cardiac output depended on the ratio of the maximal elastance of ventricle to an effective arterial elastance, a term that has been used in clinical studies of ventricular dysfunction as a measure of efficient energy transfer (168). Following this approach, the present work used the linear EDPVR relationship for the right and left ventricle (*Eqs. A4* and *A7*). As evident in the comparison of normalized sensitivities of CO^* and P_{pv}^* to parameter perturbations, the resulting algebraic formulas exhibited the same trends as the more complex

numerical model incorporating EDPVR and were also consistent with other numerical heart failure models (48, 195).

To obtain valid algebraic formulas for clinically relevant variables, the minimal closed-loop model was partitioned to investigate the interaction of left ventricle function and cardiovascular return. Previous models have followed Guyton's characterization of system equilibrium as the interaction of cardio-pulmonary performance and venous return (252, 279). This traditional approach, however, imposes several limitations for deriving algebraic formulas, namely accounting for blood redistribution between chambers, characterizing variables associated with critical symptoms, and isolating the effects of ventricular properties. These issues are resolved by partitioning model elements to study equilibrium behaviors resulting from left ventricle function and the flow resulting from the rest of the cardiovascular system (Fig. 2.2). With this novel partition, the blood volumes and unstressed volumes of the four chambers are lumped into a single compartment and can be added together (*Eqs. A13* and *A14*). Reparametrizing the difference between the total blood volume and the total unstressed volume as the system's total stressed volume simplifies the model further. The novel partition also enables system equilibrium to be characterized in terms of a pressure and flow that relate directly to the clinical profiles of "cold/warm" and "wet/dry" that have been used to characterize pump performance, predict outcomes, and devise therapies for heart failure patients (62, 101, 216). The partition also allows the effects of isolated left ventricular dysfunction on equilibrium to be evaluated (Fig. 2.4). How cardiovascular return compensates to increase cardiac output and/or lower pulmonary venous pressure can also be assessed (Fig. 2.3).

Algebraic formulas were derived by assuming equilibrium cardiac output and pulmonary venous pressure emerge from within a system that regulates arterial pressures. In contrast to

conventional modeling approaches that treat resistances as constant parameters(48, 195), the present work assumed resistances are variably controlled by baroreflex mechanisms to maintain arterial pressure homeostasis. When blood volume is increased in humans, systemic arterial pressure thus remains relatively constant whereas systemic resistance changes by several factors (74). Though less well understood, the carotid sinus baroreflex has been implicated in the direct regulation of pulmonary resistance (259). When blood volume is decreased, pulmonary arterial pressure remains relatively constant whereas a two-fold increase in total pulmonary resistance has been observed in primates (1). Arterial pressures do change over time in response to ventricular dysfunction, but are still regulated under acute conditions and relatively constant compared to resistances (99). For this reason, multi-scale heart failure models have incorporated baroreflex mechanisms using additional equations to control variable resistances (236, 275). These models, however, require numerical methods that are sensitive to parameter values and limited for purposes of identifying the most influential interactions. To obtain algebraic solutions for normal and asymptomatic heart failure cases, the present work approximated the effects of regulation by assuming that arterial pressures are perfectly regulated by variable resistances.

As with other heart failure models, equilibrium cardiac output and pulmonary venous pressure were solved in terms of total stressed volume to evaluate the net effect of multiple regulatory mechanisms. In normal physiology as well as cases of systolic dysfunction, the heightened sympathetic response to hypotension causes venoconstriction in the splanchnic vasculature to decrease overall vascular capacitance (86). A leftward shift in the pressure-volume relationship occurs. Considering compliances are unaffected, the leftward shift reflects a decrease in unstressed volume and an increase in stressed volume (86, 243). In systolic heart failure, baroreflex mediated venoconstriction attempts to restore cardiac output. Over time, total blood

volume is increased through stimulation of renal fluid reabsorption (125). To accommodate volume overload (204), the cardiopulmonary reflex becomes more active to increase vascular capacity (15, 291). Overall, the interactions among these feedback mechanisms and others is complex and can become unbalanced during heart failure (99, 169). However, by solving system equations in terms of total stressed volume, heart failure models have been able to evaluate the net effect that these compensatory mechanisms have on system equilibrium (195, 207). In a numerical heart failure model, Burkhoff and Tyberg (48) demonstrated how increasing stressed volume restores cardiac output at the cost of raising pulmonary venous pressure. This novel approach lumped long-term effects renal regulation of total blood volume as well as short-term effects of arterial and cardiopulmonary baroreflex regulation of total unstressed volume into a single parameter (94, 244). By including the nonlinear EDPVR, however, their model required numerical methods to obtain results. In contrast, the present work treated total stressed volume as a lumped, independent variable within a system of linear equations. Analyzing the system algebraically not only generalized their predictions with explicit formulas, but also extended their approach to address clinically relevant questions.

The resulting algebraic formulas predict equilibrium trends observed in a wide array of studies that alter total stressed volume. As indicated by *Eqs. 13* and *14* and illustrated in Fig. 2.5, the algebraic formulas predict elevation of both equilibrium cardiac output (CO^*) and pulmonary venous pressure (P_{pv}^*) in response to an increase in total stressed volume. When splanchnic vasoconstriction is stimulated with adrenergic agonists, stressed volume is elevated and CO^* and P_{pv}^* are increased (9, 57, 79, 113, 237). Conversely, when venoconstriction is suppressed by ganglionic blockade, stressed volume is decreased and CO^* declines (86, 307). In chronic heart failure, elevated levels of atrial natriuretic peptide (ANP) are associated with increased total blood

volume and left ventricular filling pressure (143). Experimental ANP treatment decreases total blood volume without affecting unstressed volume. Treatment reduces total stressed volume and results in decreased CO^* and $P_{pv}{}^*$ (61, 177). In heart failure, cardiopulmonary reflex activity also increases to counterbalance the sympathetic response. Increased venous capacity has been observed in patients having heart failure with reduced ejection fraction (6). In experimental heart failure, inhibition of the cardiopulmonary reflex decreases splanchnic capacitance and increases left ventricular filling pressure (289). Some interventions, which aim to reduce filling pressure, can affect both left ventricular function (LVF) and cardiovascular return (CVR). Graphical analysis (Fig. 2.3) is therefore a useful tool for evaluating pharmacological effects on equilibrium behavior. Vasodilators like nitroglycerin and enalaprilat, for instance, decrease total stressed volume while also decreasing systemic arterial pressure (112, 288). These parameter changes cause a leftward shift of LVF and CVR intercepts to lower $P_{pv}{}^*$ and sustain CO^*. Similarly, activation of adenosine-2 receptors increases venodilation and decreases systemic arterial pressure, but also increases heart rate (213, 268). With these parameter changes, LVF and CVR intercepts shift leftward and their slopes increase to lower $P_{pv}{}^*$ and increase CO^*. Overall, the algebraic formulas predict trends that are consistent with those observed in experimental and clinical studies manipulating regulatory mechanisms to change total stressed volume.

Sensitivities of cardiac output and pulmonary venous pressure to changes in stressed volume can help guide fluid management in cases of asymptomatic heart failure. While stressed volume has been rigorously measured in experimental settings for decades (194), measurements are now being taken at bedside in response to bolus infusions (192). With continued improvements in technique, CO^* and $P_{pv}{}^*$ sensitivities to stressed volume changes (α and β respectively) could be estimated for every patient. The algebraic expressions for α and β derived in the present work are

the first to identify the specific parameter interactions that determine how changes in stressed volume effect CO^* and $P_{pv}{}^*$ (Figure 2.5). Combined with patient data, the expressions (*Eqs. 11* and *12*) may be used to predict the effects of a stressed volume change on equilibrium behaviors, i.e., $\Delta CO^* = \alpha\ \Delta V_s$ and $\Delta P_{pv}{}^* = \beta\ \Delta V_s$. If changes to CO^* and $P_{pv}{}^*$ are known, then specific parameter values for patients can be deduced to assess risks to therapy. In the present work, the robustness of algebraic model was evaluated by comparing predictions to the more complete numerical model incorporating a nonlinear EDPVR for each ventricle (Fig. 2.6). For modest perturbations in total stressed volume (~300 ml), the approximation errors in CO^* and $P_{pv}{}^*$ were found to be small and comparable to measurement error. This was a conservative approach to approximation based on characterizing the nonlinear EDPVR with a single line defined by an instantaneous slope (E_{min}) and volume intercept (V_o). For larger stressed volume perturbations, the nonlinear EDPVR may be fit with a two-equation linear model that minimizes error over a specified pressure range (60, 92).

By solving equilibrium cardiac output and pulmonary venous pressure algebraically in terms of stressed volume, the physical properties determining the maximum and minimum of an asymptomatic stressed volume range could be derived. Specifically, the algebraic solutions for CO^* and $P_{pv}{}^*$ (*Eqs. 13* and *14*) can be rearranged to identify the physical interactions determining the stressed volumes at which critical symptoms of edema and hypoperfusion develop. The difference between theses "wet" and "cold" stressed volumes characterizes the homeostatic range of asymptomatic V_s fluctuation (ΔV_s). The resulting algebraic formula (*Eq. 15*) is the first to characterize this clinically-relevant range in terms of vascular-ventricular interactions. When evaluated with parameter values of normal and heart failure patients, the range for heart failure patients is relatively small (Table 2.2). When compared to the more complex numerical model, the algebraic formula overestimates ΔV_s by 58% in the normal case and 17% in the heart failure case.

Approximating the EDPVR as a single line is therefore reasonable for an algebraic solution for a small total stressed volume range such as in heart failure.

The algebraic formula for the homeostatic range of stressed volume reframes the standard clinical wet-cold paradigm to characterize how left ventricular dysfunction limits volume redistribution. In normal physiology, significant redistribution of blood volume from the splanchnic venous reservoir to the central circulation can occur in a matter of seconds to maintain cardiac filling pressures. Most heart failure patients, however, exhibit varying degrees of volume overload and high cardiac filling pressures (7, 204). Interestingly, the majority of patients who develop pulmonary edema exhibit no evidence of volume gain prior to hospitalization (58). Instead, autonomic imbalance with increased filling pressure is observed. This has led researchers to hypothesize that the mechanism of decompensation lies in the inability of a progressively sympathoexcited venous reservoir to reduce stressed volume as needed (88, 94). The present work adds to this inquiry by demonstrating how left ventricular dysfunction limits the homeostatic range of stressed volume. That is, while arterial and cardiopulmonary feedback mechanisms may become unbalanced and unable to effectively control venous reserve function, the range in which stressed volume can fluctuate may be greatly diminished. Increasing the minimal elastance of the left ventricle (E_{minlv}), for instance, will lower ΔV_s (Fig 2.8B). Further reductions in the maximal elastance of the left ventricle (E_{maxlv}) also lowers ΔV_s (Fig. 2.8A). Conversely, an increase in E_{maxlv} through exercise would can expand the range up to a point. Ventricular remodeling that increases the unstressed volume of the left ventricle (ΔV_{olv}) will also act to restore ΔV_s. (Fig 2.8C).

The linear minimal closed-loop model is a novel tool for investigators studying isolated ventricular dysfunction. In contrast to Guyton's model that relied on an empirical cardiac performance curve that includes the effects of both ventricles and the pulmonary vasculature, the

model of the present work characterizes isolated left ventricular function in terms of ventricular properties: contractility, stiffness, and unstressed volume. This improvement, as well as others previously mentioned, revamps Guyton's framework for the purposes of investigating how steady-state behaviors emerge from the interaction of ventricular and vascular properties under conditions of arterial pressure regulation. Using this framework, insights about equilibrium CO^* and $P_{pv}{}^*$, their sensitivities to altered total stressed volume, as well as the homeostatic range of asymptomatic stressed volume were developed. However, investigators may wish to adapt the methods used in the present work to address other important issues. For instance, by incorporating a pericardial pressure-volume relationship, the model can be used to investigate the role that biventricular diastolic interactions have in venodilation (278). For cases in which pulmonary arterial pressure (P_{pa}) is known to be high and mostly variable, alternate solutions can be obtained by treating pulmonary resistance (R_p) as a constant that has neared the lower limit of its physiological range. Other critical symptoms, e.g. ascites, can be investigated by partitioning minimal closed-loop model to study isolated right ventricular dysfunction. The present work therefore not only provides a novel framework for understanding asymptomatic volume fluctuations in heart failure, but also reapplies Guyton's general strategy to develop a useful modeling framework for researchers and students to better conceptualize steady-state behaviors.

CHAPTER III

RENAL FLUID BALANCE MODEL

Although implicated in the regulation of tubule fluid reabsorption, the role of renal interstitial hydrostatic pressure in diuresis has been difficult to establish. Recognized as a key intermediate in cortical fluid balance (222), renal interstitial hydrostatic pressure effects fluid inflow and outflow differently. On one hand, increased interstitial hydrostatic pressure has been associated with *decreased* fluid reabsorption from the tubule into the interstitium (104, 150). On the other hand, increased interstitial hydrostatic pressure has been associated with *increased* fluid uptake from the cortical interstitium into the peritubular capillaries (13, 30, 145). The opposing effects of interstitial hydrostatic pressure on the fluid flows into and out of the interstitium have made its role in diuresis difficult to evaluate experimentally (158, 276). Several studies have increased interstitial hydrostatic pressure directly in situ to examine factors involved in diuresis (5, 146, 149). Treating interstitial hydrostatic pressure as an independent variable, however, neglects the roles that peritubular capillaries, cortical lymphatic vessels, and distal nephron segments have in modulating both interstitial hydrostatic pressure and tubule fluid reabsorption (239, 276, 299). Moreover, diuresis in vivo does not only occur with *increased* interstitial hydrostatic pressure (242). Increased fluid excretion with *decreased* interstitial hydrostatic pressure has also been reported to occur when solute transport across the tubule epithelial barrier is inhibited (141). To better understand the seemingly contradictory effects of intermediates within a complex physiological system like the renal cortex, integrative mathematical models have been employed (64, 208).

Although mathematical models have incorporated properties of tubule and capillary compartments, the vast majority have not included the interstitium as an explicit intervening compartment. Tubule models have characterized fluid reabsorption as nonlinear fluid and solute transport driven either by transepithelial osmolality differences (253, 301) or by a hypertonic lateral interspace (43, 137, 247, 273, 294). Capillary models, in contrast, exclude tubule properties and characterize fluid uptake from the interstitium as a function of fluid permeability and pressure gradients along vessel length (76, 276). Other models incorporating both tubules and capillaries have considered fenestrated capillary vessels to be so highly permeable that interstitial and capillary osmotic pressures of small solutes may be presumed equal (224). These two-compartment models have therefore neglected capillary barrier properties (116). Notable multi-compartment models, which have included the interstitium, have further assumed fluid flow depends on solute flows into the lateral interspaces of tubule epithelia (138, 292). These nonlinear solute-coupled models, however, have required numerical methods and have limited their evaluations of pressure-flow relationships to univariate analysis techniques.

As an alternate approach, pressure-flow relationships have been investigated by using linear models to derive general algebraic formulas for pressures and flows. Linear models have been especially useful for identifying the predominant physical interactions governing emergent behaviors when many of the parameter values are not well-known (203). In contrast, inferences based on numerical solutions of nonlinear models are contingent upon the particular set of parameter values chosen (24). For example, the use of either high or low water permeability values is implicit in the competing tubule models that infer fluid reabsorption is driven either by transepithelial osmolality differences or by hypertonic lateral interspaces (254). In contrast to numerical solutions, general algebraic formulas may be used to identify the critical properties

governing system behavior without having to assume specific parameter values. Flow and pressure trends can instead be predicted by directly inspecting the parameter interactions made explicit by the algebraic expressions (273). Williams and Schafer (300), for instance, derived algebraic formulas for interstitial osmotic pressures that indicate how semi-permeable capillaries could produce interstitial osmotic pressures that differ from capillary pressures (i.e. solute polarization). Algebraic expressions for interstitial hydrostatic pressure and fluid flow have also been derived for a linear three-compartment model of peripheral tissues drained by lymphatic vessels (83). No such characterization, however, exists for fluid balance in the renal cortex. Therefore, the purpose of the present work was to derive algebraic formulas for interstitial hydrostatic pressure and tubule fluid reabsorption based on a linear three-compartment model that incorporates the cortical interstitium.

METHODS

Three-compartment model of fluid transport through the renal cortex. Similar to the approach of Williams and Schafer (300), bulk fluid reabsorption in the mammalian renal cortex was assumed to involve the pressures within three compartments (Fig. 3.1). The complex anatomical arrangement of tubule lumen, interstitial spaces, and surrounding capillary networks were thus lumped into three distinct compartments separated by two semi-permeable barriers. Appended subscripts denote whether the parameters and variables are associated with tubules (t), interstitium (i) or capillaries (c). In each compartment, there is a hydrostatic pressure (P) and an osmotic pressure (Π) exerted by each solute species (s). Semi-permeable tubule and capillary barriers were each characterized by a filtration coefficient (K_f), which is the product of their surface areas and hydraulic conductances. Barriers were also characterized by reflection coefficients (σ)

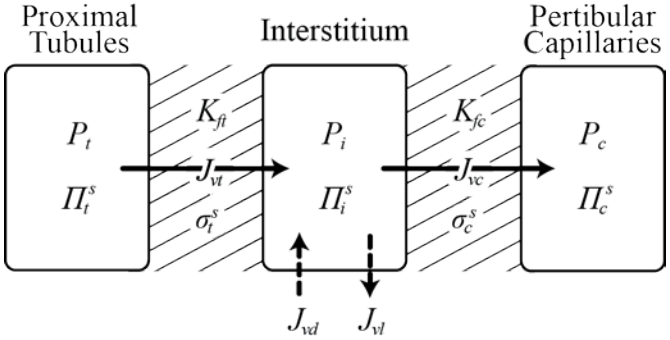

Figure 3.1 Three-compartment model characterizing fluid movement through the renal cortex. Compartments include proximal tubule (*t*), interstitium (*i*), and surrounding network of peritubular capillaries (*c*). Tubule fluid reabsorption (J_{vt}) and capillary fluid uptake (J_{vc}) depend on hydrostatic pressures (P) and osmotic pressures (Π^s) exerted by each solute species *s* in the compartments, as well as the fluid filtration coefficients (K_f) and solute reflection coefficients (σ^s) of the barriers separating the compartments (hatched). Dashed arrows indicate fluid flow into the interstitium from distal nephron segments (J_{vd}) and fluid flow out of the interstitium through cortical lymphatic vessels (J_{vl}).

for each solute species. Tubule fluid reabsorption (J_{vt}) is the rate of fluid flow from tubule to interstitium compartments. Capillary fluid uptake (J_{vc}) is the rate of fluid flow from interstitium to capillary compartments. For completeness, inflow from distal nephron segments (J_{vd}) and outflow via cortical lymphatic vessels (J_{vl}) were also included as parameters.

Governing fluid flow equations. Fluid flow across each barrier was characterized as a product of a fluid filtration coefficient and a net driving pressure. Given electrochemical forces across proximal tubule and peritubular capillary barriers are negligible (36), the standard Kedem-Katchalsky equation for fluid flow was assumed (147). To clarify analysis, the total pressure within the tubule ($\hat{P}_t$) and the total pressure within the capillary ($\hat{P}_c$) were defined,

$$\hat{P}_t = P_t - \sum_{s=1}^{n} \sigma_t^s \Pi_t^s, \quad (1)$$

$$\hat{P}_c = P_c - \sum_{s=1}^{n} \sigma_c^s \Pi_c^s, \quad (2)$$

where P_t and P_c are tubule and capillary hydrostatic pressures, respectively. The terms $\sum_{s=1}^{n} \sigma_t^s \Pi_i^s$ and $\sum_{s=1}^{n} \sigma_c^s \Pi_i^s$ represent the "total effective interstitial osmotic pressure" of *n* solutes that are weighted by either tubule (σ_t) or capillary (σ_c) reflection coefficients. The equations for tubule fluid reabsorption (J_{vt}) and capillary fluid uptake (J_{vc}) were then expressed as,

$$J_{vt} = K_{ft} \left(\hat{P}_t - P_i + \sum_{s=1}^{n} \sigma_t^s \Pi_i^s\right), \quad (3)$$

$$J_{vc} = K_{fc} \left(P_i - \hat{P}_c - \sum_{s=1}^{n} \sigma_c^s \Pi_i^s\right), \quad (4)$$

where P_i is the interstitial hydrostatic pressure, and K_{ft} and K_{fc} are tubule and capillary fluid filtration coefficients, respectively.

Graphical analysis of cortical fluid balance. Following a standard graphical analysis method (83, 119), tubule fluid reabsorption and capillary fluid uptake (*Eqs. 3* and *4*) were each plotted as a function of interstitial hydrostatic pressure (P_i). The slopes and P_i-axis intercepts were calculated for each line. To illustrate how equilibrium emerges from the interaction of reabsorption and uptake, J_{vt} and J_{vc} were then plotted simultaneously as a function of P_i. Equilibrium interstitial hydrostatic pressure (P_i^*) and reabsorption (J_{vt}^*) were indicated at the "balance point" where the two lines intersect and $J_{vt} = J_{vc}$.

Graphical representation of cortical fluid balance with changes in total tubule or total capillary pressures. To illustrate how equilibrium shifts with changes in total tubule pressure ($\hat{P}_t$) or total capillary pressure ($\hat{P}_c$), baseline tubule reabsorption and capillary uptake lines were plotted in the same manner previously described. Changes in J_{vt}^* and P_i^* resulting from either decreased $\hat{P}_t$ or increased $\hat{P}_c$ were illustrated by replotting tubule reabsorption and capillary uptake lines. Changes in slopes and intercepts, as well as the resulting shifts in equilibrium balance points were indicated.

Characterizing the properties governing cortical fluid balance in terms of equivalent pressures and resistances. To identify parameter groups governing steady-state behaviors, the three-compartment model was represented by an equivalent circuit (Fig. 3.2) commonly employed in characterizing interstitial fluid balance (85, 121, 225). In this case, the pressures were grouped to highlight the determinants of equilibrium interstitial hydrostatic pressure (P_i^*) and tubule fluid reabsorption (J_{vt}^*). Therefore, the equivalent inlet pressures that oppose P_i^* to drive fluid from the tubule to the interstitium were grouped together ($\hat{P}_t + \sum_{s=1}^{n} \sigma_t^s \Pi_i^s$), as were the equivalent outlet pressures that oppose P_i^* driving flow from the interstitium to capillary compartments ($\hat{P}_c + \sum_{s=1}^{n} \sigma_c^s \Pi_i^s$). Although a filtration coefficient (*Eqs. 3* and *4*) is by definition the ratio of the fluid flow through a semi-permeable barrier to net pressure gradient, a "resistance" is the ratio of the net pressure gradient to fluid flow. As reported by Dongaonkar et al. (83), the resistance to fluid flow between the interstitium and capillary compartments is $1/K_{fc}$. Similarly, the resistance to fluid flow between the tubule and interstitium compartments is $1/K_{ft}$. Therefore, P_i^* depends on the relative resistances, and J_{vt}^* depends on the total resistance ($1/K_{fc}$ + $1/K_{ft}$). The "effective conductance" of this system was calculated from the inverse of total resistance, and the "relative capillary conductance" and "relative tubule conductance" were calculated from the inverse of the relative resistances.

General, algebraic formulas for equilibrium interstitial hydrostatic pressure and tubule fluid reabsorption. To provide conceptual clarity, the equivalent circuit (Fig. 3.2) and balance point graph (Fig. 3.3) were represented assuming that tubule reabsorption equals capillary uptake in steady state. However, there is an additional inflow of fluid from distal nephron segments into the cortical interstitium as well as an additional outflow of fluid into cortical lymphatic vessels (231,

239). When accounting for distal flow (J_{vd}) and lymphatic flow (J_{vl}), conservation of mass within the interstitial compartment implies,

$$J_{vt} + J_{vd} = J_{vc} + J_{vl}. \quad (5)$$

To obtain algebraic formulas for equilibrium interstitial hydrostatic pressure (P_i^*) and tubule fluid reabsorption (J_{vt}^*) that includes J_{vl} and J_{vd}, *Eqs. 3*-5 were solved simultaneously for variables J_{vt}, J_{vc} and P_i. The resulting solutions were expressed in terms of constant parameters that include filtration coefficients, reflection coefficients, effective interstitial osmotic pressures, total tubule and capillary pressures, and distal and lymphatic flows.

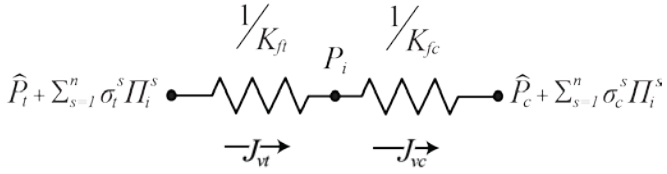

Figure 3.2 Equivalent circuit representation of three-compartment model. Equivalent inlet pressure $\left(\hat{P}_t + \sum_{s=1}^{n} \sigma_t^s \Pi_i^s\right)$ is function of total tubule pressure ($\hat{P}_t$) and sum of interstitial osmotic pressures (Π_i^s) weighted by tubule reflection coefficients (σ_t^s) for each solute species *s*. The equivalent outlet pressure ($\hat{P}_c + \sum_{s=1}^{n} \sigma_c^s \Pi_i^s$) is function of total capillary pressure ($\hat{P}_c$) and sum of Π_i^s weighted by capillary reflection coefficients (σ_c^s). Resistance to flow between tubule and interstitium compartments (J_{vt}) is $1/K_{ft}$, and resistance to flow between interstitium and capillary compartments (J_{vc}) is $1/K_{fc}$. Left half corresponds *Eq. 3*. Right half corresponds *Eq. 4*.

Validating the algebraic formulas by comparing their predictions to reported data. Algebraic formulas derived from a compartment model characterized by filtration coefficients may be used to predict behaviors at either the organ or nephron level. Given the availability of data from solute transport inhibition studies, the algebraic formulas were used to predict equilibrium tubule fluid reabsorption (J_{vt}^*) and interstitial hydrostatic pressure (P_i^*) for a cross-section of tubule, interstitium and capillaries. Treatment and baseline parameter values were thus assumed

to be equal to reported values or values calculated from reported data of comparable rat nephron studies. Treatment and corresponding baseline values, in particular, were drawn from similar micropuncture studies in which rats were administered benzolamide to inhibit carbonic anhydrase (CA) in the tubule (141, 164, 166, 277). In these studies, CA inhibition was reported to alter tubule hydrostatic and osmotic pressures (P_t, $\Pi_t^{Cl^-}$ and $\Pi_t^{HCO_3^-}$), capillary hydrostatic and protein osmotic pressures (P_c and $\Pi_c^{protein}$), interstitial protein osmotic pressure ($\Pi_i^{protein}$), and distal flow (J_{vd}). To validate the algebraic formulas, four cases were simulated: predictions accounting for all reported parameter changes, predictions neglecting only the change in distal flow, predictions neglecting only the change in interstitial protein osmotic pressure, and predictions accounting for only the change in total tubule pressure. In each case, predicted J_{vt}^* and P_i^* values were compared to the measured J_{vt}^* and P_i^* changes reported in CA-inhibited rats similarly treated with benzolamide (141).

Model sensitivity analysis. A standard one-at-a-time sensitivity analysis (176, 262) was performed to evaluate the sensitivity of the variables of the algebraic formulas to changes in baseline parameters (Table 3.1). To compare sensitivities, a nondimensional sensitivity index (*SI*) for hydrostatic pressure and tubule fluid reabsorption was calculated for each parameter,

$$SI = \frac{\Delta Var}{Var_0} \Big/ \frac{\Delta Par}{Par_0}. \quad (6)$$

The value of *SI* represents the change in the variable (ΔVar) normalized by its baseline value (Var_0) for a given change in the parameter (ΔPar) normalized by its baseline value (Par_0). Parameters with a baseline value of zero (e.g., reflection coefficients of small solutes) were necessarily excluded. To accurately calculate the *SI* values at baseline, each parameter was changed by a small amount (i.e., less than 0.0001%). The results were plotted and compared to *SI*

values calculated for a more complete, nonlinear three-compartment model that incorporated both fluid and solute flow equations.

Errors of algebraic approximation quantified by comparing results to a more complete nonlinear model that includes solute flows. The algebraic formulas derived from *Eqs. 3-5* should be interpreted as approximations that assume interstitial osmotic pressures are known parameters. In contrast, the more complete nonlinear model incorporated solute flow equations that permitted interstitial osmotic pressures to be treated as predicted variables that depend on steady-state fluid flow. The difference between the predictions of the algebraic formulas and the nonlinear solute-coupled model is the error of approximation. Using the parameter values listed in Table 3.1, approximation errors were calculated and plotted for wide ranges of total tubule pressures and total capillary pressures. In addition, algebraic formulas were derived to characterize approximation errors in equilibrium tubule fluid reabsorption and interstitial hydrostatic pressure that arise from a perturbation of a parameter at the system's boundary (i.e., a change in either total tubule pressure, total capillary pressure, distal flow, or lymphatic flow). Because the algebraic approximation treats the total effective interstitial osmotic pressures ($\sum_{s=1}^{n} \sigma_t^s \Pi_i^s$ and $\sum_{s=1}^{n} \sigma_c^s \Pi_i^s$) as constant parameters, the rate of change of the variables is characterized by its partial derivative with respect to a parameter. However, because $\sum_{s=1}^{n} \sigma_t^s \Pi_i^s$ and $\sum_{s=1}^{n} \sigma_c^s \Pi_i^s$ are variable, the true rate of change of the variables is characterized by the total derivative. Therefore, the error in each variable was estimated as the change in the parameter multiplied by the difference between the partial and total derivatives with respect to the perturbed parameter.

Predicting tubule fluid reabsorption in response to changes in total tubule or capillary pressures. To elucidate how equilibrium tubule fluid reabsorption (J_{vt}^*) varies with equilibrium interstitial pressure (P_i^*), the algebraic formulas were used to predict J_{vt}^* and P_i^* values for a wide

range of total tubule pressure ($\hat{P}_t$) and total capillary pressure ($\hat{P}_c$). For each case, J_{vt}^* and P_i^* were the plotted parametrically. For the first graph, J_{vt}^* was plotted as a function of P_i^* as total tubule pressure was altered. For the second graph, J_{vt}^* was plotted as a function of P_i^* as total capillary pressure was altered. To evaluate whether the algebraic approximations were robust, the results from the more complete nonlinear model incorporating solute flows were also plotted. In addition, the parameters governing the slopes of the two the pressure-flow relationships were predicted directly from the algebraic formulas. Specifically, the slope when total tubule pressure is altered is

$$\frac{dJ_{vt}^*}{dP_i^*} = \frac{dJ_{vt}^*}{d\hat{P}_t} \Big/ \frac{dP_i^*}{d\hat{P}_t}, \tag{7}$$

and the slope when total capillary pressure is altered is

$$\frac{dJ_{vt}^*}{dP_i^*} = \frac{dJ_{vt}^*}{d\hat{P}_c} \Big/ \frac{dP_i^*}{d\hat{P}_c}. \tag{8}$$

Nonlinear, solute-coupled three-compartment model. Neglecting the structural complexities of biological membranes, Kedem and Katchalsky (147) characterized solute transport from one compartment to another as an irreversible process of energy dissipation that occurs through flow-dependent solvent drag and independent diffusion. The resulting Kedem-Katchalsky convection-diffusion formulation has been widely used as a basis to approximate solute flow within the renal cortex (6, 116, 247, 253, 273, 292, 294, 300). Specifying this formulation for each solute (*s*) in the three-compartment model in Fig. 3.1, tubule solute reabsorption (J_{st}) and capillary solute uptake (J_{sc}) are respectively,

$$J_{st} = [J_{vt}\,(1-\sigma_t^s)\,\dot{c}\; + PS_t^s(C_t^s - C_i^s)] + J_a^s, \tag{A1}$$

$$J_{sc} = [\,J_{vc}\,(1-\sigma_c^s)\,\dot{c}\; + PS_c^s\,(C_i^s - C_c^s)], \tag{A2}$$

each expressed as a function of volume flow (J_{vt} or J_{vc}), as well as solute reflection coefficients (σ), permeability times surface area products (PS), and compartment concentrations (C). Because small and large solutes exert pressures differently, small solute concentrations were reparametrized as osmotic pressures (Π) using Van't Hoff's equation, while large solutes were reparametrized as protein osmotic pressures using Pappenheimer's empirical relationship (170). Reabsorption also includes an active solute flow term (J_a) to characterize metabolic tubule transport. The concentration term $\dot{c}$ is different for small and large solutes. For small solutes, when the ratio between the upstream and downstream concentrations (C_u^s and C_d^s, respectively) is near unity, then $\dot{c} \approx (C_u^s + C_d^s)/2$. Compared to global nonlinear transport equations in which convection and diffusion interact (43, 227), the linearization of the solute equation using this arithmetic mean provides a good approximation for a range of fluid flows when the diffusion profile does not significantly change (196, 274). For the range of flows observed in the renal cortex, this formulation works well for small solutes. However, as others have observed for general three-compartment models (202), the solute equation linearized with the arithmetic mean can predict unrealistic concentrations for macromolecules when tubule fluid reabsorption changes. As an alternate empirical linearization, the Taylor-Granger equation uses $\dot{c} \approx C_u^s$ to better approximate flows of large solutes through the interstitium (83, 269). When compared to global nonlinear equations, the Taylor-Granger approximation overestimates interstitial protein concentrations as J_{vt} is increased from baseline. Therefore, the present work assumes $\dot{c} = (C_u^s + C_d^s)/2$ for small solutes, and $\dot{c} = C_u^s$ for protein. Lymphatic solute flow (J_{vl}) is expressed as a product of interstitial solute concentration and constant lymph flow (J_{sl}),

$$J_{sl} = J_{vl}\, C_i^s. \qquad (A3)$$

Conservation of mass within the interstitial compartment implies,

$$J_{st} + J_{sd} = J_{sc} + J_{sl}, \qquad (A4)$$

where solute from distal cortical segments (J_{sd}) is regarded as a constant parameter. Using baseline parameters in Table 3.1, Newton's method was used to numerically solve *Eqs. 3*-5 and *Eqs. A1-4* for the variables J_{vt}, J_{vc}, and P_i as well as the variables J_{st}, J_{sc}, J_{sl}, and Π_i for each solute.

Baseline parameter values. Drawn from rat studies, Table 3.1 summarizes the pressure and flow values assumed to represent baseline conditions for a tubule, interstitium and surrounding capillary network. Baseline values for tubule hydrostatic and osmotic pressures, capillary hydrostatic and osmotic pressures, interstitial osmotic pressures, and distal flow were either assumed equal to reported values or estimated from data reported for control rats in benzolamide micropuncture studies (141, 164, 166, 277). Values for lymph flow and other solute parameters were drawn from control rats of other studies. Tubule and capillary hydrostatic pressures were assumed to be 13.7 and 13.5 mmHg, respectively (141, 277). To calculate tubule and capillary osmotic pressures exerted by each small solute (Π_t and Π_c), the product of temperature and universal gas constant (RT) of 19.404 L·mmHg·mmol^{-1} and Van't Hoff factors of 0.925 for Na^+, Cl^-, and HCO_3^- and 1.0 for glucose were assumed. Capillary solute concentrations (C_c) were assumed to equal the plasma concentrations of 154.4 mM Na^+, 105.5 mM Cl^-, 4.3 mM K^+, 28.1 mM HCO_3^- and 7.6 mM glucose (102, 209). Tubule solute concentrations (C_t) were assumed to be the mean of plasma and end-luminal fluid concentrations. The latter were determined from end luminal fluid to plasma concentration ratios 1.0, 1.2, 0.92, 0.18, and 0.034 for Na^+, Cl^-, K^+, HCO_3^- and glucose, respectively (102, 241). Tubule reflection coefficients (σ_t) for Na^+, Cl^-, K^+, HCO_3^-, glucose, and protein were assumed to be 0.70, 0.51, 0.56, 1.0, 1.0, and zero, respectively (6, 103, 115, 303). Capillary reflection coefficients (σ_c) were assumed to be near zero for each small solute

Table 3.1 Baseline parameter values for renal fluid model.

Parameter	Baseline
Tubule Osmotic Pressures (Π_t), mmHg	
Na^+	2771.0
Cl^-	2073.5
K^+	74.1
HCO_3^-	297.8
Glucose	76.2
Protein	0.0
Capillary Osmotic Pressures (Π_c), mmHg	
Na^+	2771.0
Cl^-	1893.6
K^+	77.2
HCO_3^-	504.4
Glucose	147.5
Protein	24.7
Interstitial Osmotic Pressures (Π_i), mmHg	
Na^+	2735.5 †
Cl^-	1896.2 †
K^+	74.6 †
HCO_3^-	503.7 †
Glucose	143.3 †
Protein	1.5
Tubule Reflection Coefficients (σ_t)	
Na^+	0.7
Cl^-	0.5
K^+	0.56
HCO_3^-	1.0
Glucose	1.0
Protein	1.0
Tubule Reflection Coefficients (σ_c)	
Na^+	0.0
Cl^-	0.0
K^+	0.0
HCO_3^-	0.0
Glucose	0.0
Protein	0.998
Hydrostatic Pressures (P), mmHg	
P_t	13.7
P_c	13.5
Distal and Lymphatic Fluid Flows, nl·min^{-1}	
J_{vd}	5.0
J_{vl}	0.031
Filtration Coefficients (K_f), nl·mmHg^{-1}·min^{-1}	
K_{ft}	0.157 †
K_{fc}	2.14 †

Baseline parameter values for three-compartment model consisting of tubule (*t*), interstitium (*i*), and capillary (*c*) compartments. †Numerically estimated from a more complete, nonlinear model incorporating both fluid and solute flow equations.

and 0.998 for protein (25, 305). For solute equations, tubule solute permeabilities were assumed to be 1.6, 1.4, 2.0, 0.35 and 0.033 μm·sec^{-1} for Na^+, Cl^-, K^+, HCO_3^- and glucose, respectively (6, 18, 22, 103). Following Williams Jr and Schafer (300), capillary permeabilities for Na^+, Cl^-, K^+, and HCO_3^- were assumed to be 10 μm·sec^{-1} while the capillary permeability for glucose was assumed to be half the value of the other solutes. The permeability times surface area product (*PS*) was calculated for each solute. Proximal tubule length was assumed to be 8 mm with a radius of 17.2 μm (103, 110). The surface area of the surrounding capillary network was assumed to be twice the cylindrical surface area of tubule (300). Active transport parameters (J_{sa}) for Na^+, Cl^-, K^+ were assumed to be 257, 155 and -4.61 pmol·min^{-1}·mm^{-1}, respectively (34). The maximum absorptive flux (J_{max}) for HCO_3^- and glucose were 265 and 100 pmol·min^{-1}·mm^{-1}, respectively, and the concentration for half-maximal proton excretion (K_m) is 11 and 1.32 mM (33, 184). With these values, active transport was calculated as a saturable function of luminal concentration, where $J_{sa} = J_{max} \cdot C_t/(K_m + C_t)$. Solute reabsorption values for the distal segment (J_{sd}) were assumed to be 330, 170, -26, 41.5, and 0.0 pmol·min^{-1} for Na^+, Cl^-, K^+, HCO_3^-, and glucose (52, 164, 165, 167). For the large protein species, the interstitial osmotic pressure (Π_i) was assumed to be 1.5 mmHg (141), and PS_t, J_{sd} and J_{sa} were assumed to be zero (198). With these values, PS_c for protein was numerically estimated to be 0.009 nl·min^{-1} using *Eqs. A1-4*. Lymph flow per nephron (J_{vl}) was estimated as a ratio of total kidney lymph flow ($J_{vl\ tot}$) to number of nephrons per kidney, which is given by $J_{vl} = (J_{vl\ tot} \cdot SNGFR)/GFR$. Baseline $J_{vl\ tot}$ was assumed to be 0.66 μl·min^{-1} (171). The glomerular filtration rate (*GFR*) and single nephron filtration rate (*SNGFR*) were assumed to be 1.10 ml·min^{-1} and 51.7 nl·min^{-1}, respectively (141). Distal flow (J_{vd}) was calculated as a product of single nephron filtration rate and the difference between the fractional fluid

reabsorption rates of late and early distal tubule. In a comparable rat study, the late and early fractional fluid reabsorption rates were measured as 0.91 and 0.81, respectively, when the single nephron filtration rate was 50.3 nl·min^{-1} (166). Finally, because simultaneous measurements have yet to be made, fluid filtration coefficients and interstitial osmotic pressures were estimated to yield baseline values appropriate for the three-compartment model. Newton's method was used to numerically solve *Eqs. 3*-5 and *Eqs. A1-4* using baseline parameters as well as equilibrium J_{vt}^{*} and P_i^{*} values, which were 26.7 nl·min^{-1} and 3.5 mmHg, respectively (141).

Altered parameter values used to simulate carbonic anhydrase inhibition. Table 3.2 summarizes treatment parameter values that were assumed to be equal to the reported values or estimated from the data available in four comparable micropuncture studies of rats administered 2 mg/kg of benzolamide to inhibit carbonic anhydrase (CA) in the tubule (141, 164, 166, 277). Tubule hydrostatic pressure (P_t) was reported to decreased to 13.4 mmHg after CA inhibition (277). The tubule fluid to plasma concentration ratios of chloride and bicarbonate decreased to 1.1 and 0.6, respectively (164). Using these ratios, treatment values for the tubule osmotic pressures of chloride and bicarbonate ($\Pi_t^{Cl^-}$ and $\Pi_t^{HCO_3^-}$) were calculated in same manner as corresponding baseline values. With CA inhibition, capillary hydrostatic pressure (P_c) was reported to increase to 16.3 mmHg, capillary protein osmotic pressure ($\Pi_c^{protein}$) was reported to increase to 25.3 mmHg, and interstitial protein osmotic pressure ($\Pi_i^{protein}$) was reported to decrease to 0.7 mmHg (141). The late and early fractional fluid reabsorption rates in distal tubule after CA inhibition were reported to be 0.80 and 0.67, respectively, when the single nephron filtration rate was 47.9 nl·min^{-1} (166). Calculated in same manner as its corresponding baseline value, the treatment value of distal flow (J_{vd}) was assumed to have increased to 6.0 nl·min^{-1}. These assumed and calculated values drawn from well-matched studies provided a set of

parameter perturbations that were sufficient for simulating carbonic anhydrase inhibition in the renal cortex. All other parameters values were assumed to remain unchanged from baseline (Table 3.1).

RESULTS

Representing the balance of tubule fluid reabsorption and capillary uptake graphically. Figure 3.3A illustrates that tubule fluid reabsorption (J_{vt}) decreases linearly with respect to interstitial hydrostatic pressure (P_i). The slope of this relationship is equal to $-K_{ft}$. The P_i -axis intercept of the reabsorption line represents the interstitial hydrostatic pressure required to drive J_{vt} to zero, and is equivalent to the inlet pressure illustrated in Fig. 3.2. In contrast to reabsorption, Fig. 3.3B illustrates that fluid uptake (J_{vc}) increases linearly with respect to P_i. The slope of this relationship is equal to K_{fc}. The P_i -axis intercept of the uptake line represents the interstitial hydrostatic pressure required to drive J_{vc} to zero, and is equivalent to the outlet pressure illustrated in Fig. 3.2. Figure 3.3C illustrates the emergence of equilibrium from the interaction of the lines representing tubule reabsorption and capillary uptake. To simplify, flow into the interstitium compartment from the distal nephron segments and flow out of the interstitium compartment via lymphatic vessels were neglected. Therefore, the intersection of these two lines (circle) represents the "balance point," where the reabsorption of fluid into the interstitium is equal to uptake by the capillaries (i.e., $J_{vt} = J_{vc}$). When the system is in steady state, the balance point represents equilibrium interstitial hydrostatic pressure (P_i^*) and tubule fluid reabsorption (J_{vt}^*).

Graphical analysis of cortical fluid balance with changes in total tubule or capillary pressures. Figure 3.4 illustrates how changes in total tubule pressure ($\hat{P}_t$, *Eq. 1*) and changes in

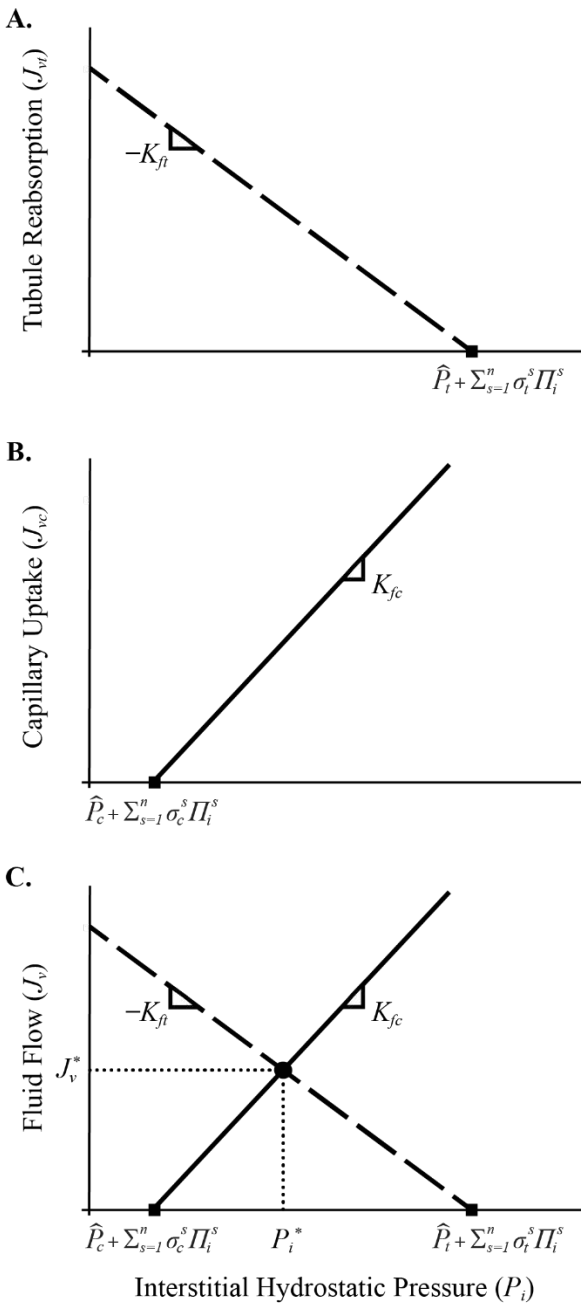

Figure 3.3 Graphical representation of interaction of tubule fluid reabsorption and capillary fluid uptake in three-compartment model. A: According to *Eq. 3*, tubule reabsorption (J_{vt}) decreases with interstitial hydrostatic pressure (P_i). The slope is $-K_{ft}$, and the intercept (square) is the equivalent inlet pressure in Fig. 3.2. B: According to *Eq. 4*, capillary uptake (J_{vc}) increases with P_i. The slope is K_{fc} and the intercept (square) is the equivalent outlet pressure in Fig. 3.2. C: In steady state, intersection (circle) represents the point where $J_{vt}=J_{vc}$. Dotted lines indicate equilibrium tubule fluid reabsorption (J_v^*) and equilibrium interstitial hydrostatic pressure (P_i^*).

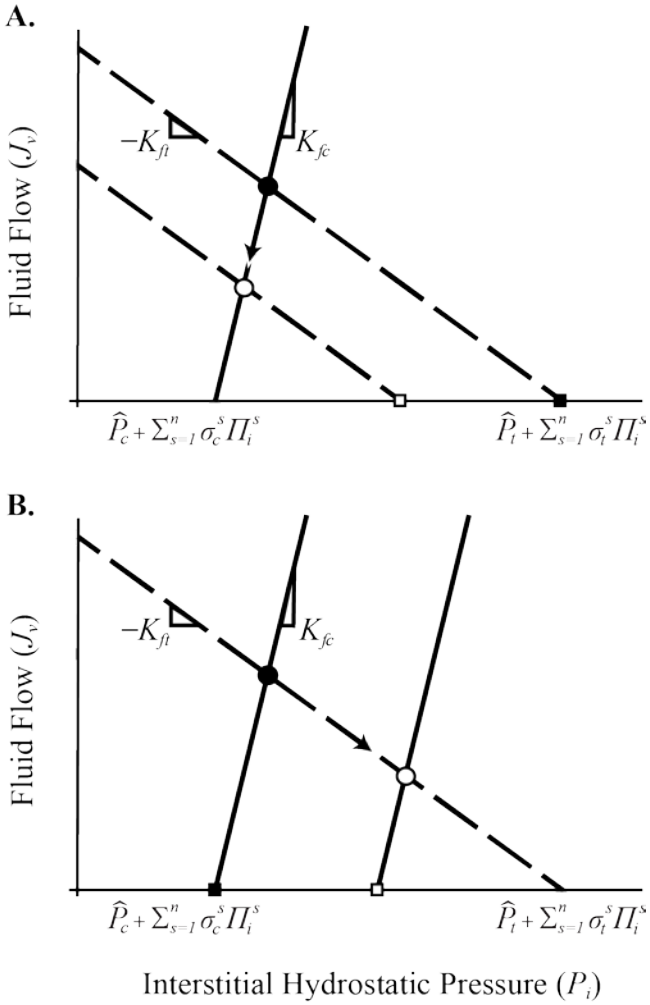

Figure 3.4 Changes in equilibrium when either total tubule pressure ($\hat{P}_t$) or total capillary pressure ($\hat{P}_c$) is altered in the three-compartment model. Equilibrium tubule reabsorption (J_v^*) and interstitial hydrostatic pressure (P_i^*) emerge at the intersection (closed circle) of the tubule reabsorption line (dashed, *Eq. 3*) and capillary uptake line (solid, *Eq. 4*). A: Decreasing $\hat{P}_t$ shifts the intercept of tubule reabsorption line to the left (closed to open square). As a result, the equilibrium point shifts (arrow from closed to open circle) such that both J_v^* and P_i^* decrease. B: Increasing $\hat{P}_c$ shifts the intercept of capillary fluid uptake line to the right (closed to open square). As a result, the equilibrium point shifts (arrow from closed to open circle) such that J_v^* decreases and P_i^* increases.

total capillary pressure ($\hat{P}_c$, *Eq. 2*) affect equilibrium tubule fluid reabsorption (J_{vt}^*) and interstitial hydrostatic pressure (P_i^*). Baseline equilibrium conditions are indicated by the intersection (closed circles) of lines representing tubule fluid reabsorption (dashed lines) and capillary fluid uptake (solid lines). Figure 3.4A illustrates how a decrease in $\hat{P}_t$ (due to a decrease in tubule hydrostatic pressure or increase in tubule osmotic pressures), shifts the P_i-axis intercept of the fluid reabsorption line to the left (closed to open square). Baseline equilibrium shifts to a new equilibrium point (arrow from closed to open circle). Thus, decreased total tubule pressure decreases both equilibrium tubule fluid reabsorption and interstitial hydrostatic pressure. Similarly, Fig. 3.4B illustrates how an increase in $\hat{P}_c$ (due to an increase in capillary hydrostatic pressure or decrease in capillary osmotic pressure), shifts the P_i-axis intercept of the fluid uptake line to the right (closed to open square). Baseline equilibrium shifts to a new equilibrium point (arrow from closed to open circle). Increased total capillary pressure thus decreases equilibrium reabsorption but increases interstitial hydrostatic pressure.

Representation of cortical fluid balance in terms of conductances. The equivalent circuit analogy in Fig. 3.2 yields expressions for composite fluid conductances for the three-compartment model. The effective fluid conductance of the two semipermeable barriers in series (K_{fe}) is

$$K_{fe} = \frac{K_{ft} K_{fc}}{K_{ft} + K_{fc}} . \qquad (9)$$

The relative tubule fluid conductance (K_{ftr}) and relative capillary fluid conductance (K_{ftr}),

$$K_{ftr} = \frac{K_{ft}}{K_{ft} + K_{fc}} , \qquad (10)$$

$$K_{fcr} = \frac{K_{fc}}{K_{ft} + K_{fc}}, \qquad (11)$$

have values between 0 and 1. From *Eqs. 10* and *11*, it can be demonstrated that $K_{ftr} + K_{fcr} = 1$.

General, algebraic formulas for equilibrium interstitial hydrostatic pressure and tubule reabsorption. At steady state (i.e., when interstitial inflow and outflow are balanced), the equilibrium interstitial hydrostatic pressure (P_i^*) has a simple algebraic formula when expressed in terms of relative tubule and capillary fluid conductances,

$$P_i^* = K_{ftr}\left(\hat{P}_t + \sum_{s=1}^{n} \sigma_t^s \Pi_i^s\right) + K_{fcr}\left(\hat{P}_c + \sum_{s=1}^{n} \sigma_c^s \Pi_i^s\right) + \frac{K_{ftr}\,K_{fcr}}{K_{fe}}(J_{vd} - J_{vl}). \quad (12)$$

The terms $\left(\hat{P}_t + \sum_{s=1}^{n} \sigma_t^s \Pi_i^s\right)$ and $\left(\hat{P}_c + \sum_{s=1}^{n} \sigma_c^s \Pi_i^s\right)$ are recognized as equivalent inlet and outlet pressures in Fig. 3.2 and the tubule fluid reabsorption and capillary uptake intercepts in Fig. 3.3. The effect of distal and lymphatic flows is modulated by $(K_{ftr}\,K_{fcr})/\,K_{fe}$, which also equals $1/(\,K_{ft} + K_{fc})$. By taking the partial derivative, the effect of each interstitial osmotic pressure on interstitial hydrostatic pressure is revealed to be modulated by $K_{ftr}\sigma_t^s + K_{fcr}\sigma_c^s$. For a small solute with σ_c^s near zero, the term modulating interstitial osmotic pressure simplifies to $K_{ftr}\sigma_t^s$. For a large solute, both σ_t^s and σ_c^s may be assumed to be near unity. In such case, the modulating term simplifies to $K_{ftr} + K_{fcr}$, which was shown above to be equal to one. Given $K_{ftr}\sigma_t^s \ll 1$, interstitial hydrostatic pressure is more sensitive to a change in the interstitial osmotic pressure of a large protein than a change in the interstitial osmotic pressure of a small solute. The equilibrium tubule fluid reabsorption (J_{vt}^*) also has a simple algebraic formula when expressed in terms of effective fluid conductance,

$$J_{vt}^* = K_{fe}\left[(\hat{P}_t - \hat{P}_c) + \sum_{s=1}^{n}(\sigma_t^s - \sigma_c^s)\,\Pi_i^s\right] - K_{ftr}(J_{vd} - J_{vl}). \quad (13)$$

The term $\left[(\hat{P}_t - \hat{P}_c) + \sum_{s=1}^{n}(\sigma_t^s - \sigma_c^s)\,\Pi_i^s\right]$ is recognized as the difference between equivalent inlet and outlet pressures in Fig. 3.2 and the difference between the tubule fluid reabsorption and capillary uptake intercepts in Fig. 3.3. The effect of distal and lymphatic flows is modulated by K_{ftr}. By taking the partial derivative, the effect of each interstitial osmotic pressure on reabsorption

is revealed to be modulated by the term $K_{fe}(\sigma_t^s - \sigma_c^s)$. For a small solute with σ_c^s near zero, the term modulating interstitial osmotic pressure simplifies to $K_{fe}\sigma_t^s$. For a large solute with σ_t^s and σ_c^s both near unity, the modulating term simplifies to zero. This suggests that interstitial osmotic pressures affect tubule fluid reabsorption, but large proteins do not.

Validating the algebraic formulas by comparing their predictions with reported data. Table 3.2 compares the measured and predicted changes in equilibrium tubule fluid reabsorption (J_{vt}^*) and interstitial hydrostatic pressure (P_i^*) caused by solute transport inhibition. Treating rats with benzolamide to inhibit carbonic anhydrase (CA) in the tubules has been reported to cause predominant changes in tubule pressures as well as changes in capillary pressures, interstitial protein osmotic pressure, and distal flow. When accounting for all of these reported changes (Table 3.2, Prediction A), the decreased values of J_{vt}^* and P_i^* predicted by the algebraic formulas (*Eqs. 12* and *13*) were within the reported SD of the measured J_{vt}^* and P_i^* values in CA-inhibited rats. Although unavailable, information of how CA inhibition altered lymph flow and the interstitial osmotic pressures of small solutes was unnecessary for making an accurate prediction. When the change in distal flow was neglected (Table 3.2, Prediction B), the decrease in both J_{vt}^* and P_i^* was still predicted with accuracy. However, when the change in interstitial protein osmotic pressure was neglected (Table 3.2, Prediction C), only J_{vt}^* was predicted to be within the reported SD. When only accounting for the changes in tubule pressures (Table 3.2, Prediction D), the 35% reduction in J_{vt}^* was still predicted within the reported SD. However, P_i^* was underestimated by approximately 1 mmHg.

Model sensitivity analysis. Figure 3.5 presents the baseline sensitivity indices (*SI*) for equilibrium interstitial hydrostatic pressure (P_i^*) and tubule fluid reabsorption (J_{vt}^*) of the three-compartment model. The solid bars indicate the sensitivity indices derived from the algebraic

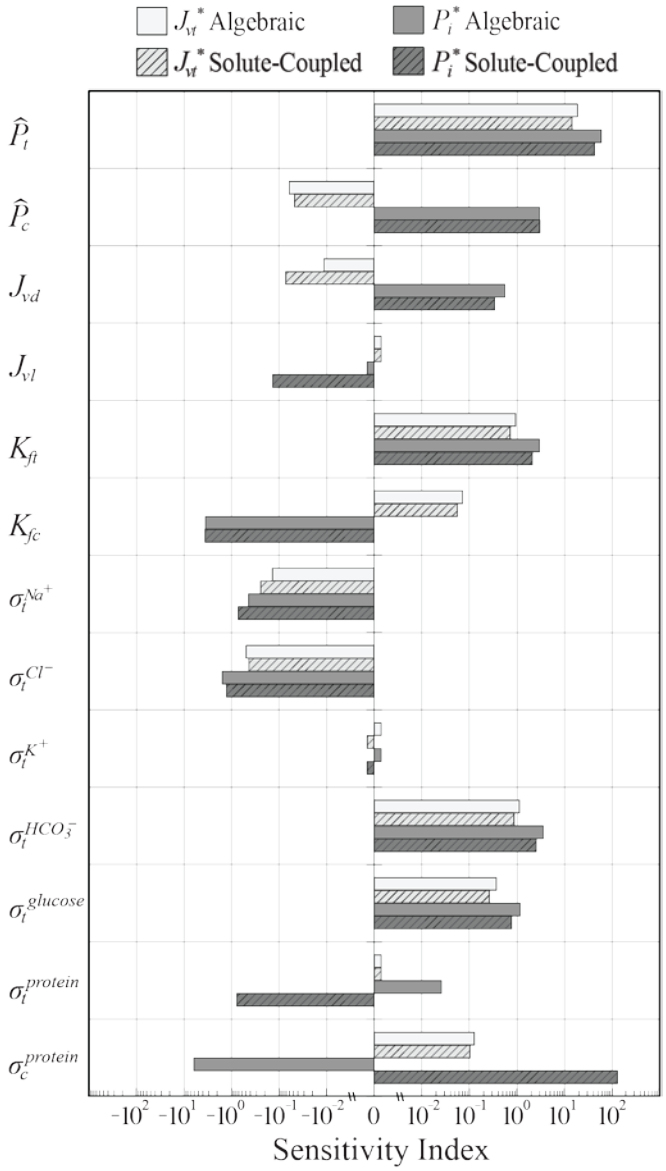

Figure 3.5 Baseline sensitivity indices (*SI*) of tubule fluid reabsorption (J_{vt}^*) and interstitial hydrostatic pressure (P_i^*) to properties of the renal cortex. Bars indicate both signs and magnitudes of J_{vt}^* and P_i^* sensitivities for the algebraic formulas (solid bars, *Eqs. 12* and *13*) and the nonlinear, solute-coupled model (hatched bars). Properties at boundaries include total tubule pressure ($\hat{P}_t$), total capillary pressure ($\hat{P}_c$), and fluid flows from distal nephron segments (J_{vd}) and cortical lymphatic vessels (J_{vl}). Properties of tubule (t) and capillary (c) barriers include fluid filtration coefficients (K_f) and solute reflection coefficients (σ). For $|SI| > 1$, the fractional change in the variable is greater than the fractional change in the parameter (*Eq. 6*). J_{vt}^* and P_i^* are interpreted to be insensitive to the parameter when $|SI| < 10^{-2}$.

Table 3.2 Comparison of predicted and measured values of equilibrium tubule fluid reabsorption and interstitial hydrostatic pressure after carbonic anhydrase inhibition.

	Altered Parameter Values after CA Inhibition	J_{vt}^*	P_i^*
		nl·min^{-1}	mmHg
Measured	P_t = 13.4 mmHg (277), $\Pi_t^{Cl^-}$ = 1988 mmHg (164), $\Pi_t^{HCO3^-}$ = 403 mmHg (164) P_c = 16.3 mmHg (141), $\Pi_c^{protein}$ = 25.3 mmHg (141) $\Pi_i^{protein}$ = 0.7 mmHg (141) J_{vd} = 6.0 nl·min^{-1} (166)	17.7±3.6 (141)	1.1±0.5 (141)
Prediction A	P_t = 13.4 mmHg (277), $\Pi_t^{Cl^-}$ = 1988 mmHg (164), $\Pi_t^{HCO3^-}$ = 403 mmHg (164) P_c = 16.3 mmHg (141), $\Pi_c^{protein}$ = 25.3 mmHg (141) $\Pi_i^{protein}$ = 0.7 mmHg (141) J_{vd} = 6.0 nl·min^{-1} (166)	17.0‡	1.3‡
Prediction B	P_t = 13.4 mmHg (277), $\Pi_t^{Cl^-}$ = 1988 mmHg (164), $\Pi_t^{HCO3^-}$ = 403 mmHg (164), P_c = 16.3 mmHg (141), $\Pi_c^{protein}$ = 25.3 mmHg (141) $\Pi_i^{protein}$ = 0.7 mmHg (141)	17.1‡	0.9‡
Prediction C	P_t = 13.4 mmHg (277), $\Pi_t^{Cl^-}$ = 1988 mmHg (164), $\Pi_t^{HCO3^-}$ = 403 mmHg (164) P_c = 16.3 mmHg (141), $\Pi_c^{protein}$ = 25.3 mmHg (141) J_{vd} = 6.0 nl·min^{-1} (166)	17.0‡	2.1
Prediction D	P_t = 13.4 mmHg (277), $\Pi_t^{Cl^-}$ = 1988 mmHg (164), $\Pi_t^{HCO3^-}$ = 403 mmHg (164)	17.4‡	-0.3

‡ Predicted results within the measured SD. Data sources are indicated in parenthesis.

Predictions of algebraic formulas (*Eqs. 12* and *13*) were compared to measured changes in equilibrium tubule fluid reabsorption (J_{vt}^*) and interstitial hydrostatic pressure (P_i^*) resulting from solute transport inhibition. Measured baseline and treatment parameters values were either assumed to equal reported values or estimated from data reported in micropuncture studies of rats treated with benzolamide to inhibit carbonic anhydrase (CA) in the tubule (141, 164, 166, 277). Ichikawa and Kon (141) reported J_{vt}^* decreased to 17.7±3.6 nl·min^{-1} and P_i^* decreased to 1.1±0.5 mmHg from baseline after CA inhibition. Four cases were investigated. A: Prediction accounting for all reported changes, i.e., tubule hydrostatic and osmotic pressures (P_t, $\Pi_t^{Cl^-}$ and $\Pi_t^{HCO3^-}$), capillary hydrostatic and protein osmotic pressures (P_c and $\Pi_c^{protein}$), interstitial protein osmotic pressure ($\Pi_i^{protein}$), and distal flow (J_{vd}). B: Prediction neglecting the distal flow change. C: Prediction neglecting the interstitial protein osmotic pressure change. D: Prediction accounting for only the tubule pressure changes. In each case, *Eqs. 12* and *13* predicted J_{vt}^* within the reported SD.

formulas, which assume interstitial osmotic pressures remain constant as another parameter is changed (*Eqs. 12* and *13*). The hatched bars indicate the sensitivity indices derived from the more complete nonlinear solute-coupled model, which accounts for the flow-dependent change in each interstitial osmotic pressure. With respect to total tubule pressure or total capillary pressures, the sensitivity indices derived from the algebraic formulas have the same sign and similar magnitude as the sensitivity indices derived from the nonlinear solute-coupled model. The small differences in magnitudes suggest that neglecting the additional changes to interstitial osmotic pressures when total tubule and capillary pressures are perturbed has little effect. The sensitivity indices indicate that both J_{vt}^* and P_i^* are highly sensitive to changes in total tubule pressure. Notably, both J_{vt}^* and P_i^* have positive sensitivity indices, indicating that increases in total tubule pressure increase both J_{vt}^* and P_i^*. In contrast, sensitivity indices indicate that J_{vt}^* and P_i^* are less sensitive to changes in total capillary pressure. Perhaps more importantly, J_{vt}^* has a negative sensitivity index, and P_i^* has a positive sensitivity index, indicating that increases in total capillary pressure decreases J_{vt}^* and increases P_i^*. With respect to the fluid filtration coefficients and solute reflection coefficients, the sensitivity indices derived from the algebraic formulas are for the most part consistent with the sensitivity indices derived from the nonlinear solute-coupled model. However, P_i^* predicted by the nonlinear solute-coupled model is highly sensitive to the capillary protein reflection coefficient. With respect to distal and lymphatic flows, sensitivity indices derived from the algebraic formulas have the same sign as those derived from the nonlinear solute-coupled model. The sensitivity index of P_i^* to lymph flow predicted by the nonlinear solute-coupled model, however, is several orders of magnitude higher than that predicted by the algebraic formula, indicating that changes in lymph flow has a large effect on interstitial osmotic pressures, particularly via changes in large proteins.

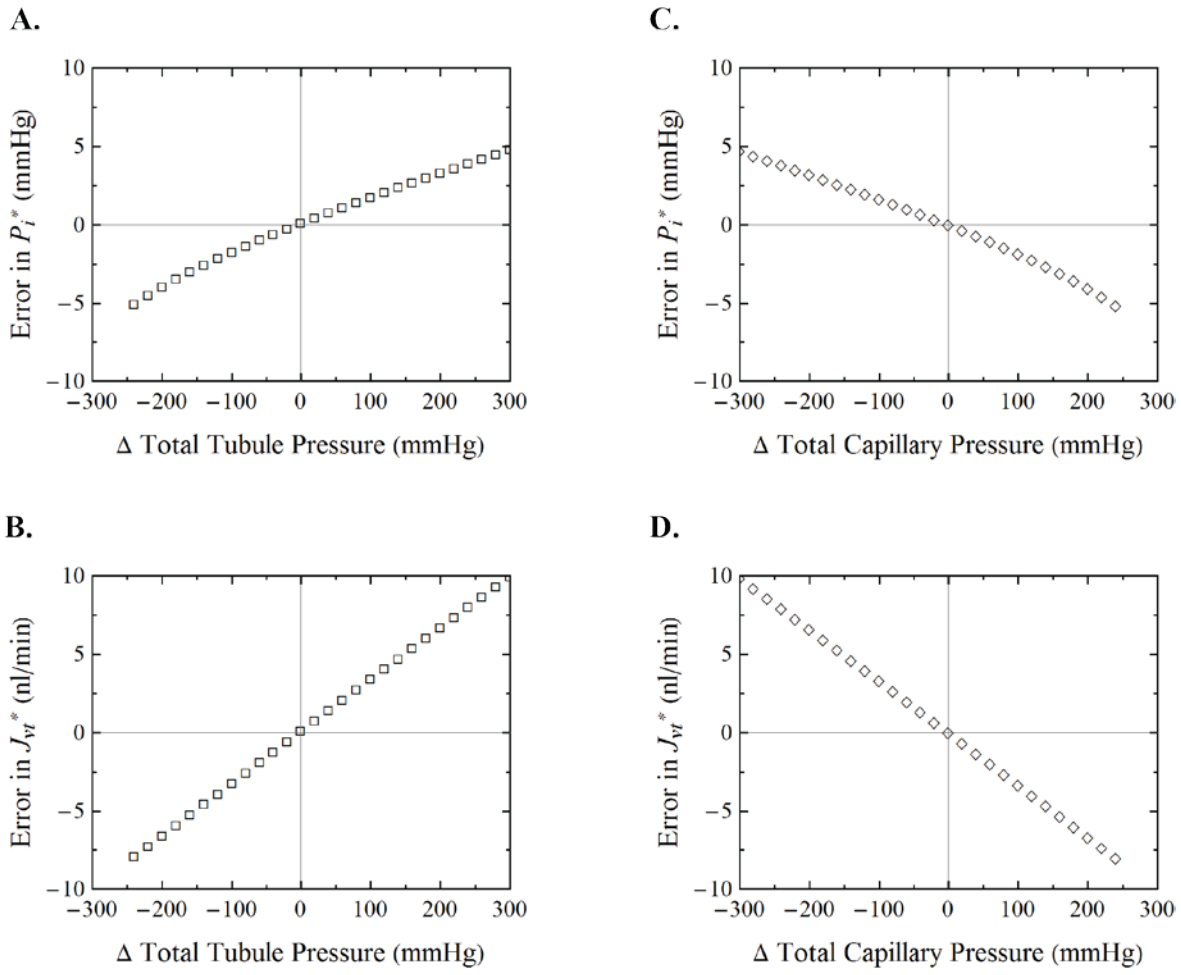

Figure 3.6 Error of approximation for equilibrium interstitial hydrostatic pressure (P_i^*) and tubule fluid reabsorption (J_{vt}^*). Using baseline values (Table 3.1), error is calculated as the difference between the results of linear algebraic model (*Eq. 12* and *13*) that assumes constant interstitial osmotic pressures and the more complete nonlinear solute-coupled model that includes solute flow equations. A & B: Errors for P_i^* and J_{vt}^* as total tubule pressure ($\hat{P}_t$) is changed (□). C & D: Errors for P_i^* and J_{vt}^* as total capillary pressure ($\hat{P}_c$) is changed (◇). Errors are zero when the predicted osmotic pressures of the nonlinear solute-coupled model are equal to the assumed osmotic pressures in the algebraic formulas.

Error of algebraic approximations quantified by comparing results to a more complete nonlinear model that includes solute flows. Figure 3.6 illustrates the error in the equilibrium interstitial hydrostatic pressure and tubule fluid reabsorption predicted by the algebraic formulas (*Eqs. 12* and *13*) as a function of total tubule pressure and total capillary pressures. The error is zero at the origin (i.e., 0 mmHg), because the algebraic formulas are equivalent to the results of the more complete nonlinear solute-coupled model that treats interstitial osmotic pressures as variables. Because the algebraic formulas do not account for the concomitant changes in interstitial osmotic pressures, errors grow as tubule and capillary pressures deviate from baseline values. The results in Fig. 3.6 only apply for the particular baseline parameter values listed in Table 3.1. Algebraic formulas for errors in equilibrium interstitial hydrostatic pressure (P_i^*) and tubule fluid reabsorption (J_{vt}^*) can provide more general results,

$$Error\ in\ P_i^* \approx \left(K_{ftr}\frac{\partial \sum_{s=1}^{n}\sigma_t^s\Pi_i^s}{\partial Par} - K_{fcr}\frac{\partial \sum_{s=1}^{n}\sigma_c^s\Pi_i^s}{\partial Par}\right)\cdot \Delta Par, \quad (14)$$

$$Error\ in\ J_{vt}^* \approx -K_{fe}\left(\frac{\partial \sum_{s=1}^{n}\sigma_t^s\Pi_i^s}{\partial Par} - \frac{\partial \sum_{s=1}^{n}\sigma_c^s\Pi_i^s}{\partial Par}\right)\cdot \Delta Par, \quad (15)$$

where *Par* represents either total tubule pressure, total capillary pressure, distal flow, or lymphatic flow. *Equations 14* and *15* indicate that the errors of approximation depend on how much one of these four parameters are perturbed (ΔPar), as well as the sensitivities of effective interstitial osmotic pressures to the parameter (i.e., $\partial \sum_{s=1}^{n}\sigma_t^s\Pi_i^s/\partial Par$ and $\partial \sum_{s=1}^{n}\sigma_c^s\Pi_i^s/\partial Par$). If the perturbation of the parameter is relatively small or if the effective interstitial osmotic pressures are insensitive to the parameter, then the error is minimal.

Tubule fluid reabsorption can increase or decrease with respect to interstitial hydrostatic pressure depending on whether tubule or capillary pressures are altered. Figure 3.7 illustrates that tubule fluid reabsorption can either increase or decrease with interstitial hydrostatic pressure

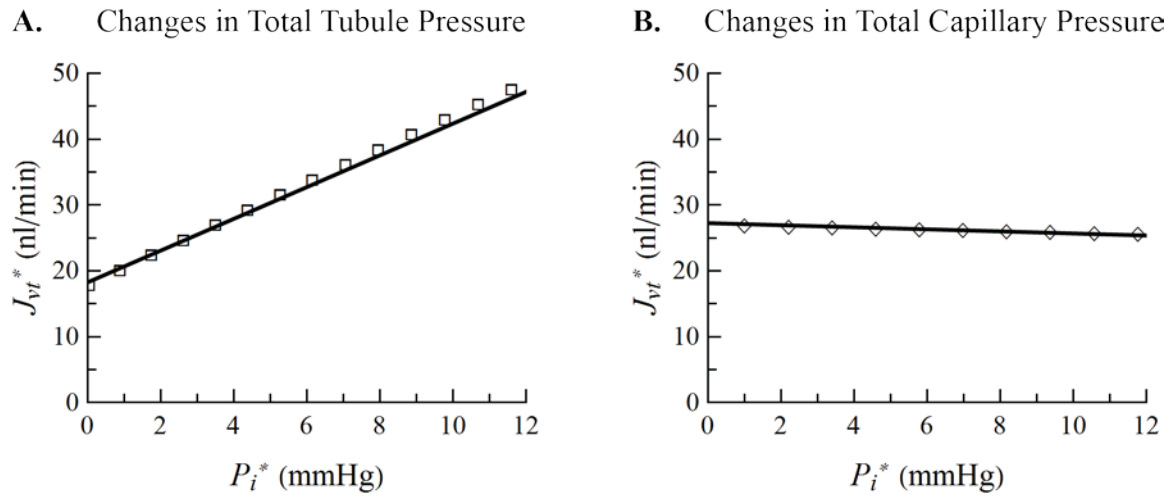

Figure 3.7 Predicted correlations of equilibrium tubule fluid reabsorption (J_{vt}^*) with equilibrium interstitial hydrostatic pressures (P_i^*). Lines represent parametric plots of algebraic formulas (*Eqs. 12* and *13*) as either $\hat{P}_t$ or $\hat{P}_c$ are altered. Tokens represent results of more complete nonlinear solute-coupled model. A: For changes in total tubule pressure, tubule fluid reabsorption is positively correlated with interstitial hydrostatic pressure. The slope of its line equals K_{fc}. The pressure-flow relationship exhibits small error when compared to the nonlinear solute-coupled model over a wide range of total tubule pressure (□). B: For changes in total capillary pressure, tubule fluid reabsorption is negatively correlated with interstitial hydrostatic pressure. The slope of its line equals $-K_{ft}$. The pressure-flow relationship exhibits small error when compared to the nonlinear solute-coupled model over a wide range of total capillary pressure (◇).

depending on how the system is perturbed. Figure 3.7A illustrates that the algebraic formulas (line) predict that increases in total tubule pressures cause an increase in both tubule fluid reabsorption and interstitial hydrostatic pressure. This result is robust, because the algebraic formulas reproduce the results of the more complete nonlinear solute-coupled model (open squares) with little error. From *Eq. 7*, the slope of this relationship is equal to K_{fc}. Figure 3.7B illustrates that the algebraic formulas (line) predict increased total capillary pressure causes a decrease in tubule fluid reabsorption, but an increase in interstitial hydrostatic pressure. This result is also robust because the algebraic formulas reproduce the results of the more complete nonlinear solute-coupled model (open diamonds) with little error. From *Eq. 8*, the slope of this relationship is equal to $-K_{ft}$.

DISCUSSION

The present work is the first to develop and validate algebraic formulas that predict interstitial hydrostatic pressure and tubule fluid reabsorption in the renal cortex. By incorporating the interstitium as an intervening third compartment, interactions among tubule and capillary properties as well as lymphatic and distal flows could be examined. The present work further demonstrates how algebraic methods are used in lieu of numerical approaches for the purpose of obtaining insights about how steady-state behaviors emerge from the interactions of a complex system. Specifically, the resulting algebraic formulas revealed three novel insights for studying cortical fluid balance. *First*, tubule fluid reabsorption is either positively or negatively correlated with interstitial hydrostatic pressure depending on whether tubule or capillary pressures are altered (Fig. 3.7). *Second*, interstitial hydrostatic pressure and tubule fluid reabsorption are governed by groupings of filtration coefficients that are not apparent when using numerical approaches (*Eqs. 9-11*). *Third*, interstitial hydrostatic pressure and tubule fluid reabsorption can be predicted with minimal error without having to invoke the solute flow equations of more complete nonlinear models (Fig 3.6). In addition to these novel findings, the discussion below details the strategies and assumptions used in developing a basic linear three-compartment model for the renal cortex, which cardiovascular and renal researchers can readily extend or modify when investigating particular processes and adaptations affecting bulk fluid flow through the renal cortex.

Algebraic formulas were derived by assuming interstitial hydrostatic pressure and tubule fluid reabsorption are emergent behaviors of cortical fluid balance. While nonlinear models coupling fluid and solute flows can predict all interstitial hydrostatic and osmotic pressure variables numerically (136, 292), the present work demonstrates that algebraic formulas can be obtained when fluid flows are uncoupled from solute flows. Limiting a model to either fluid flow

equations (*Eqs. 1-5*) or solute flow equations (*Eqs. A1-A4*) will eliminate the nonlinearities that arise from their interaction, but at the cost of reducing the number of variables that can be predicted. Such a simplification imposes a need to choose which interstitial property to regard as a constant parameter and which to retain as a variable. In a three-compartment model incorporating only solute flow equations, Williams and Schafer (300) derived algebraic formulas for interstitial osmotic pressures. These approximations were validated by assuming tubule fluid reabsorption and interstitial hydrostatic pressure were constant and comparing their results to a more complete, nonlinear model that coupled fluid and solute flows. A complementary strategy was taken in the present work (Figs. 3.6 and 3.7). By treating interstitial osmotic pressures as constant parameters, novel algebraic formulas for equilibrium tubule fluid reabsorption and interstitial hydrostatic pressure were obtained from a linear, three-compartment fluid model having a constrained scope.

To ensure model components were necessary and sufficient, the scope of the present work was constrained to the fluid flow through the cortical interstitium. The model includes inflow from the proximal tubule compartment and distal nephron segments and outflow from peritubular capillaries and lymphatic vessels (*Eq. 5*). Although regulation is beyond the scope of the present work, the feedback mechanisms involving local or global signaling ultimately work through the parameters appearing in the algebraic formulas (*Eqs. 12* and *13*). Control of efferent arteriolar resistance, for instance, alters capillary hydrostatic and protein osmotic pressures (212). Active solute transport alters tubule hydrostatic and osmotic pressures (149, 164). Fluid flows from distal nephron segments and into cortical lymphatic vessels may also be regulated (154, 231). Although feedback mechanisms are excluded to develop a basic, general model for cortical fluid balance, their effects on tubule fluid reabsorption and interstitial hydrostatic pressures can still be predicted by manipulating the pressure and flow parameters at the model's boundaries. In contrast to

previous organ or nephron models (40, 208), the present model is circumscribed by equations that characterize fluid flows into and out of the cortical interstitium.

To obtain general algebraic formulas, pressure-flow relationships were assumed to be linear. Tubule fluid reabsorption and capillary uptake were both characterized by standard linear flow equations (179, 301). Properties at a lower hierarchical level (e.g., intra-epithelial compartments) are subsumed within the filtration coefficients (K_{fc} and K_{ft}) and reflection coefficients (σ_t and σ_c). As in previous models (76, 136, 292), the transcapillary pressure-flow relationship was assumed to be linear. This assumption is supported by reports that K_{fc} remains nearly constant with significant perturbations of capillary fluid uptake induced by transport inhibition (141, 276) and volume expansion (30, 220). Investigators, however, have reported that K_{fc} increases after volume expansion (171, 239). At the tubule barrier, filtration and reflection coefficients have been reported to remain constant for small perturbations (116). Some have nonetheless speculated that K_{ft} and σ_t become pressure-sensitive when the transmural hydrostatic pressure is high (158, 292). In such a case, algebraic formulas would be valid for physiologic ranges in which the pressure-flow relationship remains sufficiently linear. To extend the use of algebraic formulas when nonlinearities in the pressure-flow relationship are significant, piecewise linearization may be used to better approximate the system by assigning a different value to a parameter (such as K_{ft} or σ_t) for each defined pressure range. Although treating the system as piecewise linear reduces prediction error, more information is required *a priori* (274).

To examine the predominant interactions governing fluid flow through the renal cortex, the present model was lumped into three compartments. Similar to previous compartment models (13, 224, 300), the cortical interstitium was assumed to be a fixed-volume, well-mixed compartment in steady state. To the extent unstirred layers are present and interstitial pressures are not uniform,

tubule reabsorption would be underestimated (26). Similarly, the physical properties of capillary and tubule compartments were also lumped. Because the difference between capillary hydrostatic and protein osmotic pressures has been argued to be nearly constant along length of vessel network (30, 171), $\hat{P}_c$ in *Eq. 2* is used to characterize the total pressure in the capillaries. Although assuming a single pressure may lead to an overestimation of capillary uptake, this approach avoids numerical methods required to address changes in pressures along vessel length (76). In the tubule, osmotic pressures change exponentially down the length of the tubule as a result of solute transport processes; and so numerical methods have been applied to more accurately account for these changes. However, since the purpose of the model in the present work is to identify the predominant parameters interactions governing steady-state behaviors, $\hat{P}_t$ in *Eq. 1* is used to approximate the total effective osmotic pressure in the tubule compartment. This approximation, however, results in tubule fluid reabsorption being slightly overestimated. As with other models (76, 301), single fluid flow pathways across tubule and capillary barriers were assumed, and structural heterogeneities (e.g. variations within the interstitium, capillary fenestrations, and tubule cell types) were neglected. Although the present model can be extended to address such complexities (302), adding more pathways and compartments would diminish the interpretive clarity exhibited by *Eqs. 12* and *13*.

The resulting algebraic formulas provide valid predictions for most parameter perturbations, despite neglecting changes in the interstitial osmotic pressures exerted by small solutes. Interstitial osmotic pressures were treated as constant parameters to derive algebraic formulas for equilibrium interstitial hydrostatic pressure (P_i^*) and tubule fluid reabsorption (J_{vt}^*) from the fluid flow equations. By integrating fluid and solute flow equations, interstitial osmotic pressures can be treated as variables. Parameter perturbations in the nonlinear solute-coupled

model therefore have additional effects on P_i^* and J_{vt}^* via changes in interstitial osmotic pressures. For most perturbations, however, neglecting these additional effects does not fundamentally alter system behavior. As illustrated in Fig. 3.5, the normalized sensitivities of P_i^* and J_{vt}^* to parameter perturbations exhibit the same trends as the nonlinear solute-coupled model. The algebraic formulas, however, do not correctly predict sensitivities of P_i^* to protein reflection coefficients. In particular, P_i^* in the nonlinear solute-coupled model is highly sensitive to changes in the capillary protein reflection coefficient (σ_c). This relatively high sensitivity is due to the higher sensitivity of P_i^* to large proteins than to small solutes. This particularly high sensitivity suggests that predictive models evaluating the effects of capillary protein permeabilities on P_i^* may also need to account for changes in interstitial protein osmotic pressure. Nonetheless, valid predictions may be obtained for most perturbations when the interstitial osmotic pressures exerted by small solutes are neglected.

Approximation errors are small for ranges of tubule and capillary pressures observed during experiments. Figure 3.6 indicates that the errors in equilibrium interstitial hydrostatic pressure (P_i^*) and tubule fluid reabsorption (J_{vt}^*) predicted by the algebraic formulas (*Eqs. 12* and *13*) are small when changing total tubule and capillary pressures over a wide range. For a 60 mmHg decrease in total tubule pressure typical of transport inhibition (141, 166), error of predicted P_i^* and J_{vt}^* would be −1 mmHg and −2 nl·min^{-1}, respectively. For a 20 mmHg increase in total capillary pressure typical of acute volume expansion (30, 306), errors would be even smaller. Such approximation errors are comparable to standard deviations reported in experimental studies (30, 141). The relatively small error is also reflected in Fig. 3.7 by the similarity of predictions made by the algebraic formulas and those of the more complete nonlinear solute-coupled model. These conclusions are based on predictions assuming the parameter values in Table 3.1. To generalize

results in contexts where parameter values might be different, approximation error formulas (*Eqs. 14* and *15*) can indicate when changes in interstitial osmotic pressures may be neglected. For given perturbations in either total tubule or capillary pressure, errors in P_i^* and J_{vt}^* depend on the values of filtration coefficients and how sensitive effective interstitial osmotic pressures are to perturbations. Taken together, the present work demonstrates that the common practice of including solute flow equations to predict tubule fluid reabsorption may not always be necessary.

Algebraic formulas predict steady-state trends observed in a wide array of experiments that alter capillary pressures. As indicated by *Eqs. 12* and *13* and illustrated in Fig. 3.7B, the algebraic formulas predict lower equilibrium tubule fluid reabsorption (J_{vt}^*) and elevated interstitial hydrostatic pressure (P_i^*) in response to an increase in total capillary pressure. Early reports indicated that acute volume expansion results in a predominant increase in total capillary pressure through an increase in capillary hydrostatic pressure and decrease in protein osmotic pressure (42, 157). Numerous volume expansion studies subsequently reported decreases in J_{vt}^* and increases in P_i^* (140, 152), with some notably exhibiting these trends without confounding effects of a changing ultrafiltration rate (151, 220, 276). Renal vein constriction has been reported to increase capillary hydrostatic pressure and decrease protein osmotic pressure, resulting in lower J_{vt}^* in rats (93) and elevated P_i^* in dogs (49). Aortic constriction can also cause a decrease in capillary protein osmotic pressure that lowers J_{vt}^* and elevates P_i^* (93, 140, 219). Conversely, when capillary protein osmotic pressure is increased, J_{vt}^* increases and P_i^* decreases (93, 111, 116, 117, 180, 221, 261). Taken together, the findings of these studies suggest J_{vt} varies inversely with P_i^* when the predominant perturbation is in capillary pressures. These observed trends are consistent with an assertion that interstitial hydrostatic pressure appears to *inhibit* tubule fluid reabsorption. Reported

correlations thus provide a measure of validation for the inverse correlation between J_{vt}^* and P_i^* that is predicted by the model when capillary pressures are changed (Fig. 3.7B).

Algebraic formulas predict steady-state trends observed in a wide array of experiments that alter tubule pressures. As indicated by *Eqs. 12* and *13* and illustrated in Fig. 3.7A, the algebraic formulas predict elevation of both equilibrium tubule fluid reabsorption (J_{vt}^*) and interstitial hydrostatic pressure (P_i^*) in response to an increase in total tubule pressure. Ureteral occlusion has been reported to cause a precipitous rise in tubule hydrostatic pressure and an increase P_i^* (104, 222). In perfused isolated tubules, increased luminal hydrostatic pressure results in increased J_{vt}^* (296). Decreasing tubule osmotic pressures exerted by Na^+ and Cl^- during in situ perfusion increases J_{vt}^* (6, 116). Conversely, increasing tubule osmotic pressures by inhibiting Na^+/H^+ exchange (284, 290) or glucose transport (29, 295) decreases J_{vt}^*. Similarly, increasing tubule osmotic pressure exerted by HCO_3^- with carbonic anhydrase inhibitors has been reported to decrease J_{vt}^* (55, 114, 164, 191, 206, 277). Ichikawa and Kon (141) reported carbonic anhydrase (CA) inhibition decreased both J_{vt}^* and P_i^*. Taken together, the findings of these studies suggest J_{vt}^* varies proportionally with P_i^* when the predominant perturbation is total tubule pressure. These experimentally observed trends are consistent with an assertion that interstitial hydrostatic pressure appears to *enhance* tubule fluid reabsorption. Reported correlations thus provide a measure of validation for the correlation between J_{vt}^* and P_i^* that is predicted by the model when the total tubule pressure is changed (Fig. 3.7A).

The validity of the algebraic formulas is exhibited by their accurate prediction of measured changes in equilibrium tubule fluid reabsorption and interstitial hydrostatic pressure. Micropuncture studies of rats treated with benzolamide to inhibit carbonic anhydrase (CA) in tubules have reported changes in tubule pressures, capillary pressures, interstitial protein osmotic

pressure, and distal flow (141, 164, 166, 277). To our best knowledge, there is no information available on how benzolamide alters the interstitial osmotic pressures of small solutes. Nonetheless, when accounting for the known parameter perturbations (Table 3.2, Prediction A), the algebraic formulas (*Eqs. 12* and *13*) predicted values of J_{vt}^* and P_i^* well within the SD of the measured values reported by Ichikawa and Kon (141). This result suggests that neglecting changes in the interstitial osmotic pressures of small solutes does not impact predictive accuracy. However, neglecting interstitial protein osmotic pressure changes does diminish the ability to accurately predict P_i^* (Table 3.2, Prediction C). If tubule pressures are the only parameters changed from baseline (Table 3.2, Prediction D), then the algebraic formulas still predict a decrease in both J_{vt}^* and P_i^*. In this case, however, J_{vt}^* is predicted accurately, and P_i^* is somewhat underestimated. The predicted 35% decrease in J_{vt}^* in the present study is also consistent with the predicted 39% decrease in J_{vt}^* reported by Weinstein et. al. (294) for a case of complete carbonic anhydrase inhibition in a nonlinear tubule model incorporating both fluid and solute flow equations. Taken together, model validation suggests that the three-compartment model can provide a simplified, alternative approach for studying the effects of tubule perturbations on cortical fluid balance.

The emergent steady-state behaviors of the three-compartment model are governed by effective and relative fluid conductances. Characterizing the three-compartment model in terms of resistance to fluid flow between compartments (Fig. 3.2) revealed interactions among filtration coefficients. Groups of interacting filtration coefficients were reparametrized as composite fluid conductances. Equilibrium tubule fluid reabsorption was thus found to be modulated by an effective fluid conductance (K_{fe}, *Eq. 9*) formed by tubule and capillary barriers in series. Equilibrium interstitial hydrostatic pressure is governed by both the relative tubule fluid conductance (K_{ftr}, *Eq. 10*) and the relative capillary fluid conductance (K_{fcr}, *Eq. 11*). If K_{ft} is lower

than K_{fc} by two orders of magnitude, then K_{fe} (*Eq. 9*) may be approximated by K_{ft} with negligible error. This approximation is consistent with mathematical models that neglect the capillary barrier and assume reabsorption is governed solely by K_{ft} (116, 273). However, if the K_{ft} is lower than K_{fc} by only one order of magnitude, then more error would be incurred with this assumption. Some support for K_{ft} being lower than K_{fc} by only one order of magnitude is found in transport inhibition studies that reported modest declines in interstitial hydrostatic pressure with reduced total tubule pressure (141, 164). If K_{ft} were instead two orders of magnitude lower, then the relative tubule conductance (K_{ftr}, *Eq. 10*) would be very small, and interstitial hydrostatic pressure would not have been significantly impacted. To our best knowledge, values of K_{ft} and K_{fc} have never been estimated simultaneously in a single experiment. In rats, K_{fc} values have been estimated to be within the range of 1.2 to 6.2 $nl \cdot min^{-1} \cdot mmHg^{-1}$ (123, 141, 201, 276). Tubule hydraulic conductance (L_p) has been estimated to be within the range of 7 to 21 $ml \cdot s^{-1} \cdot cmH_20^{-1} \cdot cm^{-2}$ (80, 116, 117, 172, 230, 235, 280, 281). Given the surface area assumed in this study, K_{ft} could have values between 0.05 to 0.15 of $nl \cdot min^{-1} \cdot mmHg^{-1}$. The values of K_{ft} and K_{fc}, therefore, could differ between one and two orders of magnitude. Further knowledge of their relative values is thus required to determine when the capillary barrier can be neglected.

The fluid conductance terms modulating distal flow provide guidance for future research. The fluid delivered to the cortical interstitium from distal nephron segments is considered large enough to impact cortical fluid balance (239, 276) and was therefore included in the three-compartment model (Fig. 3.1). When distal flow (J_{vd}) is elevated, the model predicts decreased tubule fluid reabsorption and increased interstitial hydrostatic pressure (Fig. 3.5). The algebraic formula for tubule fluid reabsorption (*Eq. 13*), however, indicates distal flow is modulated by the relative tubule fluid conductance (K_{ftr}). Because $K_{ftr} << 1$, tubule fluid reabsorption would be

insensitive to a change in distal flow (Fig. 3.5). This suggests that it may not be necessary to account for changes distal flow when investigating how other parameters effect tubule fluid reabsorption. In contrast, the algebraic formula for interstitial hydrostatic pressure (*Eq. 12*) indicates that distal flow is modulated by $1/(K_{ft} + K_{fc})$. Given the known ranges of the tubule and capillary filtration coefficients, the value of this modulating term is small such that interstitial hydrostatic pressure has a low, but still appreciable sensitivity to a change in distal flow (Fig. 3.5). Although neglecting a change in distal flow may not have much impact on interstitial hydrostatic pressure in a normal physiological state (Table 3.2, Prediction B), the value of the modulating term would be higher for disease states that reduce K_{fc}. A decrease in microvascular density, for instance, reduces K_{fc} in tissues affected by ischemic or hypertensive capillary rarefaction (90, 130), processes which affect peritubular capillary beds as well (20, 153, 185). The modulating term therefore provides guidance about whether to account for changes in distal flow changes when designing experiments involving in particular renal pathologies.

Comparison of models with and without solute flow reveals that lymph flow affects equilibrium interstitial hydrostatic pressure primarily through its effect on interstitial protein osmotic pressure. The small, positive sensitivities of tubule fluid reabsorption to lymph flow (Fig. 3.5) characterized by the algebraic formula and the nonlinear solute-coupled model are consistent with the small decrease in reabsorption observed after lymphatic vessel ligation (299). In contrast, the algebraic formula for equilibrium interstitial hydrostatic pressure exhibits a sensitivity to lymph flow that is several orders of magnitude lower than the sensitivity predicted by the nonlinear solute-coupled model (Fig. 3.5). This indicates lymph flow in the nonlinear solute-coupled model has a substantial effect on interstitial protein osmotic pressures. Sensitivities of the nonlinear solute-couple model therefore are more consistent with the dramatic increase in

interstitial hydrostatic pressure observed during lymphatic vessel ligation (299). Taken together, this lends support for the assertion of Pinter and Gärtner (231) that the function of lymph flow may be the regulation of interstitial protein osmotic pressure during diuresis. As indicated by the algebraic formulas, the interstitial pressure exerted by a large solute affects interstitial hydrostatic pressure but not tubule fluid reabsorption (*Eqs. 12* and *13*). The increased lymph flow and associated decreased interstitial protein osmotic pressure observed during volume expansion diuresis (145, 171, 220) may therefore function to ameliorate increased interstitial hydrostatic pressure without adversely impacting tubule fluid reabsorption. The present work suggests that future investigation of renal interstitial edema would benefit by considering the impact of lymph flow on interstitial protein osmotic pressure.

Algebraic formulas characterizing the three-compartment model reveal key behaviors that differ from conventional two-compartment models. Investigators using dual-perfusion models have typically assumed that tubule and capillary compartments are separated by a single effective barrier, namely the tubule epithelia (116, 293). In such two-compartment models, equilibrium tubule fluid reabsorption is equal to $K_{ft}[(P_t - P_c) - \sum_{s=1}^{n} \sigma_t^s(\Pi_t^s - \Pi_c^s)]$. When compared to equilibrium tubule fluid reabsorption predicted by the three-compartment model (*Eq. 13*), three distinct differences become apparent. First, the flow-pressure relationship of the three-compartment model is modulated by the effective fluid conductance (K_{fe}), which is smaller than the tubule fluid filtration coefficient (K_{ft}) assumed by the two-compartment model. Second, the three-compartment model can account for the flow from distal nephron segments. Modulated by the relative tubule conductance (K_{ftr}), the effective contribution to reabsorption is small, but not insignificant. Third, two-compartment models assume that the osmotic pressures exerted by small solutes are equal in the interstitial and capillary compartments (115, 116). However, there is

evidence to suggest that osmotic gradients across the capillary barrier are present (300). Studies analyzing renal lymph composition have inferred that interstitial concentrations of small solutes can differ significantly from capillary concentrations (67, 174, 199, 217, 267). This is also the case for interstitial protein osmotic pressures (25, 123). The impact of solute polarization within interstitium of the three-compartment model may be quantified algebraically as the difference in the driving pressures predicted by two- and three-compartment models. This difference is equal to $\sum_{s=1}^{n}(\Pi_c^s - \Pi_i^s)\,(\sigma_t^s - \sigma_c^s)$. By neglecting interstitial solute polarization, distal flow, and effective fluid conductance, the two-compartment model incurs more error than the three-compartment model. Assuming the baseline values in Table 3.1, the two-compartment model overestimates tubule fluid reabsorption by 26%. However, even small changes in tubule fluid reabsorption can have a large impact on urine formation. The algebraic formulas thus not only elucidate behaviors neglected by the two-compartment model, but also indicate when neglecting the interstitial compartment is not appropriate.

The linear three-compartment model of cortical fluid balance is a novel tool for investigators. The present work fills a gap between simple linear two-compartment models that neglect the interstitium and complex nonlinear models that must be solved by numerical methods. By neglecting the solute flow equations, valid algebraic formulas approximating equilibrium tubule fluid reabsorption and interstitial hydrostatic pressure (*Eqs. 12* and *13*) could be obtained. Cardiovascular and renal researchers may therefore apply these general formulas without resorting to numerical methods or assuming parameter values that are not well known. By conceptualizing the system in terms of resistances to flow between tubule and capillary compartments (Fig. 3.2), algebraic formulas could be formulated in terms of novel parameter groupings (*Eqs. 9-11*) that would not otherwise be apparent by inspecting numerical results. Multiple representations of the

system in terms of equivalent resistances and pressures (Fig. 3.2), graphical balance points (Figs. 3.3 and 3.4), and algebraic formulas (*Eqs*. *12* and *13*) can aid conceptualization. The three-compartment model can also help identify fertile areas of future research by identifying understudied parameters (e.g., lymph flow) that can have significant impact on the system in particular contexts. The methods of the present work could be particularly useful for the study of renal adaptive responses, such as those observed with hypertension (156), pregnancy (148), and diabetes mellitus (226). Taken together, the present work provides novel algebraic formulas for cardiovascular and renal researchers that are valid and broadly applicable.

CHAPTER IV

VOCATIONAL GOAL CHANGE MODEL

Participation in undergraduate research has been associated with undergraduates being more likely to pursue careers in science, technology, engineering, and mathematics (STEM) as well as other research-oriented professions (89, 246). Many studies have reported research experiences support undergraduates' development of research skills and professional habits, as well as the clarification of their career interests (2, 77, 135, 188, 257). Participation in research also has been associated with undergraduates' improved awareness of career options (3) and sustained commitment to enter fields of work and study (19, 21, 131). Undergraduate research, moreover, supports retention of students in their academic programs (118, 256). Underrepresented minority and economically disadvantaged students who have participated in university research are more likely to persist in STEM career preparation (56). Although university research can also alter undergraduates' post-graduation plans (246), less is known about the particular curricular structures of undergraduate research programs that influence undergraduates' decisions to pursue or not pursue research-oriented careers (186).

Traditional approaches to undergraduate research, namely apprenticeship and course-based research programs, have limited students' participation in the discovery-oriented knowledge production activities of university research communities. Undergraduates in apprenticeship-type programs conduct research under the guidance and time-intensive mentoring of faculty researchers (248). Research is conducted independently or in the context of a faculty-led research group (96). However, most apprenticeship programs are highly incentivized with stipends awarded to a limited number of participants (97). Academic selection criteria also result in participants being mainly

juniors and seniors and those having high grade point averages (246). The lack of access due to selection processes involved in apprenticeship programs have consequently caused some investigators to question general claims about the impact of research experiences on undergraduates' vocational goal development (39, 257). Course-based undergraduate research programs have provided additional student access to university research. These programs often use team-based structures to organize cohorts of students of the same academic level (16). The inquiry activities are still mainly guided by teaching objectives that prescribe roles and project aims for students (200). Although student input and ownership are known to promote career goal persistence, there are only a few documented cases of course-based programs that allow students to influence the productive goals of discovery-oriented research (12, 44).

In contrast to apprenticeship and course-based models, the research-intensive community (RIC) model aims to dramatically increase the number of discovery-oriented research opportunities available to all undergraduates at a university. This is achieved through programs that provide infrastructure for undergraduates, graduates, and faculty to connect and self-organize into multi-level research teams and horizontal learning communities (78, 106). Because RIC programs are co-curricular, team projects are situated in the institutional disciplinary structures supporting the production of research. In this context, more advanced students seeking leadership experience develop discovery-oriented research projects with faculty mentors that less experienced students can join (82, 96). When no qualification criteria are mandated and no monetary incentives are provided, team membership is negotiated at the team-level as a matter of participants' common interest in pursuing the knowledge production goals of the project. With faculty facilitation, horizontal affinity groups of team leaders can emerge to explore common interests in mentoring undergraduate research (298). The mentoring that occurs within the multi-level teams involving

faculty and more advanced students has been reported to promote practical competencies, epistemological knowledge, and career goal persistence, especially for low-income, first-generation, and underrepresented minority students (159, 311).

Undergraduates in RIC programs are diverse in their research experience, academic level, and academic achievement. They also have different vocational intentions motivating their participation. The teams in which they conduct research are diverse as well. Teams can involve cross-discipline interactions between team members and leaders from different departments and colleges, and the leaders themselves can have different levels of research, program, and academic experience. The diversity of multi-level interactions within teams is also evident in the different amounts of time that team members spend with their team leader, faculty mentor, and other team members. Because participation is predicated mainly on the alignment of student interests with the productive goals of a project and their ability to gain team membership, study samples drawn from RIC populations avoid some of the selection biases inherent in studies of highly incentivized, criterion-based apprenticeship programs (257). The large, diverse, minimally incentivized populations of RIC programs are thus well-suited for quantitative studies of factors promoting important outcomes of undergraduate research. Therefore, the purpose of the present work is to quantitatively identify the vocational identities and team attributes predicting undergraduate career goal change in the research-intensive community programs of a research-extensive university.

Whether general or more specific, vocational goals frame and stimulate the preparatory activities that young adults undertake during college (45). As they prepare for their future, undergraduates seek experiences and integrate goal-related information to adjust and refine conceptions of their vocational identity (17). Vocational goals therefore exist in a constellation of other socio-cognitive factors. Self-efficacy in research, for instance, mediates students' career

aspirations (2). Plans for the future are influenced by perceptions that certain professional positions are attainable and compatible with their personal values (81). Knowledge of their peers' vocational identities can also impact whether undergraduates remain motivated to pursue a research-oriented career (272). These studies highlight the many ways undergraduates refine their interests and goals relative to the normative values they encounter in university research communities.

The extent to which research experiences can impact undergraduates' vocational plans is still unsettled. In a large-scale survey of undergraduates participating in federally-funded co-curricular programs, Russell, et al. (246) reported 70% of students increased their interests in STEM careers. This is consistent with other reports that intensive research experiences are associated with students' increased curiosity in research-oriented careers (144, 161, 187). Lopatto (188), however, found less than 10% of students actually altered their post-graduation plans. Together, these studies suggest that while undergraduates' interests may change, their distal career goals may remain relatively stable. Other studies, however, have reported vocational plans are amended with contingencies to reflect awareness of a research-oriented career as a realistic option (3, 70, 135, 271). This broader conceptualization of career goal change has not yet been quantified.

Vocational Identities of Undergraduates. The propensity to explore career fields and willingness to commit to a career choice have been implicated in psychological processes of vocational identity development in young adults (197, 228). The commitment preceding an individual's specification of career goals, however, is not necessarily associated with exploration (31, 32). Investigators have therefore quantified undergraduates' exploration and commitment beliefs to identify an array of identity profiles. Figure 4.1 depicts the exploration and commitment profiles of general vocational identities proposed by Porfeli et al. (233). A *diffused* identity

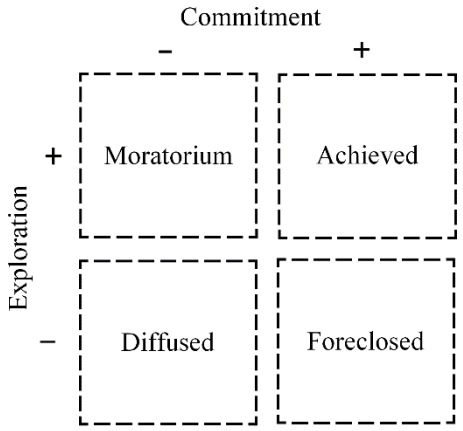

Figure 4.1 Vocational identity profiles.

characterizes individuals who are neither exploring distal career goals nor committed to one. Some studies have indicated individuals progress from diffused to an intermediate identity before reaching an *achieved* identity of high exploration and high commitment (155, 162). Individuals who place a *moratorium* on making a career choice remain uncommitted but exhibit a moderate level of exploration. A *searching moratorium* identity displays higher levels of exploration; this profile is indicative of individuals who are unsatisfied and seeking to reorient their commitments (71). A *foreclosed* identity eschews exploration and commitment to a career choice prematurely. Career goal foreclosure is associated with anxiety avoidance and nonsocial decision-making styles (31). Racial ideologies, perceived career barriers, and career myths are also associated with underrepresented minorities' early foreclosure on career goals (50, 173).

Vocational aspirations of students and faculty are influenced by the structures and polices of the institutional field in which they are situated (37, 38). Colleges organize oversight and resources around broad disciplinary concerns while departments and other similar units focus on particular academic affairs and research practices (28, 163). The fields of study organized by

colleges exhibit similar epistemological characteristics and employ similar approaches to research and teaching (214). Faculty, however, exhibit more affinity and productivity with departmental colleagues (41, 63). As a possible consequence, undergraduates across colleges and departments have been reported to value epistemic and vocational goals differently (54, 70). In practice, university research has become increasingly more interdisciplinary (234, 286), and the benefits of interdisciplinary research experiences for graduates and undergraduates have been promoted in many STEM fields (210, 245). However, lacking infrastructure to foster interactions across disciplines, undergraduate research has been bounded mainly by the discipline-oriented department and college structures that organize university faculty (73). Consequently, little is known about how cross-discipline interactions influence outcomes for undergraduate researchers (257).

Persistent multi-semester project teams managed by more advanced undergraduates and graduate students have provided an effective means for novice undergraduates to develop professional proficiencies while also contributing to the productivity of university research groups (95, 96, 108, 132). Development of career plans among undergraduate researchers occurs through interactions with socially-stratified members of these local communities of practice (2, 257). In contrast to isolated insight, individuals' reassessment of proximal and distal goals emerge from their negotiations and meaning-making efforts with more experienced community members (124, 285). Many studies have characterized the effectiveness of undergraduate and graduate student team leaders. For instance, undergraduates have reported graduate student team leaders have improved their access to research, level of project interaction, transition to independent work, insight into graduate experience, and awareness of socialization within the field of research (51, 82). In some cases, graduate student team leaders were reported to impose hierarchy that limited

undergraduates' ability to make intellectual contributions. In contrast, undergraduate mentors have been reported to elaborate on their mentee's ideas to facilitate collective knowledge-building (304). In general, effective team leaders increased team member self-efficacy by recognizing their intellectual contributions and aligning their ideas for project goals within the collective efforts of the research group (2).

METHODS

Logistic regression was used to determine significant predictors of career goal change among undergraduates who had participated in the investigative work of minimally incentivized, multi-level research teams throughout a semester at a large doctorate-granting, public university. Located in the Southern United States, the university campus serves over 44,500 undergraduates (48.9% Female, 20.9% Hispanic, 3.3% Black, 0.3% Native, and 41.6% STEM majors).

Data Sources and Sample. Study participants were recruited from two campus-wide undergraduate programs that organized research based on the RIC model. Each undergraduate team in the summer RIC program was mentored by a faculty member and led by an undergraduate team leader. In the year-around RIC program, each undergraduate research team was mentored by a faculty member and led by either an undergraduate or graduate student. Each program provided team leaders and faculty mentors the infrastructure and support needed for campus-wide recruitment of undergraduates, but left all recruitment decisions to the multi-level research teams. Data collection was conducted over a six-semester period. In total, there were 155 team leaders and 936 team members. This analysis focused on the 751 team members who were new to the program. A majority of these undergraduates (n = 457) completed the Vocational Identity Status

Assessment at the beginning of the semester. A large portion of these undergraduates (n = 330) also completed the intake and exit surveys and at least eight weekly surveys. The intake and exit surveys documented participants' post-graduation career goals, team attributes and demographic information. Weekly surveys documented the time that team members spent doing research with others. For this sample, 86% of team members were STEM majors.

Career Goal Change. To quantitatively identify the vocational identities and team-based research conditions predicting undergraduates' plans to pursue or not pursue a research-oriented career, team members were assigned to two subsamples (Table 4.1). Team members were categorized as having *a prior plan to pursue* a research-oriented career if they indicated on an intake survey item that they were (a) certain to pursue a research-oriented career or (b) considering a research-oriented career as a realistic second option. Team members were categorized as having *a prior plan to not pursue* a research-oriented career if they (c) had no interest in pursuing a research-oriented career or (d) were curious but not making plans to pursue a research-oriented career. The same item was administered on the exit survey at the end of the semester, and responses were similarly categorized. Pre- and post-responses were compared to evaluate whether prior plans were sustained or altered. For those team members having a prior plan to not pursue a research career (n = 183), almost a third altered prior plan toward pursuing a research-oriented career. For those having a prior plan to pursue a research-oriented career (n = 147), less than half altered prior plan away from pursuing a research-oriented career.

Identifying the Vocational Identity Status of Undergraduate Team Members. Measurement of team member vocational identity status was performed using the Vocational Identity Status Assessment (VISA), which has been previously validated for high school and college students (233). The instrument consists of ten items for two dimensions: career exploration and career

Table 4.1 Altered and sustained career plans after participating in team research.

Prior Plan	Total		Sustained		Altered	
	n	*%*	*n*	*%*	*n*	*%*
To Not Pursue a Research Career	183	100.0	129	70.5	54	29.5
To Pursue a Research Career	147	100.0	82	55.8	65	44.2

Table 4.2 Descriptive statistics for undergraduate team member samples.

			Research-Oriented Career			
	Total *n*=330		No Prior Plan *n*=183		Prior Plan *n*=147	
	n	*%*	*n*	*%*	*n*	*%*
TM Female	204	61.8	111	66.7	93	63.3
TM Hispanic	63	19.1	33	18.0	30	20.4
TM Black	16	4.9	10	5.5	6	4.1
TM Low Income	61	18.5	32	17.5	29	19.7
TM First & Second Year Students	75	22.7	43	23.5	32	21.8
TM Research Credit	168	55.8	99	54.1	85	57.8
TM Research Inexperience, 0 Semesters	236	71.5	141	77.1	95	64.6
TM Moratorium Identity	81	24.6	49	26.8	32	21.8
TM Searching Identity	94	28.5	48	26.3	46	31.3
TM Achieved Identity	91	27.6	36	19.7	55	37.4
TM Diffused Identity	32	9.7	27	14.8	5	3.4
TM Foreclosed Identity	32	9.7	23	12.6	9	6.1
TL Academic Level, Graduate	219	66.4	116	63.4	103	70.1
TL Research Experience, ≥ 4 Semesters	159	48.2	89	48.6	70	47.6
TL Program Experience, ≥ 1 Semesters	92	27.9	48	26.2	44	29.9
TM & TMs Different Departments	271	82.1	156	85.3	115	78.2
TM & TMs Different Colleges	206	62.4	119	65.0	87	59.2
TM & TL Different Departments	226	68.5	130	71.0	96	65.3
TM & TL Different Colleges	148	44.9	85	46.5	63	42.9
	Mean	SD	Mean	SD	Mean	SD
TM & TL Research Time, hours/week	2.75	3.10	2.56	2.39	2.99	3.79
TM & FM Research Time, hours/week	0.84	1.46	0.94	1.56	0.73	1.33
TM & TMs Research Time, hours/week	3.03	3.11	2.89	2.47	3.20	3.76

TM, team member; TL, team leader; FM, faculty mentor; TMs, other team members on research team. SD, standard deviation.

commitment. Each dimension has two subscales. Five items on in-breadth career exploration indicate whether respondent is seeking multiple experiences and considering multiple career options. Five items on in-depth career exploration indicate whether participant is seeking particular experiences for determining whether a career choice matches personal interests and talents. Five items on making a career commitment indicate whether respondent has chosen a career. Five items on career commitment identification indicate whether respondent associates career choice with personal values and relationships. To confirm that four subscales provided valid measurements for characterizing team members' vocational identity status and adequately fit collected data, confirmatory factor analysis was performed for a four-factor model. Fit indices were then computed and compared to standard cutoff values (134). To identify the vocational identity status of each of these team members, hierarchical cluster analyses was performed with standardized subscale scores (M = 0, SD = 1) using Ward's method and Euclidean distances. The choice for the number of cluster variables (*k*) to use in further analysis was evaluated with previously-established methods and standards (233). In brief, the optimal solution was characterized by having a minimum number of cluster variables, subscale patterns corresponding to recognized theoretical profiles, and a mean explained variance among clustered variables greater than 50% (109).

The robustness of cluster solutions, which ranged from three to nine variables, was evaluated using an iterative k-means cluster analysis procedure. The sample was first split into two random groups. The variable centers for each cluster solution of the whole sample were used to initialize a k-means cluster analysis for each random split-group. Centers from these clusters were retained and used to initialize a k-means analysis for the other half of the sample. This resulted in two variable assignments for each cluster solution. The inter-rater reliability of the two

assignments was then computed using Cohen's kappa (68). Mean explained variance of whole sample and inter-rater reliability for random split-groups were plotted for each cluster solution to identify the optimal number of variables. Each variable of the optimal cluster solution was then characterized by plotting mean z-scores for exploration and commitment subscales.

Confirmatory factor analysis suggested that the four subscales (i.e., exploration in-breadth, exploration in-depth, commitment making, and commitment identification) provided valid measurements for characterizing team members' vocational identity status ($\chi^2 = 290$, $df = 164$, $p < 0.001$). The Root Mean Square Error of Approximation (RMSEA) = 0.041, Comparative Fit Index (CFI) = 0.95, and the Standardized Root Mean Square Residual (SRMR) = 0.046. Fit indices thus conformed to standard cutoff values: RMSEA < 0.80, CFI > 0.90, and SRMR < 0.80 (134). This suggested that the four subscale measurements adequately fit the data provided by undergraduate team members (*n = 457*). Figure 4.2. depicts results from the cluster analysis of responses to the career exploration and commitment subscales. Cluster solutions with four to nine variables had a mean explained variance greater than the accepted 50% threshold (233). Cohen's kappa (68) was used to compute the inter-rater reliability of k-means cluster assignments when the sample was randomly split into two groups. In Fig. 4.2A, the three-, five-, and eight-variable solutions had the highest inter-rater reliabilities, which were 0.72, 0.64 and 0.60, respectively. In Fig. 4.2B, the subscale profiles of the five-variable cluster solution corresponded to the moratorium, searching, achieved, foreclosed, and diffused status identities that have been observed in other undergraduate populations (233). Moratorium, searching, and achieved were the most prevalent identities in this cluster solution with relative frequencies of 25.1%, 27.1% and 28.0%, respectively. Operationalized as five dichotomous variables, these vocational identities were similarly distributed in subsamples (Table 4.2). For the subsample having a prior plan, the counts

for diffused and foreclosed identities, however, were low and insufficient for logistic regression (4).

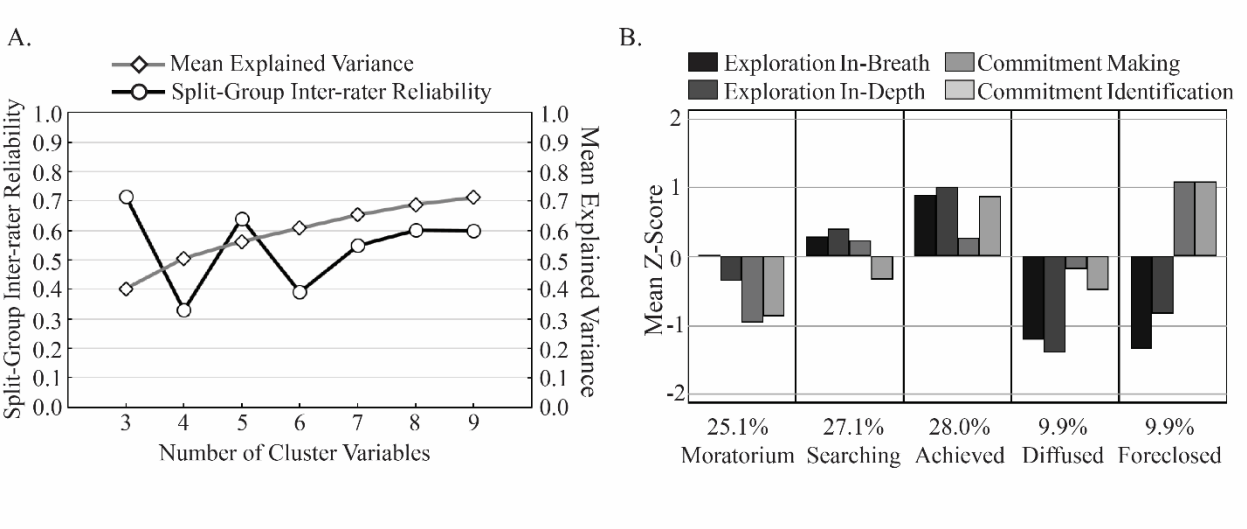

Figure 4.2 Cluster analysis of undergraduate team member responses to the Vocational Identity Status Assessment (n = 457). A: The optimal number of clusters was a five-variable solution that exhibited a mean explained variance above 0.50 as well as a moderate inter-rater reliability (Cohen's kappa) of 0.64 between the split-group cluster assignments. B: The five variables of the cluster solution were characterized by exploration and commitment subscale profiles. These profiles corresponded to the moratorium, searching, achieved, foreclosed, and diffused status identities previously observed in undergraduate populations (233).

Other Variables. Table 4.2 summarizes the descriptive statistics for the other dichotomous and continuous independent variables examined in the present work. National employment figures for bachelor degree holders indicate that Hispanic (7.6%) and Black (6.2%) graduates are underrepresented in STEM and other research-oriented careers (211). The proportion of Hispanic and Black team members in the samples reflected the university population. For the subsample having a prior research career plan, the number of Black participants was low and insufficient for logistic regression (4). No Native Americans were in the sample. Female team members were overrepresented compared to the university population. About one fifth of the team members had

parental incomes below $40,000 and were categorized as low income. Over two-thirds of team members had no prior research experience. The sample of the undergraduate participants was diverse in academic level (with almost a quarter being in their first and second year), academic achievement (with almost a quarter having a grade point average below 3.0), and motive (with just over half enrolling in research credit hours).

To investigate the influence of the multi-level conditions of team-based research, team leader traits and the research time spent with others were examined. Two-thirds of the team members in the sample had team leaders who were graduate students. Less than half had team leaders who had over four semesters of research experience; and under a third worked with team leaders who had experience in these research programs. Research time indicators included the average hours per week that team members spent with the team leader, faculty mentor, and other team members. These continuous variables had negative exponential distributions that were similar across subsamples.

To investigate the influence of cross-discipline conditions of team-based research, team members were classified as having teams with team members and leaders from different colleges and departments. Over four-fifths of the undergraduates in the sample worked with team members from different departments, whereas three-fifths worked with team members from different colleges. Over two-thirds of team members worked with a team leader from a different department, while less than half worked with team leaders from different colleges. The Phi coefficient (ϕ) and Pearson's r correlation values among these and the other independent variables provided no evidence of multicollinearity.

Analysis. Stepwise elimination was employed to remove effects of variables and interactions and produced nested models with successively lower Bayesian Information Criterion

(BIC) and deviance values (240). As terms were removed to reduce model uncertainty, BIC and deviance values decreased. Elimination was terminated when deviance began to increase. Likelihood Ratio Test ($-2LL\ \chi^2$) was then used to confirm whether further elimination was warranted. The *F*-statistic for the final model was estimated from the survey data of the weight-adjusted subsample. Archer-Lemeshow *F*-statistic was estimated to evaluate how well the final model fit survey data (10). To estimate correct classification, sensitivity and specificity were maximized (310). A McFadden's R^2 value of 0.20 or greater indicated highly satisfactory fit (189). Odds ratios were estimated to determine effect size of each selected term on distal goal change. Reported odds ratios of interaction terms are technically ratios of odds ratios. To interpret odds ratios, significant average marginal effects and interaction effects are reported in the probability metric. Each test was evaluated at a 0.05 alpha level.

RESULTS

Logistic Model for Altering Prior Plan Toward Pursuing Research-Oriented Career. In Table 4.3, we report the odds ratios for the fourteen-term final model that predicted whether team members altered their prior plan toward pursuing a research-oriented career after participating in team research ($F_{13, 170} = 2.64$, $p < 0.01$). A thirteen-term model that eliminated the interaction of TM Searching and TM Low Income in a stepwise manner exhibited a lower *BIC* (*df*) value of 247 (13) and a higher *deviance* (*df*) value of 180 (170). The Likelihood Ratio Test indicated that the final model provided a relatively better fit ($-2LL\ \chi^2 = 4.73$, $p < 0.05$). Further, the estimated Archer-Lemeshow *F*-statistic for the final model was not significant and thus provided no evidence of poor fit ($F_{9, 174} = 0.27$, $p = 0.98$). With a sensitivity of 74.0% and a specificity of 71.3%, the

final model correctly classified 72.1% of the observations. A McFadden's R^2 value of 0.212 indicated a highly satisfactory fit.

As indicated by significant odds ratio estimates, the predictors for whether a team member alters prior plan toward pursuing a research-oriented career included five independent variables. The probability of a team member with a searching identity to alter plan toward research-oriented career is on average 0.26 higher than other team members (SE = 0.06, $z = 4.03$, $p < 0.001$). A Black team member is 0.34 more likely to alter plan toward a research career (SE = 0.16, $z = 2.21$, $p < 0.05$). A team member working with team members from other departments is 0.23 more likely to alter plan toward a research career (SE = 0.06, $z = 3.92$, $p < 0.001$). In contrast, a team member working with team members from other colleges is 0.35 less likely to alter plan toward a research career (SE = 0.09, $z = -4.12$, $p < 0.001$).

As indicated by the ratios of odds ratios, the predictors for whether a team member alters their prior plan toward pursuing a research-oriented career also included four significant interactions. The probability of a team member with a searching identity to pursue a research-oriented career is decreased by 0.23 when team leader is from a different college (SE = 0.12, $z = -2.08$, $p < 0.05$). The probability of a searching team member with a low parental income to pursue a research-oriented career is 0.43 higher compared to other searching team members (SE = 0.10, $z = 4.36$, $p < 0.001$). The effect of performing research with a graduate student team leader from a different college increased the probability of a team member altering plan toward a research career by 0.21 (SE = 0.09, $z = 2.46$, $p < 0.05$). Finally, if a research inexperienced team member spends one hour per week with team leader, the probability of pursuing a research-oriented career increases by 0.04 (SE = 0.01, $z = 4.51$, $p < 0.001$).

Table 4.3 Logistic regression models of undergraduates' altered career plans.

	Research-Oriented Career Goal Change Models	
	Altered Prior Plan Toward Pursuing *n*=183	Altered Prior Plan Away from Pursuing *n*=147
	Odds Ratio	Odds Ratio
TM Hispanic	–	4.23*
TM Black	6.77*	–
TM Low Income	0.94	–
TM Moratorium	–	33.19*
TM Searching	10.66***	–
TM Achieved	–	2.12
TM Research Inexperience	0.21*	–
TL Graduate	0.73	–
TL Research Experience	–	2.17
TL Different Colleges	1.11	0.96
TL Different Departments	–	0.65
TMs Different Colleges	0.10**	–
TMs Different Departments	7.11**	–
TL Research Time	0.94	0.70*
FM Research Time	–	1.18
TMs Research Time	–	1.00
TM Searching × TL Different College	0.06**	–
TM Searching × TM Low Income	20.69**	–
TM Research Inexperience × TL Research Time	1.47*	–
TL Graduate × TL Different College	9.72*	–
TM Moratorium × TMs Research Time	–	0.28**
TMs Research Time × TL Different College	–	1.55*
TM Achieved × TL Different Department	–	0.10*
TL Research Experience × FM Research Time	–	0.18**
Constant	0.18*	1.06
F (*dfn*, *dfd*)	2.64 (13, 170)**	2.35 (13, 134) **
BIC (*df*)	248 (14)	213 (14)
deviance (*df*)	175 (169)	143 (133)
Archer-Lemeshow F (*dfn*, *dfd*)	0.27 (9, 174)	1.23 (9, 138)
Correct Classification (%)	72.2	77.6
McFadden's R^2	0.212	0.227

TM, team member; TL, team leader; FM, faculty mentor; TMs, other team members on research team.
df, degrees of freedom; *dfn*, numerator degrees of freedom; *dfd*, denominator degrees of freedom
*$p < 0.05$, **$p < 0.01$, ***$p < 0.001$

Logistic Model for Altering Prior Plan Away from Pursuing Research-Oriented Career. In Table 4.3, we report the odds ratios for the fourteen-term final model that predicted whether team members altered their prior plan away from pursuing a research-oriented career after participating in team research ($F_{13, 134} = 2.35$, $p < 0.01$). Further stepwise elimination yielded a thirteen-term model that excluded TL Different College. This constrained model had a lower *BIC* (*df*) value of 211 (12), but a higher *deviance* (*df*) value of 151 (135). The Likelihood Ratio Test indicated that the final model provided a relatively better fit ($-2LL\ \chi^2 = 8.74$, $p < 0.05$). Further, the estimated Archer-Lemeshow *F*-statistic for the final model was not significant and thus provided no evidence of poor fit ($F_{9, 138} = 1.23$, $p = 0.38$). With a sensitivity of 73.9% and a specificity of 80.5%, the final model correctly classified 77.6% of the observations. A McFadden's R^2 value of 0.291 indicated a highly satisfactory fit.

As indicated by significant odds ratio estimates, predictors for whether a team member alters their prior plan away from a pursuing a research-oriented career included two significant variables. The final model predicts that the more time spent with team leader, the less likely a team member is to alter plans away from pursuing a research-oriented career. Specifically, for each hour a team member spends per week with a team leader, the probability of a team member altering their plan away from a research-oriented career is decreased by 0.06 (SE = 0.02, $z = -2.58$, $p < 0.05$). The probability of a Hispanic team member of altering plan away from a research career, however, is 0.23 higher than other team members (SE = 0.09, $z = 2.73$, $p < 0.01$). The average marginal effect of the team member moratorium identity was not significant in the probability metric.

As indicated by the ratios of odds ratios, the predictors for whether a team member alters their prior plan away from pursuing a research-oriented career also included four significant interactions. The final model predicts that for every hour that a team member with a moratorium identity status (low commitment, moderate exploration) spends with other team members, the probability of altering plan away from a research-oriented career is decreased by 0.11 (SE = 0.03, $z = -3.93$, $p < 0.01$). For every hour a team member spends with a faculty mentor in a team whose leader has four or more semesters of research experience, the probability of altering plan away from research-oriented career is decreased by 0.25 (SE = 0.09, $z = -2.88$, $p < 0.01$). The effect of working in a team with a leader from a different department decreases the probability that a team member with an achieved identity status (high commitment, moderate career exploration) will alter plan away from research-oriented career by 0.43 (SE = 0.13, $z = -3.18$, $p < 0.01$).

DISCUSSION

The logistic models of the present work identify the vocational identities and team attributes that predict career goal change of undergraduates participating in research-intensive community (RIC) programs. Two logistic models were constructed to develop an understanding of factors that promote and also inhibit the development of research career aspirations. The first model identified factors that predict whether undergraduate researchers will alter their prior plan toward pursuing a research-oriented career. The second model identified factors that predict whether undergraduate researchers will alter their prior plan away from pursuing a research-oriented career. Together, these models provide insights on ways undergraduate research programs can be designed to amplify and diversify the nation's workforce of knowledge-producers.

Changes in Post-graduation Career Goals. In this study, we assumed distal career goals are complex cognitive constructs that can be amended to include contingency plans whereby a research-oriented career may be adopted as a realistic second option (3, 70). This is a somewhat broader operationalization of career goal change than seen in previous studies that simply asked undergraduate researchers whether their prior plan had changed. In a large-scale study of grant-funded, faculty-led apprenticeship programs, Lopatto (188) reported between 3.7% and 2.7% of undergraduate participants developed plans to attain postgraduate research positions, while between 6.7% and 4.2% discontinued their postgraduate research plans as a result of their research experience. In the present study (Table 4.1), 29.5% of undergraduate researchers altered their prior plan toward pursuing a research career while 44.2% altered their prior plan away from pursuing a research career. The trend is the same, but the magnitude of career goal change is considerably higher in the present study. This reflects the broader operationalization, but also characterizes a population of undergraduate researchers who are minimally incentivized, less experienced, and more academically diverse. The RIC programs had slightly higher proportions of first and second year students (22.7% and 17.6%) and much greater proportions of undergraduates with no prior research experience (71.5% versus 38.0%). Whereas the overall GPA for students in these apprenticeship programs was 3.63 (144), the GPA of students in RIC programs was 3.31 (SD = 0.47). These differences suggest the RIC programs offered greater access to participants having different vocational identities and potential for career goal change.

Vocational Identities. The vocational identities of undergraduates were quantified by measuring their levels career commitment and exploration. A five-cluster solution indicated that the majority of undergraduates in the RIC programs exhibited moratorium, searching, and achieved identities (25.1, 27.1 and 28.0% respectively). While there are substantial proportions of

moratorium and achieved identities in general populations of undergraduates, searching identities are a minority (233). The RIC programs, however, included a large proportion of undergraduates exhibiting high exploration and moderate commitment levels. For these students, team-based research had a significant impact on their goal development. Models revealed that team members with searching identities were more likely to alter their prior plan toward pursuing a research career as a result of RIC participation. Searching team members with low parental income were more likely to pursue a research-oriented career. This pronounced effect is consistent with findings that learning experiences that are discursive, vicarious, and productive, effectively mediate career goal development in low-income, first-generation undergraduates (105). Other studies indicate undergraduates with exploratory dispositions persist toward their career goals with learning experiences that offer opportunities for self-direction, competency, and ownership of their work (107, 228). Such opportunities for undergraduates to pursue individual goals have been previously reported to arise in RIC programs (78).

Multi-level Conditions of Team-based Research. The multi-level conditions of team-based research were found to promote undergraduate career goal change. Undergraduates in RIC programs spent approximately three times more time working with team leaders and other team members than their faculty mentor. The models indicate that the more time team members spend with faculty mentor, the less likely they are to alter their plan away from research-oriented career. However, faculty report lack of time, funding, and recognition as deterrents to engaging undergraduates in research (14). RIC programs overcome these barriers by organizing undergraduate researchers into student-led research teams. Positioning more advanced students as team mentors and managers of persistent research projects has been reported to help undergraduates gain methodological and intellectual proficiencies of the knowledge-producing

community (96). Logistic models of the present work indicate that these multi-level conditions are effective in promoting career goal change. Models indicate that the more time team members spend with a team leader, the less likely they are to alter their plans away from pursuing a research career. Research-inexperienced team members are also more likely to pursue to a research career when they are able to spend more time with their team leader. Interactions with other team members help undergraduates with moderate exploration and low commitment levels persist in their career aspirations. Models indicate that team members with moratorium identities are less likely to abandon their research-career goals if they are able to spend more time with other team members. This is consistent with studies indicating collective self-efficacy of student teams to be a positive predictor of research-oriented career intentions (75, 178).

Cross-Discipline Conditions of Team-based Research. The cross-discipline conditions of team-based research were found to promote and sometimes inhibit undergraduates' pursuit of research-oriented careers. The team members and leaders in this study were classified by their college and by their department (or equivalent unit) overseeing their program of study. The resulting logistic models reveal team members are more likely to alter plans toward a research career when working with team members from other departments and less likely to alter their plans when working with team members from other colleges. This is consistent with a study that reported university research conducted by inter-departmental teams increased the odds of undergraduates attaining employment in their field of study (133). Together, these findings suggest

inter-department programs that organize students into multidisciplinary research teams may be effective means of promoting career goal development.

Interactions of Multi-Level and Cross-Discipline Conditions with Vocational Identities. The quantified interactions of undergraduates' vocational identities with multi-level and cross-discipline conditions provides further insight on how team-based research can designed to support career goal change. In general, undergraduate team members performing research with a graduate student team leader from a different college are more likely to alter their plans toward a research-oriented career. The models, however, reveal different trends for undergraduates with searching and achieved identities. Undergraduates with searching identities are less likely to adopt research career plans when working with a team leader from a different college. In contrast, undergraduates with achieved identities are more likely to persist in their research career goals when working with a team leader from a different department. These findings correspond with studies that suggests vocational identities mediate undergraduates' interpretations of their social and institutional conditions in different ways (27). Progressing from a searching toward an achieved identity status, for instance, involves both a willingness to explore professional practices and reasonable opportunities to conduct these explorations (142). Broader cross-discipline interactions with team leaders from a different college may not provide searching undergraduates reasonable conditions for engaging in legitimate practices of a professional learning community. Cross-discipline interactions with team members from different departments, which are less broad, appear to help undergraduates sustain their research-oriented career aspirations. In contrast to direct socialization

(270), exposure to different, yet closely-related disciplinary perspectives appears to support the career aspirations of undergraduates with achieved vocational identities.

Underrepresented Minority Groups. While research experiences have been reported to promote academic retention and graduate school plans among underrepresented minority groups (19, 89, 126), participation in the team-based research of RIC programs impacts the postgraduate career goals of Black and Hispanic undergraduates differently. Models indicated Black team member are more likely to adopt plans toward pursuing research careers as a result of their research in RIC teams. This is consistent with studies that have reported undergraduate research conducted within social communities can mitigate psychological and social barriers that underrepresented students face in the attainment of their research career aspirations (53, 107, 229). However, the models also indicate that Hispanic team members are more likely to alter their post-graduate plans away from research career aspirations after RIC participation. This may mean the structures implemented in the RIC programs under study are insufficient to counter the lower likelihood of persistence toward career goals among Hispanic students. In general, students lacking traditionally-valued social and cultural capital have significantly lower chances of persisting than others students; and Hispanic students, on average, have the least amount of capital on upon entry into college (297). Closer inspection of additional data, however, suggests that there could be a strong negative relationship between Hispanic students' research career goals and graduate school intentions (Cramer's $V = -0.31$, Pearson's χ^2 $(1, n = 30) = 2.92$, $p < 0.10$). Though more data is needed to confirm this relationship, eighteen of the nineteen Hispanic students in this study who altered their postgraduate plan away from a research-career were still planning to attend graduate school. Given most studies have focused on graduate school aspirations, more research is needed

to determine whether undergraduate research can inspire and support underrepresented minorities seeking STEM and other research-oriented careers after their bachelor programs.

Implications. While much attention has been focused on the graduate school intentions of undergraduates, the present work has sought to contribute to the knowledge of designing and evaluating undergraduate research programs that amplify and diversify the nation's workforce of knowledge-producers. The present study therefore employed measurement and analysis methods for identifying the conditions and traits of RIC programs that predict changes in undergraduates' post-graduation career goals. By studying undergraduate researchers in programs that aim to maximize research opportunities for all students, and by operationalizing career goal change to include contingency plans, a substantial proportion of career goal change can be observed in a study sample that is both sizeable and diverse. Such a sample is well suited for developing logistic models that identify the interactions between participant traits and program conditions that predict career goal change. These models can examine factors that either promote or inhibit career goal change, which provides a fuller and more realistic understanding of how programs impact formative career plans of undergraduates. In addition to the evaluation and analysis methods, the logistic models in the present work provide practical insights for curriculum developers aiming to increase participation and tailor programs to support undergraduates' exploration and commitment to STEM and other research-oriented careers. These findings specifically inform how to improve programs to account for the ways career goal development is impacted by undergraduates' vocational identities, multi-level learning communities, and cross-discipline relations between team members and team leaders. The models confirm the benefits of undergraduate research for low-income and Black students, but underscore the need to provide additional infrastructure for helping Hispanic students navigate career pathways and pursue their research interests after

graduation. More broadly, this study suggests that inclusive, team-based programs like those based on the RIC model can promote career goal change among the substantial number of undergraduates who are seeking opportunities to explore and get involved in university research but who may have limited access to traditional undergraduate research programs.

CHAPTER V

SUMMARY

In Chapter II, the mechanical properties determining cardiac output and pulmonary venous pressure were investigated in a minimal closed-loop model of the cardiovascular system with arterial pressure regulation. By isolating left ventricular function, linearizing end-diastolic pressure-volume relationships (EDPVR), and assuming arterial pressures are regulated, algebraic formulas for cardiac output and pulmonary venous pressure were derived. The algebraic formulas predicted trends observed in a wide array of experimental and clinical studies. The formulas specifically account for the interactions among the properties of left ventricular function and the rest of the cardiovascular system that are not addressed by conventional heart failure models. Algebraic modeling methods thus made several novel insights possible. First, the algebraic formulas reveal that cardiac output and pulmonary venous pressure are governed by effective volume terms that are not apparent when using numerical approaches. Second, the range of asymptomatic stressed volume fluctuation is limited by the properties of the failing left ventricle. Taken together, the present work provides a novel tool for the study of blood volume distribution with isolated ventricular dysfunction.

In Chapter III, the physical properties determining renal interstitial hydrostatic pressure and tubule fluid reabsorption were investigated by modeling the renal cortex as a three-compartment system that includes the proximal tubule, cortical interstitium, and peritubular capillaries. By constructing a lumped, linear model and constraining its scope, algebraic formulas for interstitial hydrostatic pressure and tubule fluid reabsorption were derived for the integrated system. The algebraic formulas were validated with data from transport inhibition

experiments in rats and predicted trends observed in a wide array of experiments. The formulas specifically account for the interactions among tubule and capillary properties, which are not addressed by conventional tubule or capillary models. The use of algebraic methods also make several novel insights possible. First, the algebraic formulas reveal that interstitial hydrostatic pressure and tubule fluid reabsorption are governed by novel groupings of filtration coefficients that would not otherwise be apparent by inspecting the numerical results of nonlinear solute-coupled models. Second, the formulas reveal that interstitial hydrostatic pressure and tubule fluid reabsorption can be estimated with minimal error without invoking solute flow equations. Third, and most interestingly, the algebraic formulas reconcile results of in vivo experiments in which tubule fluid reabsorption is either positively or negatively correlated with interstitial hydrostatic pressure depending on whether tubule or capillary pressures are altered. Taken together, the present work provides a novel tool for the study of renal fluid balance that addresses the gap between two-compartment models that neglect tubule-capillary interactions and nonlinear solute-coupled models that require *a priori* knowledge of parameter values.

In Chapter IV, a Research-Intensive Community (RIC) model for undergraduate research was investigated. While RIC programs scale-up and sustain undergraduate research, their efficacy in promoting post-graduation participation in the nation's workforce of knowledge-producers has not been established. Therefore, the present work aimed to quantitatively identify the vocational identities and team attributes that predict undergraduate career goal change in RIC programs. Using survey data, cluster analysis revealed undergraduates with high career exploration and moderate career commitment formed a majority of participants. Logistic models predict these undergraduates were more likely to pursue research-oriented careers as a result of team-based research. Research time spent with a more advanced student team leader also promoted career goal

development, while time spent with other team members predict career goal persistence among undergraduates with low commitment. Cross-discipline relationships between team members and leaders promoted and sometimes inhibited pursuit of research-oriented careers. Effects on low income and underrepresented minority groups also varied. Findings regarding the interactions between participant traits and team attributes inform the design of undergraduate research programs that seek to amplify and diversify the nation's workforce of knowledge-producers.

REFERENCES

1. **Abel FL, Waldhausen JA, Daly WJ, Pearce WL**. Pulmonary blood volume in hemorrhagic shock in the dog and primate. *Am J Physiol* 213: 1072-8, 1967.

2. **Adedokun OA, Bessenbacher AB, Parker LC, Kirkham LL, Burgess WD**. Research skills and STEM undergraduate research students' aspirations for research careers: Mediating effects of research self-efficacy. *Journal of Research in Science Teaching* 50: 940-51, 2013.

3. **Adedokun OA, Zhang D, Parker LC, Bessenbacher A, Childress A, Burgess WD**. Research and teaching: Understanding how undergraduate research experiences influence student aspirations for research careers and graduate education. *Journal of College Science Teaching* 42: 82-90, 2012.

4. **Agresti A**. An introduction to categorical data analysis. New Jersey: Wiley-Interscience, 2007.

5. **Alberola A, Pinilla JM, Quesada T, Romero JC, Salom MG, Salazar FJ**. Role of nitric oxide in mediating renal response to volume expansion. *Hypertension* 19: 780-4, 1992.

6. **Alpern RJ**. Bicarbonate-water interactions in the rat proximal convoluted tubule. An effect of volume flux on active proton secretion. *J Gen Physiol* 84: 753-70, 1984.

7. **Androne A-S, Katz SD, Lund L, LaManca J, Hudaihed A, Hryniewicz K, Mancini DM**. Hemodilution is common in patients with advanced heart failure. *Circulation* 107: 226-9, 2003.

8. **Androne AS, Hryniewicz K, Hudaihed A, Mancini D, Lamanca J, Katz SD**. Relation of unrecognized hypervolemia in chronic heart failure to clinical status, hemodynamics, and patient outcomes. *Am J Cardiol* 93: 1254-9, 2004.

9. **Appleton CP, Lee R, Martin G, Olajos M, Goldman S**. Alpha 1-and alpha 2-adrenoceptor stimulation: Changes in venous capacitance in intact dogs. *Am J Physiol Heart Circ Physiol* 250: H1071-H8, 1986.

10. **Archer KJ, Lemeshow S**. Goodness-of-fit test for a logistic regression model fitted using survey sample data. *Stata Journal* 6: 97-105, 2006.

11. **Aroney CN, Herrmann HC, Semigran MJ, William G, Boucher CA, Fifer MA**. Linearity of the left ventricular end-systolic pressure-volume relation in patients with severe heart failure. *J Am Coll Cardiol* 14: 127-34, 1989.

12. **Auchincloss LC, Laursen SL, Branchaw JL, Eagan K, Graham M, Hanauer DI, . . . Rowland S**. Assessment of course-based undergraduate research experiences: a meeting report. *CBE—Life Sciences Education* 13: 29-40, 2014.

13. **Aukland K, Bogusky RT, Renkin EM**. Renal cortical interstitium and fluid absorption by peritubular capillaries. *Am J Physiol Renal Physiol* 266: F175-F84, 1994.

14. **Baker VL, Pifer MJ, Lunsford LG, Greer J, Ihas D**. Faculty as mentors in undergraduate research, scholarship, and creative work: Motivating and inhibiting factors. *Mentoring & Tutoring: Partnership in Learning* 23: 394-410, 2015.

15. **Balmain S, Padmanabhan N, Ferrell WR, Morton JJ, McMurray JJ**. Differences in arterial compliance, microvascular function and venous capacitance between patients with heart failure and either preserved or reduced left ventricular systolic function. *Eur J Heart Fail* 9: 865-71, 2007.

16. **Balster N, Pfund C, Rediske R, Branchaw J**. Entering research: A course that creates community and structure for beginning undergraduate researchers in the STEM disciplines. *CBE-Life Sciences Education* 9: 108-18, 2010.

17. **Bandura A**. Self-regulation of motivation through anticipatory and self-reactive mechanisms. In: *Current theory and research in motivation*, edited by Dienstbier RA. Lincoln, NE: University of Nebraska Press, 1991, p. 69-164.

18. **Barfuss DW, Schafer JA**. Differences in active and passive glucose transport along the proximal nephron. *Am J Physiol Renal Physiol* 241: F322-F32, 1981.

19. **Barlow AE, Villarejo M**. Making a difference for minorities: Evaluation of an educational enrichment program. *Journal of Research in Science Teaching* 41: 861-81, 2004.

20. **Basile DP, Donohoe D, Roethe K, Osborn JL**. Renal ischemic injury results in permanent damage to peritubular capillaries and influences long-term function. *Am J Physiol Renal Physiol* 281: F887-F99, 2001.

21. **Bauer KW, Bennett JS**. Alumni Perceptions Used to Assess Undergraduate Research Experience. *The Journal of Higher Education* 74: 210-30, 2003.

22. **Baumann K, Holzgreve H, Kolb F, Peters R, Rumrich G, Ullrich KJ**. Unidirektionale flüsse für ^{24}Na, ^{42}K, ^{45}Ca, ^{38}Cl, ^{82}Br und ^{131}I im proximalen konvolut der rattenniere (abstract). *Pflügers Arch* 289: R77-R8, 1966.

23. **Beard DA, Feigl EO**. Understanding Guyton's venous return curves. *Am J Physiol Heart Circ Physiol* 301: H629-H33, 2011.

24. **Bedell M, Lin Y, Román-Meléndez E, Sgouralis I**. Global sensitivity analysis in a mathematical model of the renal interstitium. *Involve J Math* 10: 625-49, 2017.

25. **Bell DR, Pinter GG, Wilson PD**. Albumin permeability of the peritubular capillaries in rat renal cortex. *J Physiol* 279: 621-40, 1978.

26. **Berry CA**. Water permeability and pathways in the proximal tubule. *Am J Physiol Renal Physiol* 245: F279-F94, 1983.

27. **Berzonsky MD**. The structure of identity: Commentary on Jane Kroger's view of identity status transition. *Identity: An International Journal of Theory and Research* 3: 231-45, 2003.

28. **Biglan A**. Relationships between subject matter characteristics and the structure and output of university departments. *Journal of Applied Psychology* 57: 204, 1973.

29. **Bishop JH, Green R, Thomas S**. Free-flow reabsorption of glucose, sodium, osmoles and water in rat proximal convoluted tubule. *J Physiol* 288: 331-51, 1979.

30. **Blantz RC, Tucker BJ**. Determinants of peritubular capillary fluid uptake in hydropenia and saline and plasma expansion. *Am J Physiol* 228: 1927-35, 1975.

31. **Blustein DL, Ellis MV, Devenis LE**. The development and validation of a two-dimensional model of the commitment to career choices process. *Journal of Vocational Behavior* 35: 342-78, 1989.

32. **Blustein DL, Phillips SD**. Individual and contextual factors in career exploration. *Journal of Vocational Behavior* 33: 203-16, 1988.

33. **Bode F, Chan YL, Goldner AM, Papavassilou F, Wagner M, Baumann K**. Reabsorption of D-glucose from various regions of the rat proximal convoluted tubule: evidence that the proximal convolution is not homogeneous. *Curr Probl Clin Biochem* 4: 39-43, 1975.

34. **Bomsztyk K, Wright FS**. Dependence of ion fluxes on fluid transport by rat proximal tubule. *Am J Physiol Renal Physiol* 250: F680-F9, 1986.

35. **Borlaug BA, Redfield MM, Melenovsky V, Kane GC, Karon BL, Jacobsen SJ, Rodeheffer RJ**. Longitudinal changes in left ventricular stiffness: a community-based study. *Circ Heart Fail* 6: 944-52, 2013.

36. **Boulpaep EL, Seely JF**. Electrophysiology of proximal and distal tubules in the autoperfused dog kidney. *Am J Physiol* 221: 1084-96, 1971.

37. **Bourdieu P**. The specificity of the scientific field and the social conditions of the progress of reason. *Information (International Social Science Council)* 14: 19-47, 1975.

38. **Bourdieu P, Passeron JC**. *Reproduction in education, society and culture*. Thousand Oaks, CA: Sage, 1990.

39. **Boylan M**. Undergraduate STEM research experiences: Impact on student interest in doing graduate work in STEM fields. In: *Doctoral education and the faculty of the future*, edited by Ehrenberg RG, and Kuh CVCornell University Press, 2009, p. 109–20.

40. **Braam B**. Advancement in integrated models of renal function: closing the gap between simulation and real life. *Am J Physiol Renal Physiol* 306: F284-F5, 2014.

41. **Braxton JM**. Department colleagues and individual faculty publication productivity. *The Review of Higher Education* 6: 115-28, 1983.

42. **Brenner BM, Troy JL, Daugharty TM, Ueki I, Nicholas D, Wong C**. On the mechanism of inhibition in fluid reabsorption by the renal proximal tubule of the volume-expanded rat. *J Clin Invest* 50: 1596–602, 1971.

43. **Bresler EH**. A model for transepithelial fluid transport. *Am J Physiol Renal Physiol* 235: F626-F37, 1978.

44. **Brew A**. Understanding the scope of undergraduate research: a framework for curricular and pedagogical decision-making. *Higher Education* 66: 603-18, 2013.

45. **Brown D**. Status of theories of career choice and development. In: *Career choice and development*, edited by Brown D, and Associates. New York, NY: John Wiley & Sons, 2002, p. 510–5.

46. **Brown KA, Ditchey RV**. Human right ventricular end-systolic pressure-volume relation defined by maximal elastance. *Circulation* 78: 81-91, 1988.

47. **Burkhoff D, Mirsky I, Suga H**. Assessment of systolic and diastolic ventricular properties via pressure-volume analysis: a guide for clinical, translational, and basic researchers. *Am J Physiol Heart Circ Physiol* 289: H501-H12, 2005.

48. **Burkhoff D, Tyberg JV**. Why does pulmonary venous pressure rise after onset of LV dysfunction: a theoretical analysis. *Am J Physiol Heart Circ Physiol* 265: H1819-H28, 1993.

49. **Burnett JC, Jr., Knox FG**. Renal interstitial pressure and sodium excretion during renal vein constriction. *Am J Physiol Renal Physiol* 238: F279-82, 1980.

50. **Byars-Winston AM**. Racial ideology in predicting social cognitive career variables for Black undergraduates. *Journal of Vocational Behavior* 69: 134-48, 2006.

51. **Byars-Winston AM, Branchaw J, Pfund C, Leverett P, Newton J**. Culturally diverse undergraduate researchers' academic outcomes and perceptions of their research mentoring relationships. *International Journal of Science Education* 37: 2533-54, 2015.

52. **Capasso G, Kinne R, Malnic G, Giebisch G**. Renal bicarbonate reabsorption in the rat. I. Effects of hypokalemia and carbonic anhydrase. *J Clin Invest* 78: 1558-67, 1986.

53. **Carpi A, Ronan DM, Falconer HM, Lents NH**. Cultivating minority scientists: Undergraduate research increases self-efficacy and career ambitions for underrepresented students in STEM. *Journal of Research in Science Teaching* 54: 169-94, 2017.

54. **Carter DF, Ro HK, Alcott B, Lattuca LR**. Co-curricular connections: The role of undergraduate research experiences in promoting engineering students' communication, teamwork, and leadership skills. *Research in Higher Education* 57: 363-93, 2016.

55. **Chan Y, Biagi B, Giebisch G**. Control mechanisms of bicarbonate transport across the rat proximal convoluted tubule. *Am J Physiol Renal Physiol* 242: F532-F43, 1982.

56. **Chang MJ, Sharkness J, Hurtado S, Newman CB**. What matters in college for retaining aspiring scientists and engineers from underrepresented racial groups. *Journal of Research in Science Teaching* 51: 555-80, 2014.

57. **Chang PI, Rutlen DL**. Effects of beta-adrenergic agonists on splanchnic vascular volume and cardiac output. *Am J Physiol Heart Circ Physiol* 261: H1499-H507, 1991.

58. **Chaudhry SI, Wang Y, Concato J, Gill TM, Krumholz HM**. Patterns of weight change preceding hospitalization for heart failure. *Circulation* 116: 1549-54, 2007.

59. **Chen JJS, Heldt T, Verghese G, Mark R**. Analytical solution to a simplified circulatory model using piecewise linear elastance function. Massachusetts Institute of Technology, 2003.

60. **Chen JJS, Heldt T, Verghese GC, Mark RG**. Analytical solution to a simplified circulatory model using piecewise linear elastance function. *Comput Cardiol* 45-8, 2003.

61. **Chien Y, Pegram BL, Kardon MB, Frohlich ED**. Atrial natriuretic factor does not increase total body venous compliance in conscious rats with myocardial infarction. *Am J Physiol Heart Circ Physiol* 262: H432-H6, 1992.

62. **Cicci JD, Reed BN, McNeely EB, Oni-Orisan A, Patterson JH, Rodgers JE**. Acute decompensated heart failure: Evolving literature and implications for future practice. *Pharmacotherapy* 34: 373-88, 2013.

63. **Clark BR**. Faculty organization and authority. In: *The Study of Academic Administration*, edited by Lansford T. Boulder, CO: WICHE, 1963, p. 76-93.

64. **Clemmer JS, Pruett WA, Coleman TG, Hall JE, Hester RL**. Mechanisms of blood pressure salt sensitivity: new insights from mathematical modeling. *Am J Physiol Regul Integr Comp Physiol* 312: R451-R66, 2017.

65. **Cobelli C, Carson E**. Modeling the system. In: *Introduction to Modeling in Physiology and Medicine*. Burlington, MA: Academic Press, 2008, p. 75-157.

66. **Cobelli C, Carson E**. Physiological complexity and the need for models. In: *Introduction to Modeling in Physiology and Medicine*. Burlington, MA: Academic Press, 2008, p. 7-22.

67. **Cockett AT, Roberts AP, Moore RS**. Renal lymphatic transport of fluid and solutes. *Invest Urol* 7: 10-4, 1969.

68. **Cohen J**. A coefficient of agreement for nominal scales. *Educational and psychological measurement* 20: 37-46, 1960.

69. **Coleman TG**. Mathematical analysis of cardiovascular function. *IEEE Trans Biomed Eng* 289-94, 1985.

70. **Craney C, McKay T, Mazzeo A, Morris J, Prigodich C, De Groot R**. Cross-discipline perceptions of the undergraduate research experience. *The Journal of Higher Education* 82: 92-113, 2011.

71. **Crocetti E, Sica LS, Schwartz SJ, Serafini T, Meeus W**. Identity styles, dimensions, statuses, and functions: Making connections among identity conceptualizations. *European Review of Applied Psychology* 63: 1-13, 2013.

72. **Danielsen M, Ottesen JT**. A Cardiovascular Model. In: *Applied mathematical models in human physiology*, edited by Ottesen JT, Olufsen MS, and Larsen JK. Philadelphia: Society for Industrial and Applied Mathematics, 2004, p. 137-55.

73. **Davis SN, Mahatmya D, Garner PW, Jones RM**. Mentoring undergraduate scholars: A pathway to interdisciplinary research? *Mentoring & Tutoring: Partnership in Learning* 23: 427-40, 2015.

74. **de Freitas FM, Faraco EZ, de Azevedo DF, Zaduchliver J, Lewin I**. Behavior of normal pulmonary circulation during changes of total blood volume in man. *J Clin Invest* 44: 366-78, 1965.

75. **Deemer ED, Marks LR, Miller KA**. Peer science self-efficacy: A proximal contextual support for college students' science career intentions. *Journal of Career Assessment* 25: 537-51, 2017.

76. **Deen WM, Robertson CR, Brenner BM**. A model of peritubular capillary control of isotonic fluid reabsorption by the renal proximal tubule. *Biophys J* 13: 340-58, 1973.

77. **Denofrio LA, Russell B, Lopatto D, Lu Y**. Linking student interests to science curricula. *Science* 318: 1872–3, 2007.

78. **Desai KV, Gatson SN, Stiles TW, Stewart RH, Laine GA, Quick CM**. Integrating research and education at research-extensive universities with research-intensive communities. *Advances In Physiology Education* 32: 136-41, 2008.

79. **Deschamps A, Magder S**. Baroreflex control of regional capacitance and blood flow distribution with or without alpha-adrenergic blockade. *Am J Physiol Heart Circ Physiol* 263: H1755-H63, 1992.

80. **DiBona GF**. Effect of magnesium on water permeability of the rat nephron. *Am J Physiol* 223: 1324-6, 1972.

81. **Diekman AB, Steinberg M**. Navigating social roles in pursuit of important goals: A communal goal congruity account of STEM pursuits. *Social and Personality Psychology Compass* 7: 487-501, 2013.

82. **Dolan EL, Johnson D**. The undergraduate–postgraduate–faculty triad: Unique functions and tensions associated with undergraduate research experiences at research universities. *CBE-Life Sciences Education* 9: 543-53, 2010.

83. **Dongaonkar RM, Laine GA, Stewart RH, Quick CM**. Balance point characterization of interstitial fluid volume regulation. *Am J Physiol Regul Integr Comp Physiol* 297: R6-R16, 2009.

84. **Drake R, Doursout M**. Pulmonary edema and elevated left atrial pressure: four hours and beyond. *Physiology* 17: 223-6, 2002.

85. **Drake RE, Allen SJ, Katz J, Gabel JC, Laine GA**. Equivalent circuit technique for lymph flow studies. *Am J Physiol Heart Circ Physiol* 251: H1090-H4, 1986.

86. **Drees JA, Rothe CF**. Reflex venoconstriction and capacity vessel pressure-volume relationships in dogs. *Circ Res* 34: 360-73, 1974.

87. **Dunlap ME, Bibevski S, Rosenberry TL, Ernsberger P**. Mechanisms of altered vagal control in heart failure: influence of muscarinic receptors and acetylcholinesterase activity. *Am J Physiol Heart Circ Physiol* 285: H1632-H40, 2003.

88. **Dunlap ME, Sobotka PA**. Fluid re-distribution rather than accumulation causes most cases of decompensated heart failure. *J Am Coll Cardiol* 62: 165-6, 2013.

89. **Eagan MK, Hurtado S, Chang MJ, Garcia GA, Herrera FA, Garibay JC**. Making a difference in science education the impact of undergraduate research programs. *American educational research journal* 50: 683-713, 2013.

90. **Edwards MT, Diana JN**. Effect of exercise on pre-and postcapillary resistance in the spontaneously hypertensive rat. *Am J Physiol Heart Circ Physiol* 234: H439-H46, 1978.

91. **Efstratiadis S, Michaels AD**. Acute hemodynamic effects of intravenous nesiritide on left ventricular diastolic function in heart failure patients. *J Card Fail* 15: 673-80, 2009.

92. **Ellwein LM, Pope SR, Xie A, Batzel J, Kelley CT, Olufsen MS**. Modeling cardiovascular and respiratory dynamics in congestive heart failure. *Math Biosci* 241: 56-74, 2013.

93. **Falchuk KH, Brenner BM, Tadokoro M, Berliner RW**. Oncotic and hydrostatic pressures in peritubular capillaries and fluid reabsorption by proximal tubule. *Am J Physiol* 220: 1427-33, 1971.

94. **Fallick C, Sobotka PA, Dunlap ME**. Sympathetically mediated changes in capacitance redistribution of the venous reservoir as a cause of decompensation. *Circ Heart Fail* 4: 669-75, 2011.

95. **Feldman A, Divoll K, Rogan-Klyve A**. Research education of new scientists: Implications for science teacher education. *Journal of Research in Science Teaching* 46: 442-59, 2009.

96. **Feldman A, Divoll KA, Rogan-Klyve A**. Becoming researchers: The participation of undergraduate and graduate students in scientific research groups. *Science Education* 97: 218-43, 2013.

97. **Felix A, Zovinka E**. One STEP: Enhancing student retention through early introduction of research for STEM majors. *Council on Undergraudate Research Quarterly* 29: 30-5, 2008.

98. **Fermoso JD, Richardson TQ, Guyton AC**. Mechanism of decrease in cardiac output caused by opening the chest. *Am J Physiol* 207: 1112-6, 1964.

99. **Floras JS**. Sympathetic nervous system activation in human heart failure: Clinical implications of an updated model. *J Am Coll Cardiol* 54: 375-85, 2009.

100. **Forrester JS, Diamond G, Chatterjee K, Swan H**. Medical therapy of acute myocardial infarction by application of hemodynamic subsets. *N Engl J Med* 295: 1404-13, 1976.

101. **Forrester JS, Waters DD**. Hospital treatment of congestive heart failure: Management according to hemodynamic profile. *Am J Med* 65: 173-80, 1978.

102. **Frohnert PP, Höhmann B, Zwiebel R, Baumann K**. Free flow micropuncture studies of glucose transport in the rat nephron. *Pflügers Arch* 315: 66-85, 1970.

103. **Frömter E, Rumrich G, Ullrich KJ**. Phenomenologic description of Na^+, Cl^- and HCO_3^- absorption from proximal tubules of the rat kidney. *Pflügers Archiv* 343: 189-220, 1973.

104. **Garcia-Estan J, Roman RJ**. Role of renal interstitial hydrostatic pressure in the pressure diuresis response. *Am J Physiol Renal Physiol* 256: F63-F70, 1989.

105. **Garriott PO, Flores LY, Martens MP**. Predicting the math/science career goals of low-income prospective first-generation college students. *Journal of Counseling Psychology* 60: 200, 2013.

106. **Gatson SN, Stewart RH, Laine GA, Quick CM**. A case for centralizing undergraduate summer research programs: the DeBakey Research-Intensive Community. *The FASEB Journal* 23: 633.8-.8, 2009.

107. **Gazley JL, Remich R, Naffziger-Hirsch ME, Keller J, Campbell PB, McGee R**. Beyond preparation: Identity, cultural capital, and readiness for graduate school in the biomedical sciences. *Journal of research in science teaching* 51: 1021-48, 2014.

108. **Gonzalez C, Gonzalez**. Undergraduate research, graduate mentoring, and the university's mission. *Science* 293: 1624-6, 2001.

109. **Gore PAJ**. Cluster analysis. In: *Handbook of applied multivariate statistics and mathematical modeling*, edited by Tinsley HEA, and Brown SD. San Diego, CA: Academic Press, 2000, p. 297–321.

110. **Gottschalk CW, Mylle M**. Micropuncture study of pressures in proximal tubules and peritubular capillaries of the rat kidney and their relation to ureteral and renal venous pressures. *Am J Physiol* 185: 430-9, 1956.

111. **Granger JP, Haas JA, Pawlowska D, Knox FG**. Effect of direct increases in renal interstitial hydrostatic pressure on sodium excretion. *Am J Physiol Renal Physiol* 254: F527-32, 1988.

112. **Gray R, Chatterjee K, Vyden JK, Ganz W, Forrester JS, Swan H**. Hemodynamic and metabolic effects of isosorbide dinitrate in chronic congestive heart failure. *Am Heart J* 90: 346-52, 1975.

113. **Green JF**. Mechanism of action of isoproterenol on venous return. *Am J Physiol Heart Circ Physiol* 232: H152-H6, 1977.

114. **Green R, Bishop JH, Giebisch G**. Ionic requirements of proximal tubular sodium transport. III. Selective luminal anion substitution. *Am J Physiol Renal Physiol* 236: F268-F77, 1979.

115. **Green R, Giebisch G**. Reflection coefficients and water permeability in rat proximal tubule. *Am J Physiol Renal Physiol* 257: F658-F68, 1989.

116. **Green R, Giebisch G, Unwin R, Weinstein AM**. Coupled water transport by rat proximal tubule. *Am J Physiol Renal Physiol* 261: F1046-F54, 1991.

117. **Green R, Windhager EE, Giebisch G**. Protein oncotic pressure effects on proximal tubular fluid movement in the rat. *Am J Physiol* 226: 265-76, 1974.

118. **Gregerman SR, Lerner JS, von Hippel W, Jonides J, Nagda BA**. Undergraduate student-faculty research partnerships affect student retention. *The Review of Higher Education* 22: 55-72, 1998.

119. **Guyton AC**. Determination of cardiac output by equating venous return curves with cardiac response curves. *Physiol Rev* 35: 123-9, 1955.

120. **Guyton AC, CE Coleman T**. *Circulatory physiology: cardiac output and its regulation*. Philadelphia: WB Saunders, 1973.

121. **Guyton AC, Coleman TG, Granger HJ**. Circulation: overall regulation. *Annu Rev Physiol* 34: 13-44, 1972.

122. **Guyton AC, Lindsey AW, Kaufmann BN**. Effect of mean circulatory filling pressure and other peripheral circulatory factors on cardiac output. *Am J Physiol* 180: 463-8, 1955.

123. **Hargens AR, Tucker BJ, Blantz RC**. Renal lymph protein in the rat. *Am J Physiol Renal Physiol* 233: F269-F73, 1977.

124. **Harré R**. *Personal being: A theory for individual psychology*. Oxford: Blackwell, 1983.

125. **Hasking GJ, Esler MD, Jennings GL, Burton D, Johns JA, Korner PI**. Norepinephrine spillover to plasma in patients with congestive heart failure: evidence of increased overall and cardiorenal sympathetic nervous activity. *Circulation* 73: 615-21, 1986.

126. **Hathaway RS, Nagda BA, Gregerman SR**. The relationship of undergraduate research participation to graduate and professional education pursuit: an empirical study. *Journal of College Student Development* 43: 614-31, 2002.

127. **Heldt T, Chernyak Y**. Analytical solution to a minimal cardiovascular model. In: *Computers in Cardiology*. Valencia, Spain: IEEE, 2006, p. 785-8.

128. **Heldt T, Shim EB, Kamm RD, Mark RG**. Computational modeling of cardiovascular response to orthostatic stress. *J Appl Physiol* 92: 1239-54, 2002.

129. **Henderson WR, Griesdale DE, Walley KR, Sheel AW**. Clinical review: Guyton-the role of mean circulatory filling pressure and right atrial pressure in controlling cardiac output. *Crit Care* 14: 243, 2010.

130. **Henrich HA, Romen W, Heimgärtner W, Hartung E, Bäumer F**. Capillary rarefaction characteristic of the skeletal muscle of hypertensive patients. *J Mol Med* 66: 54-60, 1988.

131. **Hippel Wv, Lerner JS, Gregerman SR, Nagda BA, Jonides J**. Undergraduate student-faculty research partnerships affect student retention. *The Review of Higher Education* 22: 55-72, 1998.

132. **Horowitz J, Christopher KB**. The research mentoring program: Serving the needs of graduate and undergraduate researchers. *Innovative Higher Education* 38: 105-16, 2013.

133. **Hotaling N, Fasse BB, Bost LF, Hermann CD, Forest CR**. A quantitative analysis of the effects of a multidisciplinary engineering capstone design course. *Journal of Engineering Education* 101: 630-56, 2012.

134. **Hu Lt, Bentler PM**. Cutoff criteria for fit indexes in covariance structure analysis: Conventional criteria versus new alternatives. *Structural Equation Modeling: A Multidisciplinary Journal* 6: 1-55, 1999.

135. **Hunter AB, Laursen SL, Seymour E**. Becoming a scientist: The role of undergraduate research in students' cognitive, personal, and professional development. *Science Education* 91: 36-74, 2007.

136. **Huss R, Stephenson J**. A mathematical model of proximal tubule absorption. *J Membr Biol* 47: 377-99, 1979.

137. **Huss RE, Marsh DJ**. A model of NaCl and water flow through paracellular pathways of renal proximal tubules. *J Membr Biol* 23: 305-47, 1975.

138. **Huss RE, Stephenson JL**. A mathematical model of proximal tubule absorption. *J Membr Biol* 47: 377-99, 1979.

139. **Hussain J, Ahmed HA, Grant WA, Hernandez MD, Quick CM, Stewart RH**. Predicting regression of a Ductus Arteriosus. *FASEB J* 31: 860.9-.9, 2017.

140. **Ichikawa I, Brenner BM**. Mechanism of inhibition of proximal tubule fluid reabsorption after exposure of the rat kidney to the physical effects of expansion of extracellular fluid volume. *J Clin Invest* 64: 1466-74, 1979.

141. **Ichikawa I, Kon V**. Role of peritubular capillary forces in the renal action of carbonic anhydrase inhibitor. *Kidney Int* 30: 828-35, 1986.

142. **Irving PW, Sayre EC**. Identity statuses in upper-division physics students. *Cultural Studies of Science Education* 11: 1155-200, 2016.

143. **JC B, Kao P, Hu D, Heser D, Heublein D, Granger J, . . . Reeder G**. Atrial natriuretic peptide elevation in congestive heart failure in the human. *Science* 231: 1145-7, 1986.

144. **Junge B, Quiñones C, Kakietek J, Teodorescu D, Marsteller P**. Promoting undergraduate interest, preparedness, and professional pursuit in the sciences: an outcomes evaluation of the SURE program at Emory University. *CBE-Life Sciences Education* 9: 119-32, 2010.

145. **Källskog Ö, Wolgast M**. Driving forces over the peritubular capillary membrane in the rat kidney during antidiuresis and saline expansion. *Acta Physiol Scand* 89: 116-25, 1973.

146. **Kato T, Kassab S, Wilkins FC, Kirchner KA, Granger JP**. Decreased sensitivity to renal interstitial hydrostatic pressure in Dahl salt-sensitive rats. *Hypertension* 23: 1082-6, 1994.

147. **Kedem O, Katchalsky A**. Thermodynamic analysis of the permeability of biological membranes to non-electrolytes. *Biochim Biophys Acta* 27: 229-46, 1958.

148. **Khraibi AA, Dobrian AD, Yu T, Solhaug MJ, Billiar RB**. Role of RIHP and renal tubular sodium transporters in volume retention of pregnant rats. *Am J Hypertens* 18: 1375-83, 2005.

149. **Khraibi AA, Granger JP, Haas JA, Burnett JC, Knox FG**. Intrarenal pressures during direct inhibition of sodium transport. *Am J Physiol Regul Integr Comp Physiol* 263: R1182-R6, 1992.

150. **Khraibi AA, Haas JA, Knox FG**. Effect of renal perfusion pressure on renal interstitial hydrostatic pressure in rats. *Am J Physiol Renal Physiol* 256: F165-F70, 1989.

151. **Khraibi AA, Heublein DM, Burnett JC, Knox FG**. Renal interstitial hydrostatic pressure and ANF in exaggerated natriuresis of the SHR. *Am J Physiol Regul Integr Comp Physiol* 258: R1380-R5, 1990.

152. **Khraibi AA, Solhaug MJ, Dobrian AD, Berndt TJ**. Renal interstitial hydrostatic pressure and natriuretic responses to volume expansion in pregnant rats. *Am J Physiol Renal Physiol* 282: F821-F5, 2002.

153. **Kimura N, Kimura H, Takahashi N, Hamada T, Maegawa H, Mori M, . . . Iwano M**. Renal resistive index correlates with peritubular capillary loss and arteriosclerosis in biopsy tissues from patients with chronic kidney disease. *Clin Exp Nephrol* 19: 1114-9, 2015.

154. **Kishore BK, Mandon B, Oza NB, DiGiovanni SR, Coleman RA, Ostrowski NL, . . . Knepper MA**. Rat renal arcade segment expresses vasopressin-regulated water channel and vasopressin V2 receptor. *J Clin Invest* 97: 2763-71, 1996.

155. **Klimstra TA, Hale III WW, Raaijmakers QA, Branje SJ, Meeus WH**. Identity formation in adolescence: change or stability? *Journal of Youth and Adolescence* 39: 150-62, 2010.

156. **Kneedler SC, Phillips LE, Hudson KR, Beckman KM, Gelston CAL, Rutkowski JM, . . . Mitchell BM**. Renal inflammation and injury are associated with lymphangiogenesis in hypertension. *Am J Physiol Renal Physiol* 312: F861-F9, 2017.

157. **Knox FG, Cuche JL, Ott CE, Diaz-Buxo JA, Marchand G**. Regulation of glomerular filtration and proximal tubule reabsorption. *Circ Res* 36: 107-18, 1975.

158. **Knox FG, Granger JP**. Control of sodium excretion: an integrative approach. In: *Comprehensive Physiology*, edited by Pollock DM. Bethesda, MD: Wiley Blackwell, 2011, p. 927-67.

159. **Kobulnicky HA, Dale DA**. A community mentoring model for STEM undergraduate research experiences. *Journal of College Science Teaching* 45: 17, 2016.

160. **Kovacs G, Berghold A, Scheidl S, Olschewski H**. Pulmonary arterial pressure during rest and exercise in healthy subjects: a systematic review. *Eur Respir J* 34: 888-94, 2009.

161. **Kremer JF, Bringle RG**. The effects of an intensive research experience on the careers of talented undergraduates. *Journal of Research & Development in Education* 1990.

162. **Kroger J, Martinussen M, Marcia JE**. Identity status change during adolescence and young adulthood: A meta-analysis. *Journal of adolescence* 33: 683-98, 2010.

163. **Kuh GD**. Guiding principles for creating seamless learning environments for undergraduates. *Journal of college student development* 37: 135-48, 1996.

164. **Kunau Jr RT**. The influence of the carbonic anhydrase inhibitor, benzolamide (CL-11,366), on the reabsorption of chloride, sodium, and bicarbonate in the proximal tubule of the rat. *J Clin Invest* 51: 294-306, 1972.

165. **Kunau Jr RT, Webb HL, Borman SC**. Characteristics of sodium reabsorption in the loop of Henle and distal tubule. *Am J Physiol* 227: 1181-91, 1974.

166. **Kunau Jr RT, Weller DR, Webb HL**. Clarification of the site of action of chlorothiazide in the rat nephron. *J Clin Invest* 56: 401-7, 1975.

167. **Kunau Jr RT, Whinnery MA**. Potassium transfer in distal tubule of normal and remnant kidneys. *Am J Physiol Renal Physiol* 235: F186-F91, 1978.

168. **Ky B, French B, May Khan A, Plappert T, Wang A, Chirinos JA, . . . Cappola TP**. Ventricular-arterial coupling, remodeling, and prognosis in chronic heart failure. *J Am Coll Cardiol* 62: 1165-72, 2013.

169. **La Rovere MT, Specchia G, Mortara A, Schwartz PJ**. Baroreflex sensitivity, clinical correlates, and cardiovascular mortality among patients with a first myocardial infarction. A prospective study. *Circulation* 78: 816-24, 1988.

170. **Landis EM, Pappenheimer JR**. Exchange of substances through the capillary walls. In: *Handbook of Physiology: Circulation*. Washington, DC: Am Physiol Soc, 1963, p. 961-1034.

171. **Larson M, Hermansson K, Wolgast M**. Hydraulic permeability of the peritubular and glomerular capillary membranes in the rat kidney. *Acta Physiol Scand* 117: 251-61, 1983.

172. **Lassiter WE, Frick A, Rumrich G, Ullrich KJ**. Influence of ionic calcium on the water permeability of proximal and distal tubules in the rat kidney. *Pflügers Arch* 285: 90-5, 1965.

173. **Leal-Muniz V, Constantine MG**. Predictors of the career commitment process in Mexican American college students. *Journal of Career Assessment* 13: 204-15, 2005.

174. **LeBrie SJ, Mayerson HS**. Influence of elevated venous pressure on flow and composition of renal lymph. *Am J Physiol* 198: 1037-40, 1960.

175. **Ledder G**. Mathematical Modeling. In: *Mathematics for the Life Sciences: Calculus, Modeling, Probability, and Dynamical Systems*. New York, NY: Springer-Verlag, 2013, p. 83-143.

176. **Lee C-J, Gardiner BS, Ngo JP, Kar S, Evans RG, Smith DW**. Accounting for oxygen in the renal cortex: A computational study of factors that predispose the cortex to hypoxia. *Am J Physiol Renal Physiol* 313: F218-F36, 2017.

177. **Lee RW, Gay RG, Goldman S**. Atrial natriuretic peptide reverses angiotensin-induced venoconstriction in dogs. *Am J Physiol Heart Circ Physiol* 257: H1062-H7, 1989.

178. **Lent RW, Schmidt J, Schmidt L**. Collective efficacy beliefs in student work teams: Relation to self-efficacy, cohesion, and performance. *Journal of Vocational Behavior* 68: 73-84, 2006.

179. **Levick JR, Michel CC**. Microvascular fluid exchange and the revised Starling principle. *Cardiovasc Res* 87: 198-210, 2010.

180. **Levy M, Levinsky NG**. Proximal reabsorption and intrarenal pressure during colloid infusions in the dog. *Am J Physiol* 220: 415-21, 1971.

181. **Levy MN**. The cardiac and vascular factors that determine systemic blood flow. *Circ Res* 44: 739-47, 1979.

182. **Lewis GD, Murphy RM, Shah RV, Pappagianopoulos PP, Malhotra R, Bloch KD, . . . Semigran MJ**. Pulmonary vascular response patterns during exercise in left ventricular systolic dysfunction predict exercise capacity and outcomes clinical perspective. *Circ Heart Fail* 4: 276-85, 2011.

183. **Liang F, Liu H**. A closed-loop lumped parameter computational model for human cardiovascular system. *JSME Int J., Ser. C* 48: 484-93, 2005.

184. **Liu FY, Cogan MG**. Kinetics of bicarbonate transport in the early proximal convoluted tubule. *Am J Physiol Renal Physiol* 253: F912-F6, 1987.

185. **Liu S, Soong Y, Seshan SV, Szeto HH**. Novel cardiolipin therapeutic protects endothelial mitochondria during renal ischemia and mitigates microvascular rarefaction, inflammation, and fibrosis. *Am J Physiol Renal Physiol* 306: F970-F80, 2014.

186. **Lopatto D**. Survey of Undergraduate Research Experiences (SURE): First Findings. *Cell Biol Educ* 3: 270-7, 2004.

187. **Lopatto D**. Undergraduate research experiences and the epigenesis of a science career. In: *64th Annual Meeting of the Society for Development Biology*. San Francisco, CA: Academic Press, 2005, p. 586-7.

188. **Lopatto D**. Undergraduate research experiences support science career decisions and active learning. *CBE-Life Sciences Education* 6: 297-306, 2007.

189. **Louviere JJ, Hensher DA, Swait JD**. *Stated choice methods: analysis and applications*. Cambridge: Cambridge University Press, 2000.

190. **Lu K, Clark JW, Ghorbel FH, Ware DL, Bidani A**. A human cardiopulmonary system model applied to the analysis of the Valsalva maneuver. *Am J Physiol Heart Circ Physiol* 281: H2661-79, 2001.

191. **Lucci MS, Warnock DG, Rector F**. Carbonic anhydrase-dependent bicarbonate reabsorption in the rat proximal tubule. *Am J Physiol Renal Physiol* 236: F58-F65, 1979.

192. **Maas JJ, Pinsky MR, Aarts LP, Jansen JR**. Bedside assessment of total systemic vascular compliance, stressed volume, and cardiac function curves in intensive care unit patients. *Anesth Analg* 115: 880-7, 2012.

193. **Magder S**. Point: Counterpoint: The classical Guyton view that mean systemic pressure, right atrial pressure, and venous resistance govern venous return is/is not correct. *J Appl Physiol* 101: 1523-5, 2006.

194. **Magder S, De Varennes B**. Clinical death and the measurement of stressed vascular volume. *Crit Care Med* 26: 1061-4, 1998.

195. **Magder S, Veerassamy S, Bates JH**. A further analysis of why pulmonary venous pressure rises after the onset of LV dysfunction. *J Appl Physiol* 106: 81-90, 2009.

196. **Manning GS, Bresler EH, Wendt RP**. Irreversible thermodynamics and flow across membranes. *Science* 166: 1438, 1969.

197. **Marcia JE**. The status of the statuses: Research review. In: *Ego identity: A handbook for psychosocial research*, edited by Marcia JE, Waterman AS, Matteson DR, Archer SL, and Orlofsky JL. New York: Springer-Verlag, 1993, p. 22-41.

198. **Maunsbach AB**. Cellular mechanisms of tubular protein transport. *Int Rev Physiol* 11: 145-67, 1975.

199. **McIntosh GH, Morris B**. The lymphatics of the kidney and the formation of renal lymph. *J Physiol* 214: 365-76, 1971.

200. **Meixner C, Rosch D**. Powerful pedagogies. In: *The handbook for student leadership development*, edited by Komives SR, Dugan JP, Owen JE, Slack C, and Wagner W. New York: John Wiley & Sons, 2011, p. 307-37.

201. **Mertz J, Haas JA, Berndt TJ, Burnett Jr JC, Knox F**. Effects of secretin on peritubular capillary physical factors and proximal fluid reabsorption in the rat. *J Clin Invest* 72: 622-5, 1983.

202. **Mikulecky DC**. A simple network thermodynamic method for series-parallel coupled flows II. The non-linear theory, with applications to coupled solute and volume flow in a series membrane. *J Theor Biol* 69: 511-41, 1977.

203. **Mikulecky DC, Thomas SR**. A simple network thermodynamic method for series-parallel coupled flows III: Application to coupled solute and volume flows through epithelial membranes. *J Theor Biol* 73: 697-710, 1978.

204. **Miller WL, Albers DP, Gansen DN, Mullan BP**. Intravascular volume profiles in patients with class I and II systolic heart failure: heterogeneity and volume overload are common even in mild heart failure. *J Card Fail* 2017.

205. **Miller WL, Grill DE, Borlaug BA**. Clinical features, hemodynamics, and outcomes of pulmonary hypertension due to chronic heart failure with reduced ejection fraction: pulmonary hypertension and heart failure. *JACC: Heart Failure* 1: 290-9, 2013.

206. **Miracle CM, Rieg T, Blantz RC, Vallon V, Thomson SC**. Combined effects of carbonic anhydrase inhibitor and adenosine A1 receptor antagonist on hemodynamic and tubular function in the kidney. *Kidney Blood Press Res* 30: 388-99, 2007.

207. **Morley D, Litwak K, Ferber P, Spence P, Dowling R, Meyns B, . . . Burkhoff D**. Hemodynamic effects of partial ventricular support in chronic heart failure: results of simulation validated with in vivo data. *The Journal of Thoracic and Cardiovascular Surgery* 133: 21-8. e4, 2007.

208. **Moss R, Thomas SR**. Hormonal regulation of salt and water excretion: a mathematical model of whole kidney function and pressure natriuresis. *Am J Physiol Renal Physiol* 306: F224-F48, 2014.

209. **Muntwyler E, Griffin GE**. Effect of potassium on electrolytes of rat plasma and muscle. *J Biol Chem* 193: 563-73, 1951.

210. **National Academy of Sciences, National Academy of Engineering, Institute of Medicine**. *Facilitating interdisciplinary research*. Washington, DC: The National Academies Press, 2005, p. 332.

211. **National Science Foundation**. Women, minorities, and persons with disabilities in science and engineering: 2017 Arlington, VA: National Center for Science and Engineering Statistics, 2017.

212. **Navar LG, Arendshorst WJ, Pallone TL, Inscho EW, Imig JD, Bell PD**. The renal microcirculation. In: *Handbook of Physiology, Microcirculation*, edited by Tuma R, and Wa L. San Diego: Elsevier, 2008, p. 550-683.

213. **Nekooeian AA, Tabrizchi R**. Haemodynamic effects of a selective adenosine A2A receptor agonist, CGS 21680, in chronic heart failure in anaesthetized rats. *British journal of pharmacology* 125: 651-8, 1998.

214. **Neumann R, Parry S, Becher T**. Teaching and learning in their disciplinary contexts: A conceptual analysis. *Studies in higher education* 27: 405-17, 2002.

215. **Nishikawa T, Dohi S**. Errors in the measurement of cardiac output by thermodilution. *Canadian Journal of Anaesthesia* 40: 142-53, 1993.

216. **Nohria A, Tsang SW, Fang JC, Lewis EF, Jarcho JA, Mudge GH, Stevenson LW**. Clinical assessment identifies hemodynamic profiles that predict outcomes in patients admitted with heart failure. *J Am Coll Cardiol* 41: 1797-804, 2003.

217. **O'Morchoe CC, O'Morchoe PJ, Donati EJ**. Comparison of hilar and capsular renal lymph. *Am J Physiol* 229: 416-21, 1975.

218. **Olansen JB, Clark J, Khoury D, Ghorbel F, Bidani A**. A closed-loop model of the canine cardiovascular system that includes ventricular interaction. *Comput Biomed Res* 33: 260-95, 2000.

219. **Osgood RW, Lameire NH, Sorkin MI, Stein J**. Effect of aortic clamping on proximal reabsorption and sodium excretion in the rat. *Am J Physiol Renal Physiol* 232: F92-F6, 1977.

220. **Ott CE**. Effect of saline expansion on peritubule capillary pressures and reabsorption. *Am J Physiol Renal Physiol* 240: F106-F10, 1981.

221. **Ott CE, Haas JA, Cuche JL, Knox FG**. Effect of increased peritubule protein concentration on proximal tubule reabsorption in the presence and absence of extracellular volume expansion. *J Clin Invest* 55: 612-20, 1975.

222. **Ott CE, Navar LG, Guyton AC**. Pressures in static and dynamic states from capsules implanted in the kidney. *Am J Physiol* 221: 394-400, 1971.

223. **Ottesen JT, Olufsen MS, Larsen JK**. A Cardiovascular Model. In: *Applied mathematical models in human physiology*SIAM, 2004.

224. **Palatt PJ, Saidel GM, Macklin M**. Transport processes in the renal cortex. *J Theor Biol* 29: 251-74, 1970.

225. **Pappenheimer JR, Soto-Rivera A**. Effective osmotic pressure of the plasma proteins and other quantities associated with the capillary circulation in the hindlimbs of cats and dogs. *Am J Physiol* 152: 471-91, 1948.

226. **Patel KP, Carmines PK**. Renal interstitial hydrostatic pressure and sodium excretion during acute volume expansion in diabetic rats. *Am J Physiol Regul Integr Comp Physiol* 281: R239-R45, 2001.

227. **Patlak CS, Patlak DA, Goldstein JF, Hoffman**. The flow of solute and solvent across a two-membrane system. *J Theor Biol* 5: 426-42, 1963.

228. **Perez T, Cromley JG, Kaplan A**. The role of identity development, values, and costs in college STEM retention. *Journal of educational psychology* 106: 315, 2014.

229. **Perna L, Lundy-Wagner V, Drezner ND, Gasman M, Yoon S, Bose E, Gary S**. The contribution of HBCUs to the preparation of African American women for STEM careers: A case study. *Research in Higher Education* 50: 1-23, 2009.

230. **Persson AEG, Schnermann J, Ågerup B, Eriksson NE**. The hydraulic conductivity of the rat proximal tubular wall determined with colloidal solutions. *Pflügers Archiv* 360: 25-44, 1975.

231. **Pinter GG, Gärtner K**. Peritubular capillary, interstitium, and lymph of the renal cortex. In: *Reviews of Physiology, Biochemistry and Pharmacology*. Berlin: Springer, 1984, p. 183-202.

232. **Pironet A, Desaive T, Chase JG, Morimont P, Dauby PC**. Model-based computation of total stressed blood volume from a preload reduction manoeuvre. *Math Biosci* 265: 28-39, 2015.

233. **Porfeli EJ, Lee B, Vondracek FW, Weigold IK**. A multi-dimensional measure of vocational identity status. *Journal of Adolescence* 34: 853-71, 2011.

234. **Porter A, Rafols I**. Is science becoming more interdisciplinary? Measuring and mapping six research fields over time. *Scientometrics* 81: 719-45, 2009.

235. **Preisig PA, Berry CA**. Evidence for transcellular osmotic water flow in rat proximal tubules. *Am J Physiol Renal Physiol* 249: F124-F31, 1985.

236. **Prevorovská S, Musil J, Maršık F**. Human cardiovascular system with heart failure under baroreflex control (numerical model). *Acta Bioeng Biomech* 3: 39-52, 2001.

237. **Price HL, Cooperman LH, Warden JC**. Control of the splanchnic circulation in man: role of beta-adrenergic receptors. *Circ Res* 21: 333-40, 1967.

238. **Quick CM, Young WL, Noordergraaf A**. Infinite number of solutions to the hemodynamic inverse problem. *Am J Physiol Heart Circ Physiol* 280: H1472-9, 2001.

239. **Quinn MD, Marsh DJ**. Peritubular capillary control of proximal tubule reabsorption in the rat. *Am J Physiol Renal Physiol* 236: F478-F87, 1979.

240. **Raftery AE**. Bayesian model selection in social research. *Sociological methodology* 111-63, 1995.

241. **Rector FC**. Sodium, bicarbonate, and chloride absorption by the proximal tubule. *Am J Physiol Renal Physiol* 244: F461-F71, 1983.

242. **Roman RJ**. Pressure-diuresis in volume-expanded rats. Tubular reabsorption in superficial and deep nephrons. *Hypertension* 12: 177-83, 1988.

243. **Rose WC, Shoukas AA**. Two-port analysis of systemic venous and arterial impedances. *Am J Physiol Heart Circ Physiol* 265: H1577-H87, 1993.

244. **Rothe CF**. Mean circulatory filling pressure: its meaning and measurement. *J Appl Physiol* 74: 499-509, 1993.

245. **Roy ED, Morzillo AT, Seijo F, Reddy SM, Rhemtulla JM, Milder JC, . . . Martin SL**. The elusive pursuit of interdisciplinarity at the human-environment interface. *BioScience* 63: 745-53, 2013.

246. **Russell SH, Hancock MP, McCullough J**. Benefits of undergraduate research experiences. *Science* 316: 548-9, 2007.

247. **Sackin H, Boulpaep EL**. Models for coupling of salt and water transport: proximal tubular reabsorption in Necturus kidney. *J Gen Physiol* 66: 671-733, 1975.

248. **Sadler TD, Burgin S, McKinney L, Ponjuan L**. Learning science through research apprenticeships: A critical review of the literature. *Journal of Research in Science Teaching* 47: 235-56, 2010.

249. **Sagawa K**. The ventricular pressure-volume diagram revisited. *Circ Res* 43: 677-87, 1978.

250. **Sagawa K, Eisner A**. Static pressure-flow relation in the total systemic vascular bed of the dog and its modification by the baroreceptor reflex. *Circ Res* 36: 406-13, 1975.

251. **Sagawa K, Lie RK, Schaefer J**. Translation of Otto frank's paper "Die Grundform des arteriellen Pulses" zeitschrift für biologie 37: 483–526 (1899). *J Mol Cell Cardiol* 22: 253-4, 1990.

252. **Sakamoto T, Kakino T, Sakamoto K, Tobushi T, Tanaka A, Saku K, . . . Tsutsumi T**. Changes in vascular properties, not ventricular properties, predominantly contribute to baroreflex regulation of arterial pressure. *Am J Physiol Heart Circ Physiol* 308: H49-H58, 2015.

253. **Schafer JA, Patlak CS, Andreoli TE**. Fluid absorption and active and passive ion flows in the rabbit superficial pars recta. *Am J Physiol Renal Physiol* 233: F154-F67, 1977.

254. **Schafer JA, Reeves WB, Andreoli TE**. Mechanisms of fluid transport across renal tubules. In: *Comprehensive Physiology*, edited by Pollock DM. Bethesda, MD: Wiley Blackwell, 2011, p. 659–713.

255. **Schwartzenberg S, Redfield MM, From AM, Sorajja P, Nishimura RA, Borlaug BA**. Effects of vasodilation in heart failure with preserved or reduced ejection fraction: implications of distinct pathophysiologies on response to therapy. *J Am Coll Cardiol* 59: 442-51, 2012.

256. **Seymour E, Hewitt NM**. *Talking about leaving: Why undergraduates leave the sciences*. Boulder, CO: Westview Press, 1997.

257. **Seymour E, Hunter A, Laursen SL, DeAntoni T**. Establishing the benefits of research experiences for undergraduates in the sciences: First findings from a three-year study. *Science Education* 88: 493-534, 2004.

258. **Shoukas AA**. Pressure-flow and pressure-volume relations in the entire pulmonary vascular bed of the dog determined by two-port analysis. *Circ Res* 37: 809-18, 1975.

259. **Shoukas AA, Brunner MJ, Frankle AE, Greene AS, Kallman CH**. Carotid sinus baroreceptor reflex control and the role of autoregulation in the systemic and pulmonary arterial pressure-flow relationships of the dog. *Circ Res* 54: 674-82, 1984.

260. **Smith BW, Andreassen S, Shaw GM, Jensen PL, Rees SE, Chase JG**. Simulation of cardiovascular system diseases by including the autonomic nervous system into a minimal model. *Computer methods and programs in biomedicine* 86: 153-60, 2007.

261. **Spitzer A, Windhager EE**. Effect of peritubular oncotic pressure changes on proximal tubular fluid reabsorption. *Am J Physiol* 218: 1188-93, 1970.

262. **Stachowska-Pietka J, Waniewski J, Flessner MF, Lindholm B**. Computer simulations of osmotic ultrafiltration and small-solute transport in peritoneal dialysis: a spatially distributed approach. *Am J Physiol Renal Physiol* 302: F1331-F41, 2012.

263. **Staub NC**. Pulmonary edema. *Physiological Reviews* 54: 678-811, 1974.

264. **Suga H, Sagawa K**. Instantaneous pressure-volume relationships and their ratio in the excised, supported canine left ventricle. *Circ Res* 35: 117-26, 1974.

265. **Sunagawa K, Sagawa K, Maughan WL**. Ventricular interaction with the loading system. *Annals of Biomedical Engineering* 12: 163-89, 1984.

266. **Sunagawa K, Sagawa K, Maughan WL**. Ventricular interaction with the vascular system in terms of pressure-volume relationships. In: *Ventricular/Vascular Coupling*, edited by Yin FCP. New York: Springer, 1987, p. 210-39.

267. **Swann HG, Ormsby AA, Delashaw JB, Tharp WW**. Relation of lymph to distending fluids of the kidney. *Exp Biol Med* 97: 517-22, 1958.

268. **Tabrizchi R**. Effects of adenosine and adenosine analogues on mean circulatory filling pressure and cardiac output in anesthetized rats. *Naunyn Schmiedebergs Arch Pharmacol* 356: 69-75, 1997.

269. **Taylor AE, Granger DN**. Exchange of macromolecules across the microcirculation. In: *Handbook of Physiology: The Cardiovascular System - Microcirculation*. Bethesda, MD: Am Physiol Soc, 1984, p. 467-520.

270. **Thiry H, Laursen SL**. The role of student-advisor interactions in apprenticing undergraduate researchers into a scientific community of practice. *Journal of Science Education and Technology* 20: 771-84, 2011.

271. **Thiry H, Laursen SL, Hunter A-B**. What experiences help students become scientists?: A comparative study of research and other sources of personal and professional gains for STEM undergraduates. *The Journal of Higher Education* 82: 357-88, 2011.

272. **Thoman DB, Muragishi GA, Smith JL**. Research microcultures as socialization contexts for underrepresented science students. *Psychological science* 28: 760-73, 2017.

273. **Thomas SR, Mikulecky DC**. A network thermodynamic model of salt and water flow across the kidney proximal tubule. *Am J Physiol Renal Physiol* 235: F638-F48, 1978.

274. **Thomas SR, Mikulecky DC**. Transcapillary solute exchange: A comparison of the Kedem-Katchalsky convection-diffusion equations with the rigorous nonlinear equations for this special case. *Microvasc Res* 15: 207-20, 1978.

275. **Tsuruta H, Sato T, Shirataka M, Ikeda N**. Mathematical model of cardiovascular mechanics for diagnostic analysis and treatment of heart failure: Part 1 model description and theoretical analysis. *Med Biol Eng Comput* 32: 3-11, 1994.

276. **Tucker BJ, Mundy CA, Blantz RC**. Can causality be determined from proximal tubular reabsorption and peritubular physical factors? *Am J Physiol Renal Physiol* 250: F169-F75, 1986.

277. **Tucker BJ, Steiner RW, Gushwa LC, Blantz RC**. Studies on the tubulo-glomerular feedback system in the rat: the mechanism of reduction in filtration rate with benzolamide. *J Clin Invest* 62: 993-1004, 1978.

278. **Tyberg JV, Belenkie I, Manyari DE, Smith ER**. Ventricular interaction and venous capacitance modulate left ventricular preload. *Can J Cardiol* 12: 1058-64, 1996.

279. **Uemura K, Sugimachi M, Kawada T, Kamiya A, Jin Y, Kashihara K, Sunagawa K**. A novel framework of circulatory equilibrium. *Am J Physiol Heart Circ Physiol* 286: H2376-H85, 2004.

280. **Ullrich KJ, Rumrich G, Baldamus CA**. Mode of urea transport across the mammalian nephron. In: *Urea and the Kidney*, edited by Kerr D, and Schmidt-Nielsen B. Amsterdam: Excerpta Medica Foundation, 1970, p. 175-85.

281. **Ullrich KJ, Rumrich G, Fuchs G**. Wasserpermeabilität und transtubulärer Wasserfluß corticaler Nephronabschnitte bei verschiedenen Diuresezuständen. *Pflügers Arch* 280: 99-119, 1964.

282. **Ursino M, Antonucci M, Belardinelli E**. Role of active changes in venous capacity by the carotid baroreflex: analysis with a mathematical model. *Am J Physiol Heart Circ Physiol* 267: H2531-H46, 1994.

283. **Vaduganathan M, Gheorghiade M**. A roadmap to inpatient heart failure management. *J Cardiol* 65: 26-31, 2015.

284. **Vallon V, Schwark J-R, Richter K, Hropot M**. Role of Na^+/H^+ exchanger NHE3 in nephron function: micropuncture studies with S3226, an inhibitor of NHE3. *Am J Physiol Renal Physiol* 278: F375-F9, 2000.

285. **Vygotsky LS**. *Mind in society: The development of higher psychological processes*. Cambridge, MA: Harvard University Press, 1980.

286. **Wagner CS, Roessner JD, Bobb K, Klein JT, Boyack KW, Keyton J, . . . Börner K**. Approaches to understanding and measuring interdisciplinary scientific research (IDR): A review of the literature. *Journal of informetrics* 5: 14-26, 2011.

287. **Wallace AW, Tunin CM, Shoukas AA**. Effects of vasopressin on pulmonary and systemic vascular mechanics. *Am J Physiol Heart Circ Physiol* 257: H1228-H34, 1989.

288. **Wang SY, Manyari DE, Scott-Douglas N, Smiseth OA, Smith ER, Tyberg JV**. Splanchnic venous pressure–volume relation during experimental acute ischemic heart failure: differential effects of hydralazine, enalaprilat, and nitroglycerin. *Circulation* 91: 1205-12, 1995.

289. **Wang SY, Manyari DE, Tyberg JV**. Cardiac vagal reflex modulates intestinal vascular capacitance and ventricular preload in anesthetized dogs with acute myocardial infarction. *Circulation* 94: 529-33, 1996.

290. **Wang T, Yang C-L, Abbiati T, Schultheis PJ, Shull GE, Giebisch G, Aronson PS**. Mechanism of proximal tubule bicarbonate absorption in NHE3 null mice. *Am J Physiol Renal Physiol* 277: F298-F302, 1999.

291. **Webb S, Adgey A, Pantridge J**. Autonomic disturbance at onset of acute myocardial infarction. *Br Med J* 3: 89-92, 1972.

292. **Weinstein AM**. Glomerulotubular balance in a mathematical model of the proximal nephron. *Am J Physiol Renal Physiol* 258: F612-F26, 1990.

293. **Weinstein AM, Stephenson JL**. Models of coupled salt and water transport across leaky epithelia. *J Membr Biol* 60: 1-20, 1981.

294. **Weinstein AM, Weinbaum S, Duan Y, Du Z, Yan Q, Wang T**. Flow-dependent transport in a mathematical model of rat proximal tubule. *Am J Physiol Renal Physiol* 292: F1164-F81, 2007.

295. **Weinstein SW, Klose R, Szyjewicz J, Moore L**. Evidence for an osmotic effect of glucose in the in vivo rat proximal tubule. *Pflügers Archiv* 394: 320-8, 1982.

296. **Welling LW, Grantham JJ**. Physical properties of isolated perfused renal tubules and tubular basement membranes. *J Clin Invest* 51: 1063-75, 1972.

297. **Wells R**. Social and cultural capital, race and ethnicity, and college student retention. *Journal of College Student Retention: Research, Theory & Practice* 10: 103-28, 2008.

298. **Wernette P, Houser C, Quick C**. Team-based multidisciplinary research scholarship in the geosciences. In: *American Geophysical Union's 49th Fall Meeting*. San Francisco, CA: 2016.

299. **Wilcox CS, Sterzel RB, Dunckel PT, Mohrmann M, Perfetto M**. Renal interstitial pressure and sodium excretion during hilar lymphatic ligation. *Am J Physiol Renal Physiol* 247: F344-51, 1984.

300. **Williams Jr JC, Schafer JA**. Cortical interstitium as a site for solute polarization during tubular absorption. *Am J Physiol Renal Physiol* 254: F813-F23, 1988.

301. **Williams Jr JC, Schafer JA**. A model of osmotic and hydrostatic pressure effects on volume absorption in the proximal tubule. *Am J Physiol Renal Physiol* 253: F563-F75, 1987.

302. **Wilson PD, Pinter GG**. A model for heterogeneity of kinetics of albumin transport in the renal cortical interstitium. *Math Biosci* 46: 1-10, 1979.

303. **Wilson RW, Wareing M, Green R**. The role of active transport in potassium reabsorption in the proximal convoluted tubule of the anaesthetized rat. *J Physiol* 500: 155-64, 1997.

304. **Wilson SB, Varma-Nelson P**. Small groups, significant impact: a review of peer-led team learning research with implications for STEM education researchers and faculty. *Journal of Chemical Education* 93: 1686-702, 2016.

305. **Windhager EE**. Sodium chloride transport. In: *Membrane Transport in Biology*, edited by Giebisch G, Tosteson DC, and Ussing HH. New York: Springer, 1979, p. 145-214.

306. **Wolgast M, Larson M, Nygren K**. Functional characteristics of the renal interstitium. *Am J Physiol Renal Physiol* 241: F105-F11, 1981.

307. **Yamamoto J, Trippodo NC, Ishise S, Frohlich E**. Total vascular pressure-volume relationship in the conscious rat. *Am J Physiol Heart Circ Physiol* 238: H823-H8, 1980.

308. **Yancy CW, Jessup M, Bozkurt B, Butler J, Casey DE, Drazner MH, . . . Wilkoff BL**. ACCF/AHA guideline for the management of heart failure. American College of Cardiology Foundation: American Heart Association Task Force, 2013.

309. **Yip GW-K, Zhang Q, Xie J-M, Liang Y-J, Liu Y-M, Yan B, . . . Yu C-M**. Resting global and regional left ventricular contractility in patients with heart failure and normal ejection fraction: insights from speckle-tracking echocardiography. *Heart* 97: 287-94, 2011.

310. **Youden WJ**. Index for rating diagnostic tests. *Cancer* 3: 32-5, 1950.

311. **Zhao C, Kuh GD**. Adding value: Learning communities and student engagement. *Research in higher education* 45: 115-38, 2004.